

A Comparative Analysis of the Two-Bladed and the Three-Bladed Wind Turbine for Offshore Wind Farms

Anish John Paul
Sustainable Energy Technology



MASTER OF SCIENCE THESIS

A Comparative Analysis of the Two-Bladed and the Three-Bladed Wind Turbine for Offshore Wind Farms

in partial fulfillment of the requirements
for the degree of
Master of Science
in
Sustainable Energy Technology
at the
Technical University of Delft

Anish John Paul
September 2010

Technical University of Delft
Faculty of Aerospace Engineering – Section Wind Energy

Technical University of Delft
Faculty of Aerospace Engineering – Section Wind Energy

The undersigned hereby certify that they have read and recommend to the Faculty of Applied Sciences for acceptance a thesis entitled 'A Comparative Analysis of the Two-Bladed and Three-Bladed Wind Turbine for Offshore Wind Farms' by Anish John Paul in partial fulfillment of the requirements for the Degree of Master of Science.

September 2010

Committee:

Prof. dr. Gerard .J.W. van Bussel

ir. Michiel Zaaijer

ir. Niels Diepeveen

ir. Turaj Ashuri

Acknowledgements

First, I would like to thank my supervisor Michiel Zaaijer for his constant guidance during the last 12 months at TU Delft. The numerous discussions we had have contributed greatly in shaping my thesis. I also thank the committee for their contributions in shaping my thoughts.

I would also like to thank the Master students at Section Wind Energy whose contributions, via informative discussions, were invaluable and also everyone at Section Wind Energy for making my experience here most memorable.

I would like to take this opportunity to thank all my friends. Their comraderie, entertainment and caring cannot be overstated. They made this a truly eventful two years.

Finally, I would like to thank my family for their continuous support and motivation.

Abstract

Background: As the installation of offshore wind farms continues to increase, the need to optimize on costs involved is a constant factor in the industry. In this regard, research into the two-bladed rotor has garnered some interest in the recent past, to see if the optimum cost can be shifted in the favor of the two-bladed wind turbine.

Objective: The objective of this thesis was to determine the costs of energy delivered by a two-bladed wind turbine and a three-bladed wind turbine and to determine which turbine's cost is lower. Energy cost was treated as the main discerning factor between the turbines.

Method: Two concepts were defined; the two-bladed wind turbine and the three-bladed turbine. For the three-bladed concept two cases were considered; one with a design tip speed ratio equal to that of the two-bladed concept and another with a design tip speed ratio lower than the first case. Only the rotor and the support structure were designed. For the rotor, Delft University airfoils were used. The Blade Element Momentum theory was used to design the rotors and to obtain the rotor power and thrust. Support structures were designed based on the Rayleigh method for stepped piles. Bladed 3.80 was used to determine fatigue damage of the rotors and support structures. Components in the nacelle were not designed but their masses were estimated using scaling relations. These masses along with rotor and support structure masses were translated into Euro's using cost factors obtained from literature.

An offshore site roughly 70km from shore was selected and hundred of these designed turbines were hypothetically installed at this site. Cost of installation and electrical infrastructure was obtained from data available. From this and the rotor and support structure costs the investment cost was obtained. The Annual Energy Yield of the turbines was also calculated. These, along with operation and maintenance costs were used to calculate the energy cost.

Main Results: From the design iterations it was seen that the energy cost of the two-bladed turbine was slightly lower than that of the three-bladed concept with a lower design tip speed ratio. Another important result of this report was that a three-bladed turbine with a tip speed ratio equal to that of the two-bladed turbine gave the lowest energy costs. It was also seen that the energy yield of the two-bladed concept is lower than that of the three-bladed concept and support structure costs for the two-bladed concept is higher.

Keywords: *wind turbine, two-bladed, three-bladed, rotor, tip speed ratio, blade, support structure, nacelle, LPC*

Contents

Acknowledgements..... i

Abstract.....iii

Contents.....v

List of Symbolsix

 Greek Symbolsix

 Alphabetsix

List of Abbreviationsxi

1 Introduction 1

 1.1 Steps towards Optimal concepts for Offshore Wind Turbines..... 1

 1.2 Thesis Objective 2

 1.3 Approach..... 2

 1.4 Report Layout..... 3

2 Turbine Configurations and Definitions..... 5

 2.1 Wind Farm Size 5

 2.2 Definitions..... 5

 2.2.1 Wind Turbine 6

 2.2.2 Rotor 6

 2.2.3 Nacelle..... 6

 2.2.4 Support Structure 6

 2.2.5 Offshore Electrical Network..... 7

 2.3 Turbine Configurations 7

 2.3.1 Power Control: Stall control vs. Pitch control..... 7

 2.3.2 Rotor Orientation: Upwind vs. Downwind 7

 2.3.3 Yaw Control: Passive Yaw vs. Active Yaw 8

 2.3.4 Drive train: Direct Drive Generators vs. High Speed Generators with
Gearbox..... 8

 2.3.5 Gearbox..... 9

 2.3.6 Blades..... 10

 2.3.7 Hub..... 10

 2.3.8 Other Nacelle Components 11

 2.3.9 Support Structure 12

 2.4 Final Note 12

3 Site Conditions 13

 3.1 General Information 13

 3.2 Soil Profile 13

 3.3 Water Level 14

 3.4 Sea Floor Depth..... 15

 3.5 Wind and Wave Data 15

 3.5.1 50 year maximum wave height..... 15

 3.5.2 Platform height and hub height..... 15

 3.5.3 50 year maximum wind speed..... 17

 3.5.4 Wind speed distribution 18

3.5.5	Turbulence Intensity	19
3.5.6	Sea States	19
3.5.7	Wave Spectrums	19
3.6	Current Data.....	20
4	The Design Process	23
5	Procedure for Investment Cost Estimation and LPC.....	27
5.1	Levelised Production Cost (LPC) of Energy	27
5.2	Cost and Scaling Model.....	28
5.2.1	Suitability of the NREL model for the selected wind farm	28
5.2.2	Cost of Offshore Electrical Network	29
5.2.3	Cost of Turbine components per unit mass.....	31
5.2.4	Cost of Installation	33
5.2.5	Cost of Operation and Maintenance	35
5.3	Final Note	38
6	Design Tip Speed Ratio	41
6.1	Definition	41
6.2	Influence of Design tip speed ratio on certain parameters.....	41
6.2.1	Blade Geometry and Design tip speed ratio.....	41
6.2.2	Power Coefficient and Design tip speed ratio	43
6.2.3	Aerodynamic considerations stemming from Design tip speed ratio	44
6.2.4	Structural design considerations stemming from Design tip speed ratio	48
6.2.5	Practical considerations stemming from Design tip speed ratio.....	49
6.2.6	Today's Offshore Turbines.....	50
6.3	Summary of selection parameters for λ_{design}	50
6.4	Selection of λ_{design}	51
7	Component Design and Installation Procedure.....	55
7.1	Rotor Design.....	55
7.1.1	Airfoil selection and properties	55
7.1.2	Chord and Twist Selection	60
7.1.3	Blade Element Momentum theory	61
7.1.4	Internal structure of the airfoil	63
7.1.5	Material Selection	65
7.2	Nacelle.....	67
7.2.1	Generator	68
7.2.2	Gearbox.....	68
7.2.3	Hub.....	69
7.2.4	Pitch mechanism.....	70
7.2.5	Yaw System	70
7.3	Support Structure Design.....	70
7.3.1	Design based on Natural Frequency	70
7.3.2	Scour	72
7.3.3	Pile Penetration and Soil Stiffness	72
7.3.4	Buckling checks	73
7.3.5	S-N curve	74

7.4	Fatigue Analysis of the Blades and Support structure.....	75
7.5	Installation Procedure.....	75
8	Implementation and Results.....	81
8.1	Rotor	81
8.1.1	Blade dimensions.....	81
8.1.2	Blade Strength and Mass	83
8.1.3	Rated Wind Speed	86
8.1.4	Design and Operating curves from the BEM code.....	86
8.1.5	Blade verification checks	86
8.2	Nacelle.....	88
8.3	Support Structure	88
8.3.1	Foundation Pile.....	88
8.3.2	Tower	89
8.4	Installation	90
8.5	Results.....	91
8.5.1	Rotor	91
8.5.2	Nacelle.....	94
8.5.3	Support Structure	95
8.5.4	Results for all iterations	96
8.5.5	LPC.....	99
8.6	Final note	101
9	Conclusions and Recommendations.....	103
9.1	Conclusions	103
9.1.1	Rotor Cost	103
9.1.2	AEY	103
9.1.3	Nacelle.....	103
9.1.4	Support Structure	103
9.1.5	Installation	104
9.2	Recommendations.....	104
9.2.1	Better blade design.....	104
9.2.2	New airfoils	104
9.2.3	New Support Structure	105
9.2.4	Teetering Hub Effects	105
	References	107
	Appendix I: Example Design and Operating curves for one iteration	111
	Design Curves.....	111
	Operating Curves	117

List of Symbols

Greek Symbols

1. δ – internal friction angle of soil [degrees]
2. γ – effective unit weight of soil [kN/m^3]
3. ζ^* – highest water level above mean sea level [m]
4. ψ – azimuth angle [degrees]
5. δ_3 – delta 3 angle
6. $\Delta\beta$ – the change in pitch angle
7. ζ – the teeter angle
8. λ – tip speed ratio
9. λ_r – local speed ratio
10. ϕ – Inflow angle [rad]
11. Ω – Rotor rotational speed [rad/s]
12. θ_p – Section pitch angle
13. θ_T – Section twist angle
14. α – angle of attack
15. α_s – critical angle of attack
16. ρ – density of air [kg/m^3]
17. μ – Mass per unit length of the monopile [kg/m]
18. ρ_{steel} – steel density [kg/m^3]
19. $\Delta\sigma$ – Stress range [N/m^2]

Alphabets

1. a – axial induction factor
2. a' – tangential induction factor
3. a_n – annuity factor
4. AEY – annual energy yield [kW-hr/year]
5. B – Number of blades
6. C_l – Lift coefficient of the airfoil
7. C_d – Drag coefficient of the airfoil
8. $C_{l,\text{design}}$ – Chosen Lift coefficient of the airfoil
9. C_p – Power coefficient
10. C_c – Investment costs including interest during construction [€]
11. $C_{O\&M,y}$ – annual operation and maintenance cost [€]
12. d – Water depth [m]
13. D – rotor diameter [m]
14. D_{spur} – Diameter of the spur gear [m]
15. E_{steel}, E – Young's modulus of steel [210 GPa]
16. F_n – Thrust force [N]
17. f is electrical frequency [Hz]
18. f_{nat} – Natural frequency of the support structure [Hz]
19. H_s – significant wave height [m]

20. I_j – Second moment of area of section j [m^4]
21. K_{rot} – Rotational stiffness of the soil [Nm/rad]
22. K_{lat} – Lateral stiffness of the soil [N/m]
23. l_j – Length of section j [m]
24. L – Length of support structure from seabed to hub height [m]
25. LPC – Levelised Production Cost [$€/kW-hr$]
26. m – Inverse slope of S-N curve
27. $Mass_{spur}$ – Mass of the spur gear [kg]
28. m_j – Mass of section j [kg]
29. M_{top} – Tower top mass [kg]
30. N – Number of cycles to fatigue failure
31. N_{spur} – Ratio between generator shaft speed and spur gear speed
32. n_s is the synchronous speed of the generator [rpm]
33. P – Power [W]
34. p – number of magnetic poles
35. r – Real interest rate [%]
36. T' – Economic lifetime of the wind farm [years]
37. T_t – natural Period [s]
38. r_i – Distance of the annulus i from the hub [m]
39. R – Blade length [m]
40. R_{tip} – Distance of the blade tip from the hub [m]
41. T_z – Zero Crossing Period [s]
42. U_r – Wind velocity at rotor [m/s]
43. U, U_o – Free stream wind velocity [m/s]
44. U_{rated} – Rated wind speed [m/s]
45. U_{ss} – Sub surface current [m/s]
46. $U_{ss}(0)$ – Current velocity at MSL [m/s]
47. V_{10} – Wind speed at 10m above MSL (where data was measured) [m/s]
48. V_{hub} – Wind Velocity at hub [m/s]
49. V_{rated} – Turbine rated wind speed [m/s]
50. x_j – Distance of midpoint of section j to the seabed [m]
51. z – Height with reference to the MSL [m]
52. z_o – ‘internal roughness length’ within the wind farm [m].
53. Z_{10} – 10 m above MSL
54. Z_{hub} – Turbine hub height from MSL [m]
55. $Z_{platform}$ – Platform Level from MSL [m]

List of Abbreviations

1. AEY - Annual Energy Yield
2. BEM - Blade Element Momentum
3. DFIG – Double Fed Induction Generator
4. DOWEC – Dutch Offshore Wind Energy Converter
5. GFRP – Glass Fibre Reinforced Plastic
6. HAT - Highest Astronomical Tide
7. LAT - Lowest Astronomical Tide
8. LPC - Levelised Production Cost
9. MSL - Mean Sea Level
10. NREL – National Renewable Energy Laboratory

1 Introduction

Offshore wind farms are poised to produce a large amount of green electricity. The reasons that wind farm developers look offshore include steady winds, low wind shear, low turbulence and a larger amount of space as compared to that available for onshore turbines. As the present situation stands, the capital costs of offshore wind farms are higher than that of onshore wind farms. Most reports estimate that the investment cost of offshore wind is around 1600 €/kW, and that of onshore wind is 1000 €/kW (BWEA, N.D. & offshorewindenergy.org, 2008). This investment cost of offshore wind is based on the Horns Rev project which consists of 80 wind turbines each with a rating of 2MW. With the introduction of larger turbines in newer offshore wind farms it is quite conceivable that this figure will have changed.

A cost break up of an onshore wind farm and an offshore wind farm is shown below in Figure 1-1. It should be noted that these percentages vary according to the number of wind turbines in the farm, distance of the farm from the shore, the size and rating of each turbine, etc.

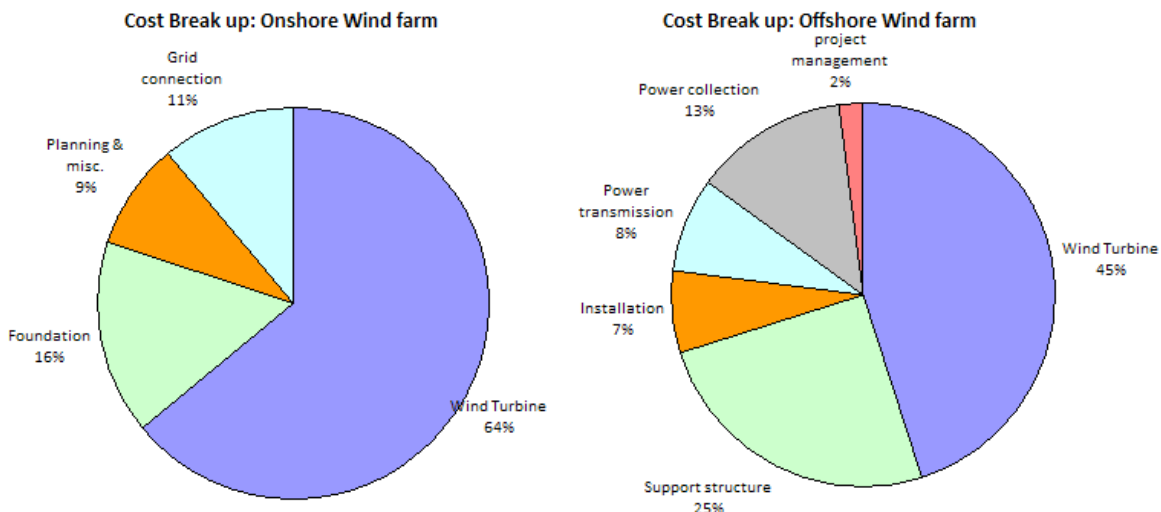


Figure 1-1: Investment cost Break up for Offshore and Onshore Wind Farms
www.offshorewindenergy.org

As can be seen in the above figure the cost break up for offshore wind farms is quite different than that for onshore wind farms. The costs associated with the offshore grid, installation costs and support structure take up significant amounts of the pie. In addition to this, offshore maintenance costs (not shown in the figure) are significantly more than onshore maintenance costs.

1.1 Steps towards Optimal concepts for Offshore Wind Turbines

Most wind turbines used in offshore wind farms are variants of onshore wind turbines, which have simply been treated to withstand offshore conditions, i.e. the salty offshore environment. To bring down the investment cost of offshore wind energy it is necessary

to design and use a wind turbine which has been optimized for offshore use. Some examples of such concepts are:

- Large multi-MW wind turbines: Offshore wind energy research in the 70's and 80's showed that offshore wind energy was economically feasible only when turbines crossed a certain size threshold. In recent times, offshore wind turbine rotor diameters have peaked at about 125 meters. This trend in size increase shows that the economic viability of offshore wind turbines is higher when turbines are larger. Furthermore, present research into wind turbines is geared toward crossing this barrier.
- Simple and robust wind turbines: In this discussion simple implies a lesser number of components and robust implies a lesser number of failures. Figure 1-1 shows that the maintenance costs for offshore wind are quite large. Wind turbine design with respect to maintenance costs would mean a lesser number of components (which means there are lesser parts to fail) and robust design (which means each component has a higher reliability). No such trend is observed in the industry so this example is speculative.

The two-bladed turbine seems to offer an alternative to the now established three-bladed turbine as an optimal offshore wind turbine. Optimal turbine in this discussion refers to the turbine which delivers energy at the lowest cost. This is because the absence of the third blade means lower manufacturing costs, lower transportation costs and lower installation costs. The two-bladed wind turbine is an old concept but its development was largely ignored. However as the offshore wind industry matures, reducing investment cost, installation cost and maintenance costs has gained more importance. This has in turn led to renewed interest in the two-bladed turbine.

1.2 Thesis Objective

The objective of this report is to compare the Levelised Production Cost (LPC) of a 'typical' wind farm utilizing 5MW three-bladed turbines and one using 5MW two-bladed turbines and to find out which concept offers the lowest LPC.

This is the next step, after what was done in System Integration Project – II, where the two-bladed turbine was qualitatively compared with the three-bladed turbine (Paul, 2010).

1.3 Approach

For this thesis a three-bladed wind turbine and a two-bladed wind turbine will be designed. LPC will be treated as the objective function during the design process. LPC will be a function of the rotor, support structure, nacelle and the number of wind turbines in the wind farm. In the design process, minimizing the LPC will be the primary goal thus leading to a trade-off between the energy yield of the turbine and loads on the turbine.

Although the primary focus is on the design of the rotor and the support structure, it is important to consider the effect of the concept change on other aspects of the wind farm. These include electrical infrastructure, installation and operation & maintenance.

In this manner the impact of the concept change can be witnessed in a 'real' situation. Therefore a wind farm design approach will be used.

For the design process, realistic wind and ocean data is required. The data required include the annual wind speed distribution which will be used to determine the Annual Energy Yield (AEY) and the sea states which will be used to simulate the wind and wave loading on the rotor and support structure during the 20 year lifetime of the wind turbine.

The blades will be aerodynamically designed using the Blade Element Momentum (BEM) theory. Blade structure will be designed based on the stress developed due to aerodynamic loading. The support structure will be designed based on the rotational frequency of the rotor and the weight of the nacelle-rotor assembly. The designed turbines will then be analyzed using Bladed 3.80. A fatigue analysis and an ultimate load analysis will be performed based on which the designs will be finalized. The cost contribution of the rotor and support structure to LPC will be determined on a unit weight basis. There will be no design of the components in the nacelle. Instead their cost contribution to the LPC will be determined based on scaling relations available in literature.

1.4 Report Layout

The layout of the report will follow the steps involved in the approach described above. In Chapter 2 the size of the wind farm and some definitions and turbine configurations selected will be discussed. Chapter 3 details the site chosen and the conditions prevalent at the site. The design process followed is briefly sketched in Chapter 4. In Chapter 5 costs of components per unit weight, installation costs/unit time and the operation and maintenance costs are obtained. This chapter also gives the procedure to determine LPC. Chapter 6 discusses the selection of the design tip speed ratio of both concepts. Chapter 7 describes procedures for rotor design according to the BEM theory, the modeling of the relevant components in the nacelle, the procedure for design of the turbine support structure and the determination of the installation costs. The implementation of these design procedures along with the results is given in Chapter 8. The conclusions and recommendations are discussed in Chapter 9.

2 Turbine Configurations and Definitions

This section will deal primarily with the configurations of the two-bladed turbine and the three-bladed turbine. First, the size of the wind farm was fixed based on present day wind farms. Definitions of components are then assigned. These definitions will be used throughout the report. Lastly turbine configurations are chosen based on designs prevalent in the industry.

2.1 Wind Farm Size

It was decided that the designed wind turbines will operate in wind farms with one hundred turbines each i.e. one hundred two-bladed turbines in one farm and one hundred three-bladed turbines in another farm. One hundred turbines in an offshore wind farm is a reasonable number considering the trend in the industry. Horns Rev I and II have 80 and 91 wind turbines respectively, Rødsand I has 72 wind turbines. Other large offshore wind farms in the planning/construction phase are BARD Offshore 1 (80 turbines), Greater Gabbard Offshore Wind Farm (140 turbines), Sheringham Shoal Offshore Wind Farm (88 turbines), Thanet Offshore Wind Farm (100 turbines) and Rødsand II Offshore Wind Farm (72 turbines).

Of course the sites of both wind farms will experience the same wind and wave conditions and have the same soil data. The turbines in each farm will be placed in a rectangular grid with an array spacing of $7D$ by $7D$, where D is the rotor diameter.

2.2 Definitions

Before the turbine configurations are discussed, some terms need to be defined. Figure 2-1 shows the parts of an offshore wind turbine. Most of the terms in the figure are self-explanatory. For the definitions of more commonly used terms please refer to IEC 61400-3.

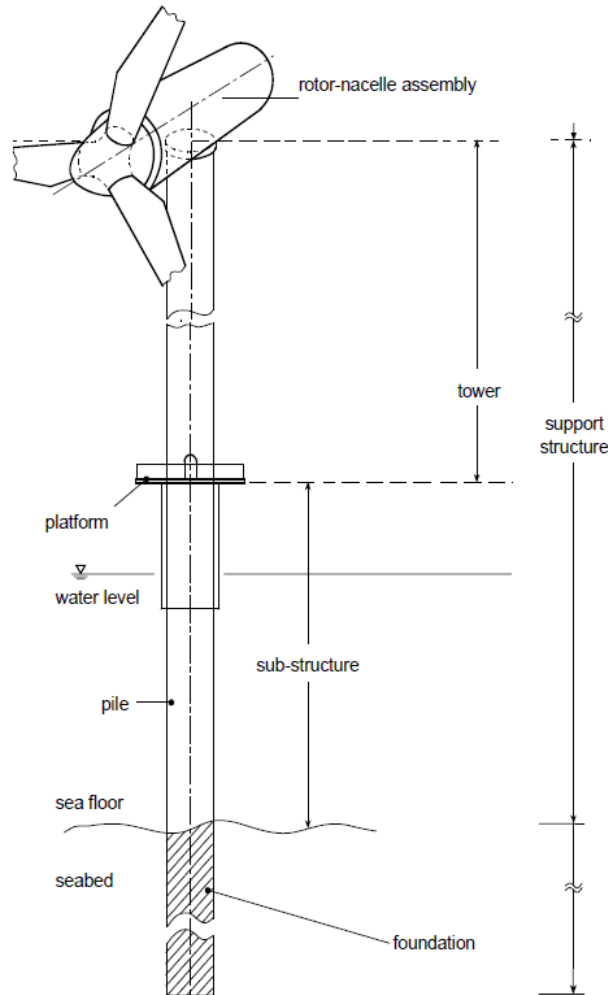


Figure 2-1: Parts of an offshore wind turbine (Source: IEC 61400-3)

Other terms and definitions that will specifically be used in this report are:

2.2.1 Wind Turbine

In this report, wind turbine will mean the entire structure i.e. the rotor-nacelle assembly, the tower, the substructure and the foundation.

2.2.2 Rotor

In this report, rotor will mean the blades and the hub.

2.2.3 Nacelle

In this report, the nacelle will mean housing which contains components (drive train, generator and their accompanying systems) and the components themselves.

2.2.4 Support Structure

In this report, support structure will mean all parts below the rotor-nacelle assembly i.e. the tower, the substructure and the foundation.

2.2.5 Offshore Electrical Network

The electricity generated in the turbine needs to be transported to shore. This involves two aspects:

Power Collection

In this report power collection means the collection of the energy generated by each turbine and bringing it to a certain point in the wind farm from where it can be transported to shore. This involves the electrical cabling from the turbine to the collection point.

Power Transmission

In this report power transmission means transmitting the energy from the collection point mentioned above, to the shore. Depending on the distance from the shore and the amount of energy collected the necessity of an offshore transformer station will be evaluated.

For purposes of simplicity, power collection and power transmission will be combined and will be referred to as Offshore Electrical Network.

2.3 **Turbine Configurations**

To arrive at a suitable conclusion when making the comparison between the two-bladed and the three-bladed turbine, design features prevalent in modern, state-of-the-art, multi-MW turbines need to be chosen. This means that the configurations chosen are based on designs witnessed in the industry and no study will be performed on the inherent advantage each configuration provides. These design features are discussed below.

2.3.1 Power Control: Stall control vs. Pitch control

Stall control machines were popular in the early 1990's. With the advent of multi MW wind turbines pitch control machines became more popular. This was mostly due to better output power quality and assisted start up. Modern multi-MW offshore wind turbines use pitch control to restrict the power developed by the rotor at wind speeds higher than the wind turbine's rated wind speed. For this reason, both turbines in this report will be pitch controlled. Power control will be achieved by pitching to feather.

2.3.2 Rotor Orientation: Upwind vs. Downwind

The choice of rotor orientation is based on many factors (which are not discussed here). See Figure 2-2 for a pictorial representation of both upwind and downwind concepts.

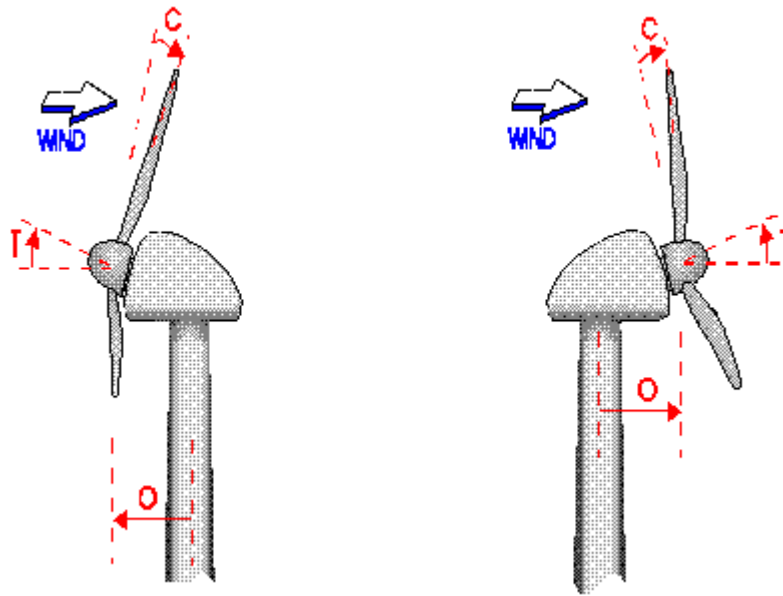


Figure 2-2: Illustration of cone angle(C), tilt angle (T) and overhang (O) for a upwind turbine (Left) and a downwind turbine (Right) (Source: Bladed software)

In this report the rotor orientation for the three-bladed turbine will be upwind. This choice is justified based on present designs witnessed in offshore wind turbines. The orientation for the two-bladed turbine will also be upwind. This choice can be justified based on the fact that all large two-bladed turbines constructed so far have been upwind machines. Admittedly, there have been very few large two-bladed turbines constructed thus far. The largest of these was the Mod 5B with a 100 meter rotor diameter.

For an upwind rotor, to avoid the possibility of a tower strike, the rotor overhang, the nacelle tilt angle and the blade cone angle can be suitably modified.

2.3.3 Yaw Control: Passive Yaw vs. Active Yaw

Active Yaw systems of multi-MW machines generally use an electric motor to yaw the rotor into the wind via a large yaw gear. Passive yaw systems use the yaw moment developed due to the difference in loading over the rotor to orient the rotor into the wind. In this report both turbines will employ an active yaw system. This is in line with present industry practice.

2.3.4 Drive train: Direct Drive Generators vs. High Speed Generators with Gearbox

There are plenty of configurations which can be adopted for the drive train. These include the double fed induction Generator (DFIG) with a gearbox, direct drive synchronous generator, the synchronous generator with a gearbox, among others. There are many advantages and disadvantages for each system and therefore many reasons to make an appropriate design choice. See (for example) H. Polinder and J. Morren, 2005. However, such a study will not be done here. Instead, in keeping with the

offshore wind industry practice, the drive train selected will be a high speed generator with gearbox.

For this report, the generator chosen is a DFIG. The number of magnetic poles chosen is six. The Bard 5MW turbine and the RE Power 5MW turbine use this configuration (RE Power, 2010 and Bard Offshore, 2010). This means that the rated rotational (synchronous) speed of the generator is 1000rpm, considering that the network operates at 50Hz. See Equation 2.1.

$$n_s = \frac{120f}{p} \quad \text{Equation 2.1}$$

n_s is the synchronous speed of the generator [rpm]

f is electrical frequency [Hz]

p is the number of magnetic poles

For a good energy yield, an operating speed range of 60% to 110% is sufficient (Polinder and Morren, 2005). From this, the operating speed range of the DFIG was set at 600rpm to 1100 rpm.

2.3.5 Gearbox

The gearbox steps up the rotational speed of the rotor to a value suitable for the generator i.e. up to 1000 rpm. A typical value of an overall gear ratio for a 5MW wind turbine is 1:97 (RE Power, 2010 and Bard Offshore, 2010). This step up is achieved usually by three separate stages, because each stage has a maximum step up ratio of 1:6 due to size restrictions (Manwell et al, 2006). In keeping with industry practice a gearbox with a combination of two planetary stages and a spur gear stage will be used.



Figure 2-3: Two planetary stages + a spur gear gearbox (GE Drivetrain technologies, ND)

2.3.6 Blades

The diameter of the rotors of both concepts was chosen as 126m. This number was based on the length of the RE Power 5MW turbine blade which is LM Glasfiber's LM 61.5 P (LM Glasfiber, 2010) and allowing 3 meters diameter for the rotor hub. Most scaling models determine component costs as a function of the rotor diameter (or blade length). If the diameters of the two-bladed and three-bladed rotor are different this will not serve in accurately differentiating between the costs of the two-bladed turbine and the three-bladed turbine as the concept changes. For this reason the diameters of the rotors of both concepts were kept the same. For a straightforward and fair comparison the material used for the blades will also be kept the same.

2.3.7 Hub

The hubs of both concepts are quite different. Again, the merits and demerits of each hub will not be discussed but the hub was chosen based on industry practice.

2.3.7.1 *Three-bladed turbine*

The hub of the three-bladed turbine will be a rigid hub. A rigid hub is one that has all its major parts fixed with respect to the main shaft. Rigid hubs are generally used for wind turbines with three blades. This is due to the benign nature of the aerodynamic loading on a three-bladed rotor. Each blade of a turbine experiences a cyclic load at its root due to wind shear, turbine yawing, etc. For the three-bladed turbine these cyclic loads, when combined together at the main shaft, are balanced. In this respect a three-bladed rotor is 'symmetric'.

2.3.7.2 *Two-bladed turbine*

As mentioned in section 2.3.7.1, each blade experiences cyclic loading at the root. While the load is constant at the drive train of the three-bladed turbine, this is not so for the two-bladed turbine. The loading, in this case, is a function of the azimuth angle ψ . This fluctuating load leads to high fatigue damage in the drive train. To mitigate this, teetering hubs are generally used on two-bladed wind turbines. Although most teetering hubs have been built for fixed-pitch turbine, they can also be constructed for variable pitch turbines. But this involves a higher degree of complexity.

Figure 2-4 below shows a teetering hub with a non-zero δ_3 angle. For a discussion on the load alleviating benefits of the teetering hub and the δ_3 angle refer to Chapter 6 of *The Wind Energy Handbook* (Burton et al, 2001). The hub of the two-bladed turbine in this report will be a teetering hub with a non-zero δ_3 angle.

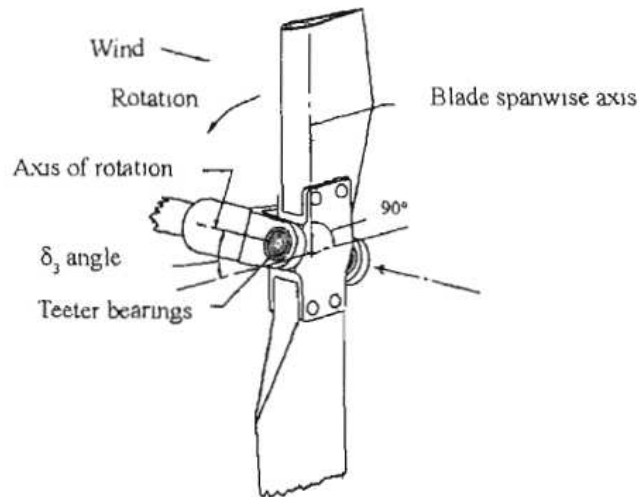


Figure 2-4: Teetering hub with a non-zero δ_3 angle (Manwell et al, 2006)

2.3.8 Other Nacelle Components

Figure 2-5 shows the nacelle of the turbine. The costs of the following components will also be taken into consideration in this report

- Low speed shaft
- Yaw drive and bearing
- Brake
- Pitch mechanism.
- Control system.
- Main frame and cover
- Hydraulics and cooling
- Main bearings

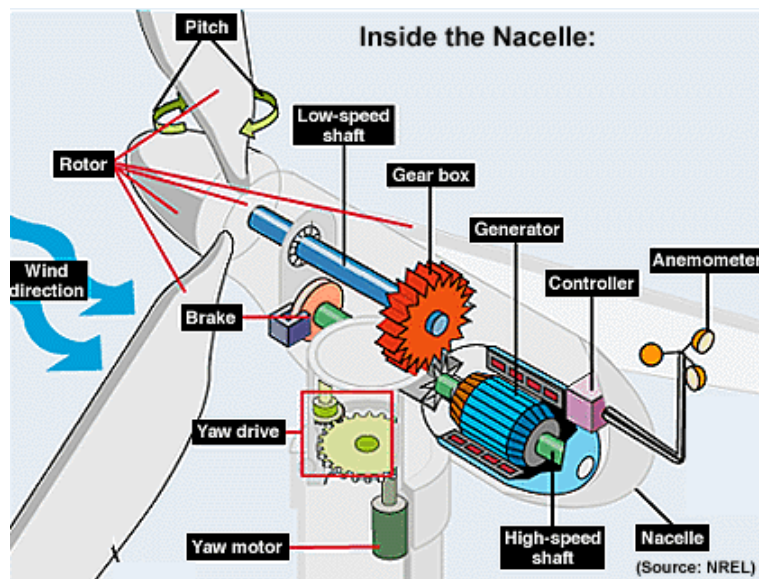


Figure 2-5: Nacelle

2.3.9 Support Structure

The monopile type support structure will be used in this report. It is a hollow steel cylinder that is driven into the sea bed. A transition piece fits over the monopile. The tower is bolted on to the transition piece and supports the nacelle-rotor assembly. Most offshore wind farms which have a water depth up to 25m use the monopile as it is the most cost-effective. This was the main reason to choose the monopile.

2.4 Final Note

From the above discussions it can be seen that the design choices for the two-bladed turbine and the three-bladed turbine were kept the same whenever this would not compromise the performance of each concept. This was done so that the differences inherent to both turbines would stand out, thus providing a clearer comparison.

3 Site Conditions

The location and weather conditions of the site chosen for the wind farm will be described in this section.

3.1 General Information

The site chosen is located in the North Sea roughly 70 kilometers from the Danish coastline which is the nearest land mass. In this report it will be assumed that all electricity generated will be transported to a point on the coastline.

The density of air is assumed to be 1.225 kg/m^3 and the density of sea water is assumed to be 1025 kg/m^3 .

3.2 Soil Profile

The soil properties at the site are determined by drilling for soil samples at a certain number of locations within the area earmarked for the wind turbine support structure and testing these samples. It is quite possible for a wind farm to have several soil profiles within its boundary. In this report the soil profile will be assumed to be uniform everywhere in the site. This means that all support structures will be designed for the same soil profile.

A soil profile was obtained from data available (de Vries and Krolis, 2007). See Table 3-1. Although this data is not for the site chosen (Section 3.1), it can be treated as data representative of soil conditions in the North Sea.

Table 3-1: Soil Profile at the site

Layers	Depth (m)	Soil Type	δ (deg)	γ (kN/m^3)
	0	seabed		
1	0.5	Sand	15	8.5
2	1	Sand	20	8
3	1.6	Sand	35	11
4	2.3	Sand	25	9.5
5	3.5	Sand	35	11.5
6	4.5	Sand	15	9.5
7	6	Sand	25	10.5
8	20	Sand	30	11

(δ is the internal friction angle of soil in degrees and γ is the effective unit weight of soil in kN/m^3)

Each soil layer acts as a spring and the resistance of the soil plays a role in determining the natural frequency of the structure and deflections at the end of the pile (otherwise known as the toe kick) and at the seabed.

3.3 Water Level

The water level was obtained from data measured over 22 years (de Vries, 2009). This data included the deviation of the water from the mean sea level i.e. the tidal range and it also included surge data. The tide data and the surge data was combined to give the total deviation from the mean sea level (i.e. the water levels). The return period of these water levels was calculated and plotted. A trendline was included to obtain the water levels with a return period greater than 22years. See Figure 3-1. From the plot the 5 year maximum and the 50 year maximum water level were obtained. See Table 3-2.

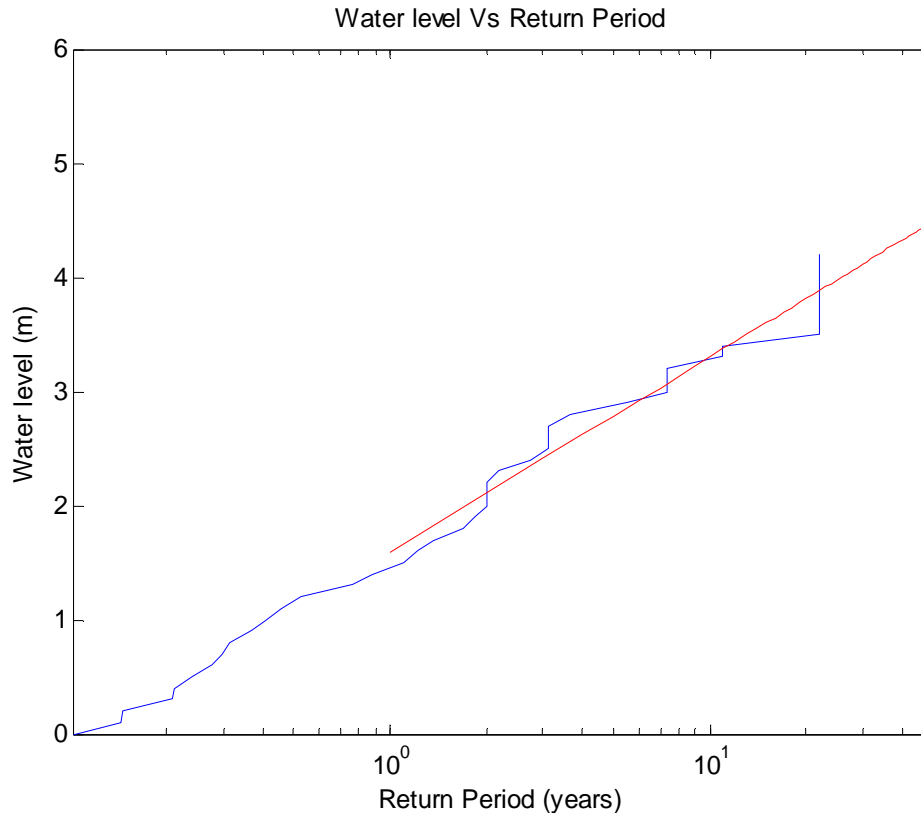


Figure 3-1: Water level Vs Return Period

Mean Sea Level (MSL) is used as the reference level for all other water levels.

Table 3-2: 5 year and 50 year maximum water level at the site

5 Year Maximum Water level	2.8 m
50 year Maximum Water level	4.5 m

Also, from the data, the lowest astronomical tide and the highest astronomical tide were obtained. See Table 3-3.

Table 3-3: LAT and HAT

Lowest Astronomical Tide (LAT)	-1.8m
Highest Astronomical Tide (HAT)	2 m

3.4 Sea Floor Depth

The sea floor depth at the site ranges from 25 to 30m from the Lowest Astronomical Tide (LAT) at different locations within the site (de Vries, 2009). For straightforwardness and simplicity an average sea floor depth of 27m from LAT will be considered. This means that the lengths of the support structures from LAT to the sea floor are the same for all wind turbines. With reference to the MSL the sea floor depth is 28.8m.

3.5 Wind and Wave Data

3.5.1 50 year maximum wave height

The fitted curves for the return periods of the significant wave height (H_s) for the site are shown below in Figure 3-2 (de Vries, 2009). (Only data up to 50 years have been plotted). To calculate the highest water level above MSL, Germanischer Lloyd standard IV-2: Guideline for the Certification of Offshore Wind Turbines was used. The 50 year maximum significant wave height is used to determine the interface height of the turbine.

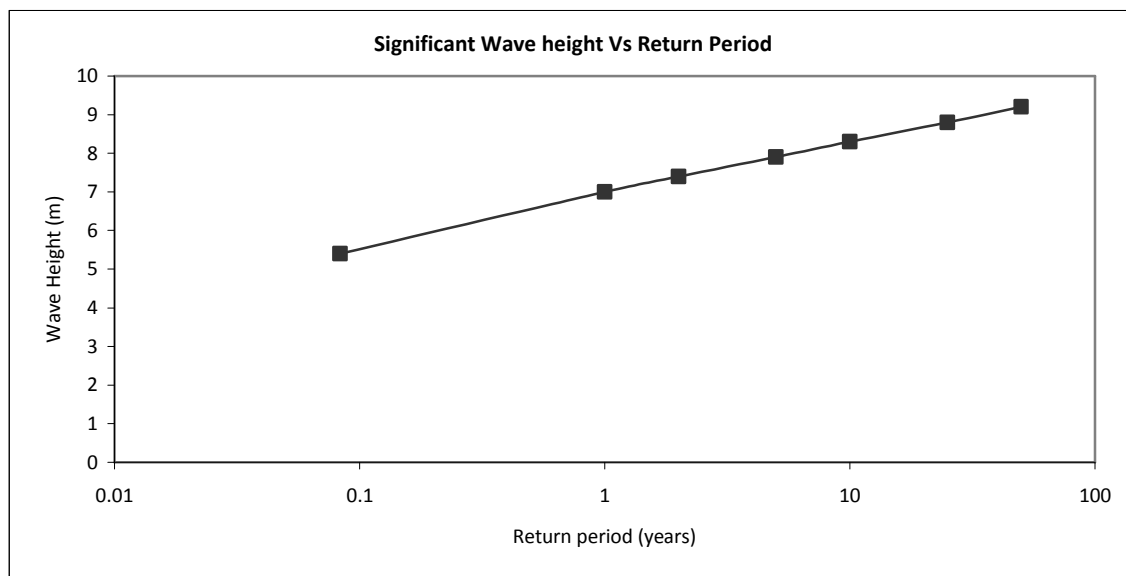


Figure 3-2: Significant Wave Height Vs Return Period

3.5.2 Platform height and hub height

The platform height and the hub height were calculated from the data available from preceding sections. The platform is the level at which the transition piece is connected to the tower. The hub height is needed because the wind speed at this height needs to be determined and is used to calculate the aerodynamic loading on the wind turbine and power obtained from the turbine.

Table 3-4 shows the important design levels for the turbine and Figure 3-3 shows some of these design levels. All data is with respect to the MSL (the reference level).

Table 3-4: Important design levels for the turbine

Sea Floor Depth(m)	-28.8	from depth data
Lowest Astronomical Tide (m)	-1.8	from water level data
Mean Sea Level (m)	0.0	Reference level
Highest Astronomical Tide (m)	2.0	from water level data
ζ^* (highest water level above MSL) (m)	11.6	from Germanischer Lloyd IV-Part 2, page 4-15
50 year maximum water level (m)	4.5	from water level data
air gap (m)	2.0	assumed
Platform Height (Z_{platform})(m)	20.1	$\zeta^* + 50 \text{ year max water level} + \text{air gap}$
Rotor Diameter (m)	126	from turbine configuration data (Chapter 2)
Blade clearance (m)	5.0	assumed
Hub Height (Z_{hub})(m)	88.1	$Z_{\text{platform}} + \text{blade clearance} + \frac{1}{2} \text{ Rotor Diameter}$

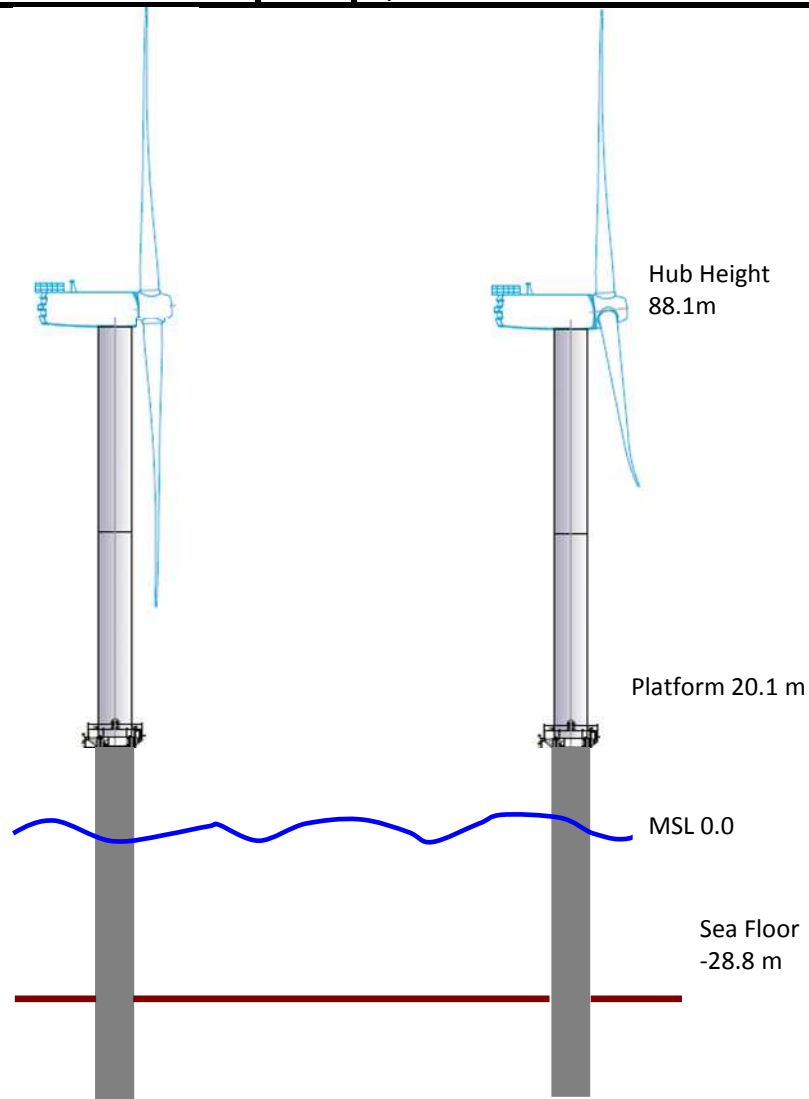


Figure 3-3: Important design levels for the turbines. All levels are with reference to the MSL. (Diagram is not to scale.)

3.5.3 50 year maximum wind speed

The wind speed at hub height is calculated using the wind shear law and assuming a logarithmic profile. A roughness length of 0.0002m is normally used for a calm sea without waves. Using this would have led to an over reduction in the wind speed values, because a wind farm generates its own 'wind climate' due to downstream wind effects (DNV-OS-J101, 2004). Based on this a roughness length of 0.05m was used. This value is based on suggestions by some researchers (Benschop, 1996, Sørensen & Thøgersen, 2006). The wind speed at hub height was then calculated using Equation 3.1.

$$V_{hub} = V_{10} \frac{\ln(Z_{hub} / z_o)}{\ln(Z_{10} / z_o)} \quad \text{Equation 3.1}$$

IEC 61400-3

V_{hub} – Wind speed at hub [m/s]

V_{10} – Wind speed at 10m above MSL (where data was measured) [m/s]

Z_{hub} – Hub height from MSL [m]

Z_{10} – 10 m above MSL

z_o – 'internal roughness length' within the wind farm [m].

The fitted curves for the return periods of the wind speeds for the site are shown below in Figure 3-4. The 50 year wind speed will be used while simulating the loads on a parked wind turbine.

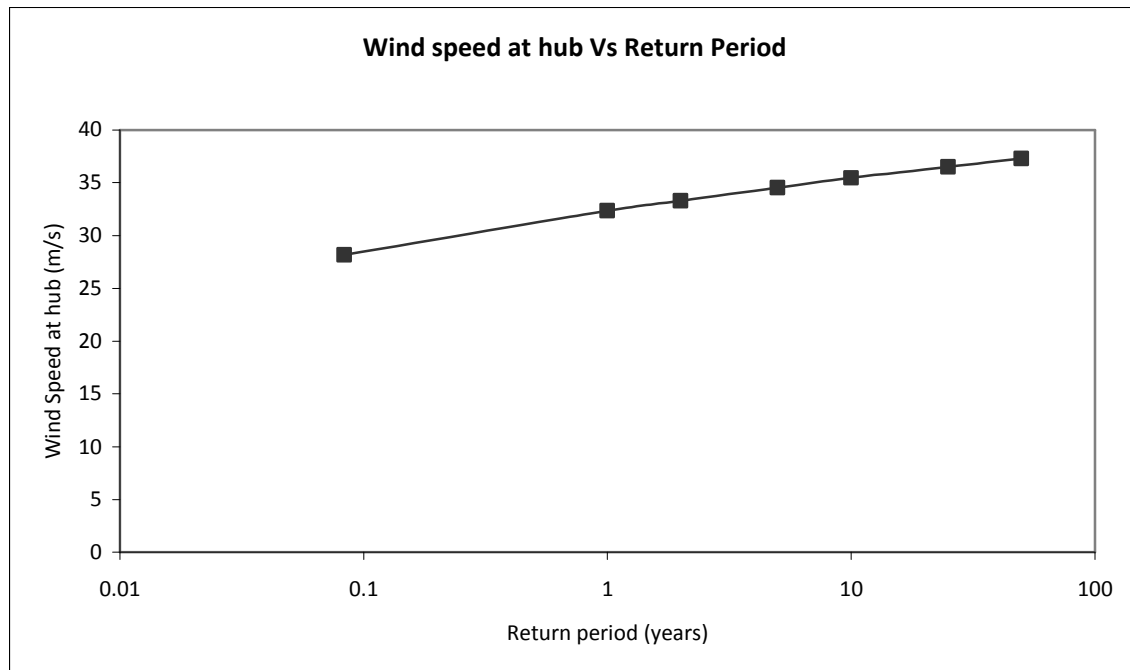


Figure 3-4: Wind Speed Vs Return Period

3.5.4 Wind speed distribution

The wind speed distribution at hub height is shown below in Figure 3-5 along with the associated data in Table 3-5. The wind speed at hub height was obtained by applying Equation 3.1 to the original data that was measured at 10m above MSL (de Vries, 2009).

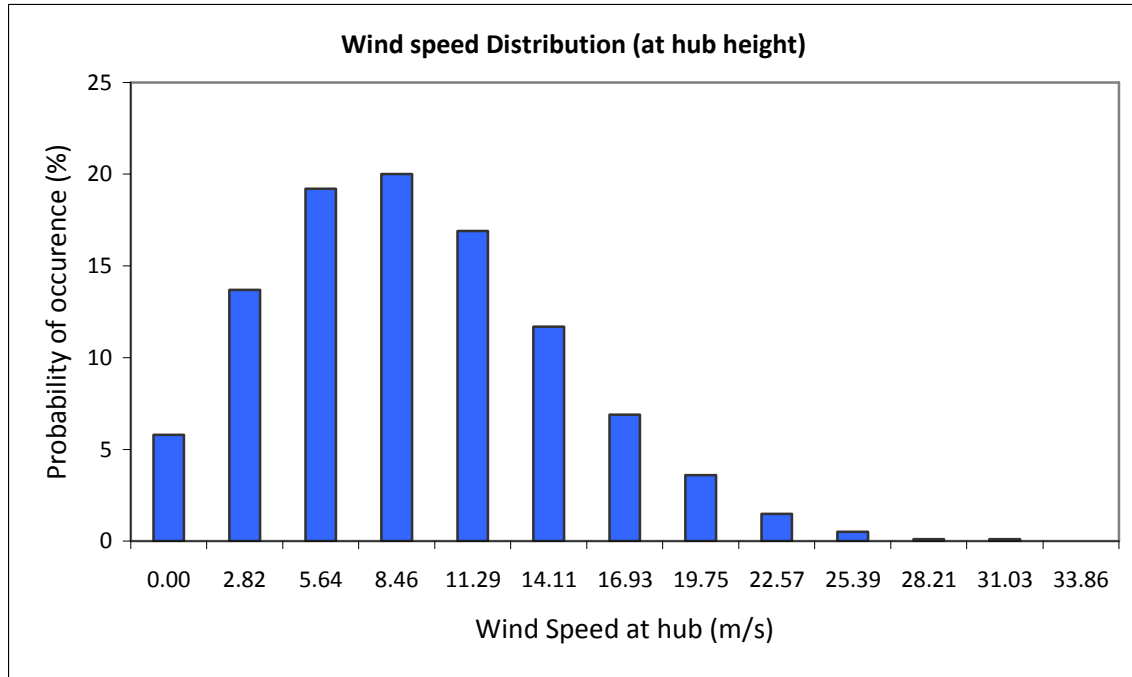


Figure 3-5: Histogram of the Wind Speed Distribution at the site.

Table 3-5: Wind Speed Distribution at the site

Wind speed at hub height (m/s)	Probability of occurrence (%)
0.00	5.8
2.82	13.7
5.64	19.2
8.46	20
11.29	16.9
14.11	11.7
16.93	6.9
19.75	3.6
22.57	1.5
25.39	0.5
28.21	0.1
31.03	0.1
33.86	0

Mean wind speed at hub height	10.72 m/s
--------------------------------------	-----------

3.5.5 Turbulence Intensity

The turbulence intensity will be set at 12% according to the Germanischer Lloyd standards for the Extreme Wind model (GL IV-2 2004).

3.5.6 Sea States

From the measured data (de Vries, 2009) the following sea states were identified. These will be used to simulate the fatigue loading on the turbine during its lifetime. See Table 3-6.

Table 3-6: Sea states

Sl. No.	Hs(m)	V _{hub} (m/s)	Tz(s)	Occurrence (%)
1	4.25	23.51	7.17	0.60
2	4.75	23.28	7.50	0.40
3	3.75	21.33	6.68	1.70
4	3.25	19.34	6.34	3.10
5	2.75	17.03	5.72	5.80
6	1.75	16.58	4.61	5.60
7	2.25	15.06	5.39	9.90
8	1.25	13.61	4.40	9.90
9	1.75	11.62	4.93	8.40
10	1.25	9.87	4.58	7.30
11	0.75	9.62	3.50	9.00
12	0.75	8.27	4.50	9.50
13	0.25	7.32	3.88	3.20
14	1.75	6.07	5.45	2.00
15	1.25	5.74	4.98	7.30
16	0.75	4.73	5.63	4.50
17	0.25	3.95	5.90	2.00
18	0.75	3.51	4.50	4.30
19	0.25	3.43	4.15	4.90

3.5.7 Wave Spectrums

A wave spectrum shows the distribution of wave energy over the frequencies of the waves. The Pierson-Moskowitz spectrum and the Jonswap spectrum are the most used spectra for wind developed seas. The Pierson-Moskowitz spectrum describes a fully developed sea. The site suits this situation so the Pierson-Moskowitz spectrum will be used for the fatigue analysis. The Jonswap spectrum describes a developing sea and is used only in analysis of extreme events.

The Pierson-Moskowitz spectrum for sea state 6, 8, 10, 13 and 16 are shown below in Figure 3-6. These sea states were shown because of their (comparatively) high frequency of occurrence. The figure shows that most of the wave energy is concentrated at frequencies between 0.1 and 0.2 Hz. Care must be taken during the

design process to ensure that the natural frequency of the support structure is not in this region.

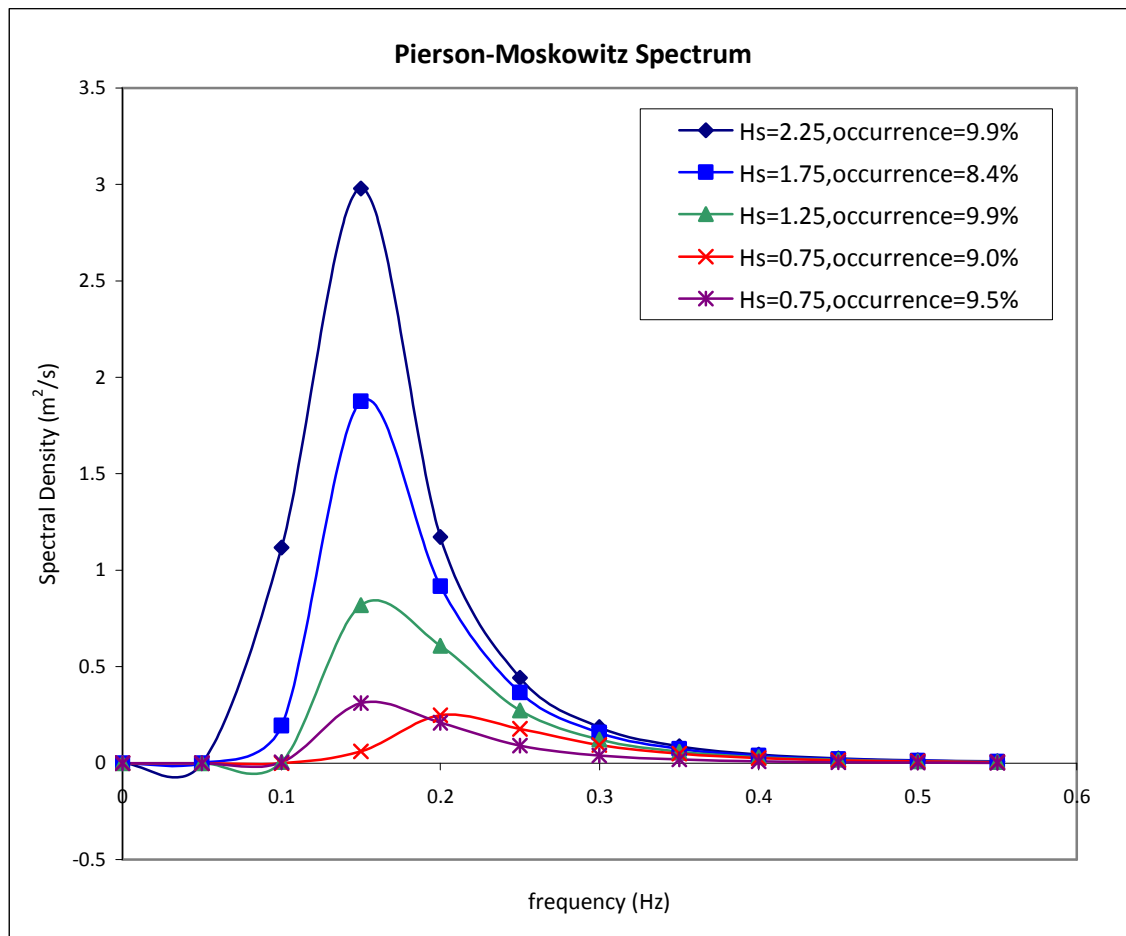


Figure 3-6: Pierson-Moskowitz spectrum for 5 sea states

3.6 Current Data

The total current speed was obtained from data measured over a period of 30.5 years (de Vries, 2009). The data was measured at MSL. Current data is used in the calculation for extremes, and is required also during installation & maintenance. A procedure similar to the one used to determine the water level data was followed and the 5-year maximum and the 50-year maximum were calculated. See Figure 3-7 and Table 3-7.

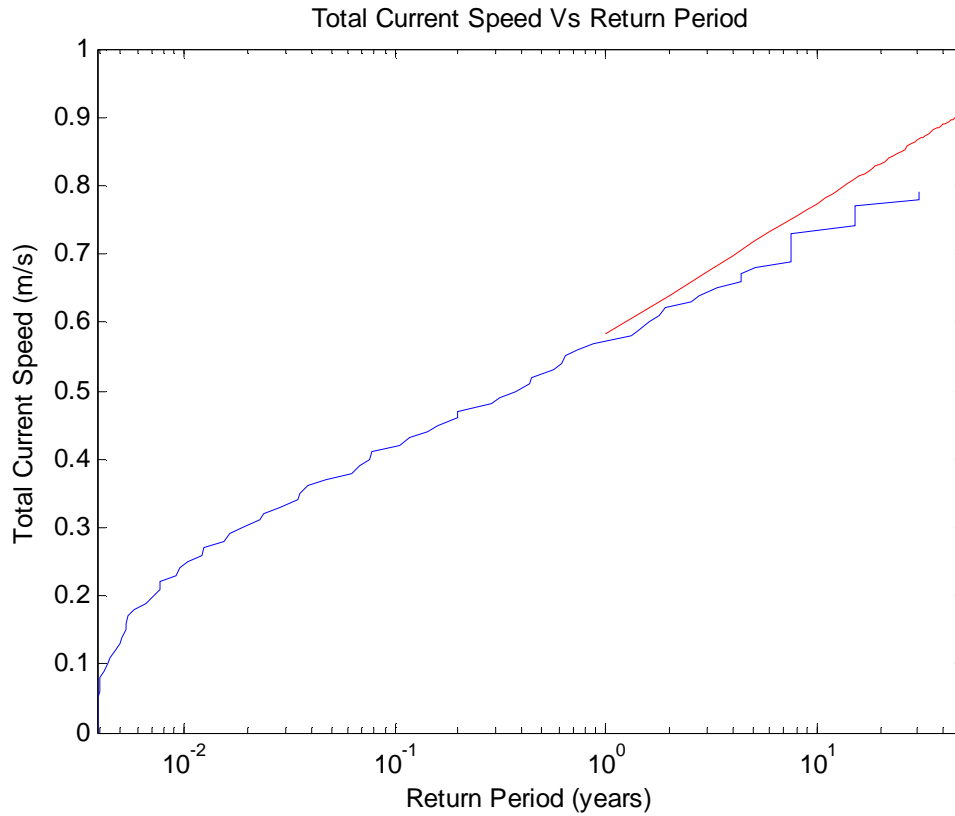


Figure 3-7: Total Current Speed Vs Return Period

Table 3-7: 5 year and 50 year current speeds at the site

5 year Total Current Speed	0.63 m/s
50 year Total Current Speed	0.91 m/s

The current speed was assumed to vary with water depth according to the power law given by IEC 61400-3. See Equation 3.2.

$$U_{ss}(z) = U_{ss}(0)[(z + d) / d]^{1/7} \tag{Equation 3.2}$$

- U_{ss} –Sub surface current [m/s]
- z – Height with reference to the MSL [m]
- d – Water depth [m]
- $U_{ss}(0)$ – Current velocity at MSL [m/s]

4 The Design Process

The design process followed in this report will be briefly described in this section.

Before initiating the design process it is necessary to prepare the cost calculations of the different components of the wind turbine and procedures such as installation and operation and maintenance. This was done using literature available and the costs of the components are obtained in terms of Euro per unit mass. The costs of procedures are obtained in terms of Euro per unit time or Euro per turbine. This process is shown in Chapter 5. Thus, the component masses and procedure times obtained after the design stage can be converted into money and ultimately the LPC can be obtained.

A flowchart of the design process is shown in Figure 4-1. The two-bladed and three-bladed turbines are designed for their rated wind speed and design tip speed ratios. The design tip speed ratio is chosen primarily on aerodynamic considerations and secondarily on turbine cost. Selection of the design tip speed ratio is discussed in Chapter 6. The aerodynamic design of the blades and a natural frequency based design of the support structure are then undertaken.

In the design approach adopted in this report, the axial induction factor is treated as an independent variable. The axial induction factor is varied to obtain chord and twist distributions for the blades of the two-bladed and three-bladed turbines. This was thought important because as turbines become larger the mass of the blade increases and this contributes to the investment cost. In this manner, it is possible for the investment costs to be varied in the design process. This trade off between blade cost and energy yield will ultimately be reflected in the LPC.

Based on the design tip speed ratio, airfoil properties for the blades are selected and the BEM theory was used to determine the rotor thrust and rotor power. These parameters along with the wind and site conditions are used to determine the AEY and to finalize the dimensions of the blade internal structure and the support structure. The stiffness of the blades is then determined and a fatigue analysis is performed to ensure that the design stiffness is sufficient. A mass estimate of the components in the nacelle is also made. Since it is expected that the two-bladed turbine will rotate faster, there will be changes in the masses of certain components in the nacelle. Only the gearbox mass is expected to change significantly due to the difference in design tip speed ratio (of the three-bladed turbine and the two-bladed turbine). In the following discussions the nacelle includes the nacelle body (frame and cover), the low speed shaft, the main bearings, mechanical brake and the hydraulics and cooling found within the nacelle. A two-bladed rotor is expected to rotate faster than an equivalent three-bladed rotor. This has implications for the nacelle body, the low speed shaft, the main bearings and the mechanical brake, but in this report the differences for these components was not evaluated. For both concepts these components were lumped into the 'nacelle' and were treated as one component. Next, the installation and O&M costs are calculated.

With the rotor mass, nacelle mass and support structure mass obtained for these different designs, their cost is determined using the information from Chapter 5. Along with installation and operation and maintenance costs and the AEY, the LPC is calculated. This LPC is a function of the axial induction factor. Thus, different LPC's are obtained for

blades designed with different axial induction factors and the wind turbine design corresponding to the lowest LPC is chosen as the optimal design.

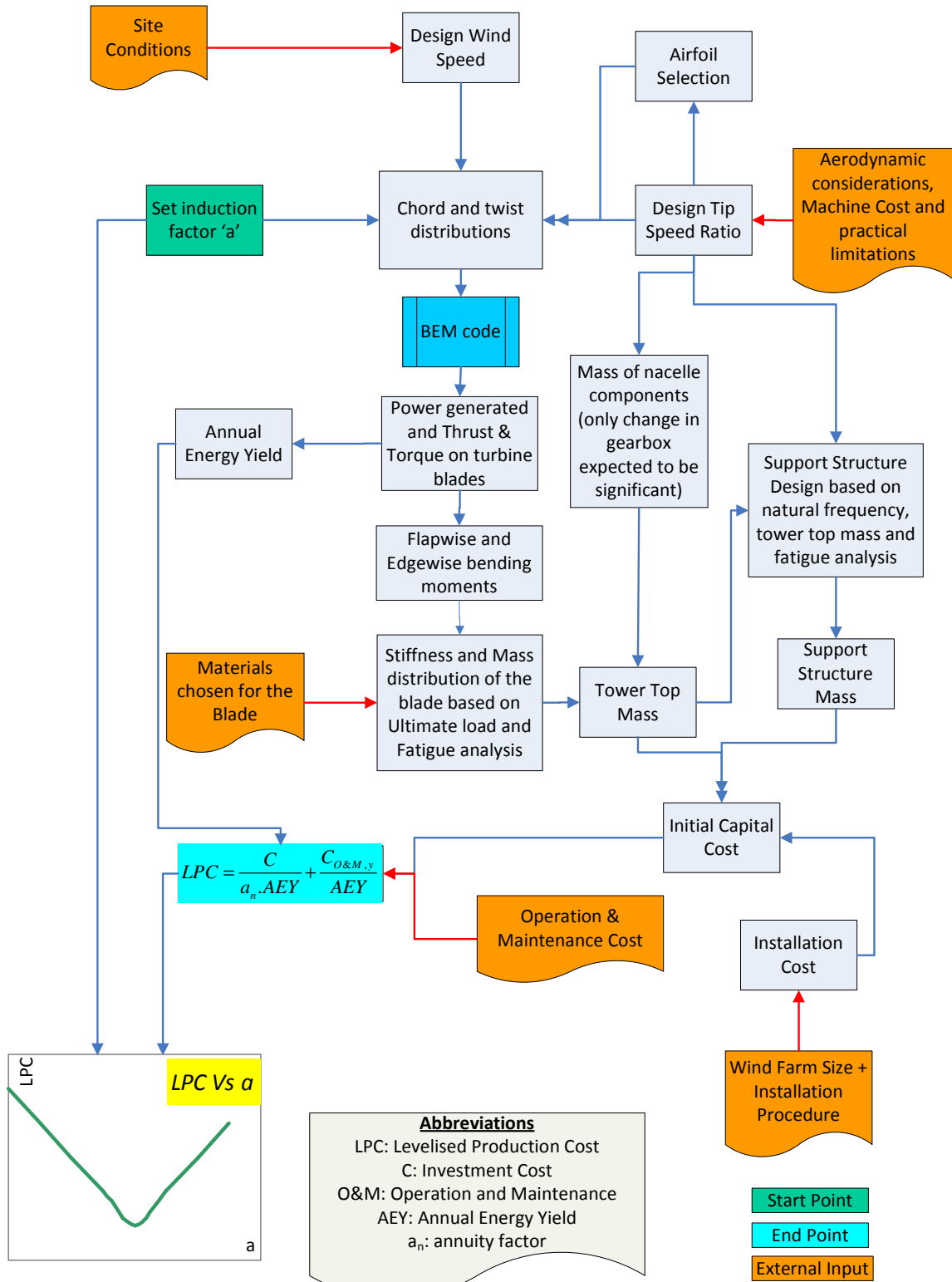


Figure 4-1: Design Process Flowchart

The details of the design procedures of individual components and establishment of installation times are described in Chapter 7 and the implementation of this iterative process and the results obtained are presented in Chapter 8. The optimal three-bladed turbine will be compared with the optimal two-bladed turbine to determine which concept is economically preferred for offshore use.

5 Procedure for Investment Cost Estimation and LPC

Estimating the investment costs involved for the two turbine concepts with the view to ultimately determine the difference in costs between them is the next step. This chapter describes the procedure to obtain the investment cost and the LPC. Literature available regarding cost and scaling models of wind turbines was used to tailor a cost estimate which is suitable for this project. To obtain accurately the investment costs and the cost of energy per kWh, an integrated approach was followed which included aspects such as the rotor, the support structure, installation, operation and maintenance, electrical networks, etc. With the change in the number of blades and a conceivable difference in the design tip speed ratio, a number of components need to be designed separately for the two-bladed and three-bladed turbines. Chief among them are the rotor blades, the gearbox and the support structure. With these design differences, difference in mass and therefore difference in cost is inevitable. The aim of this chapter is to set up factors to capture the difference in cost via the difference in mass as the concept changes.

The actual value of energy depends on market conditions, avoided costs (like cost of fuel), environmental benefits, etc. In this report, the cost estimation will only include the cost of energy since this thesis seeks mainly to differentiate between the two-bladed and the three-bladed concepts. Other factors like insurance, subsidies, permits etc will also not be considered to keep the analysis as straightforward as possible. What is important is that the two-bladed and the three-bladed concept are given the same treatment.

5.1 Levelised Production Cost (LPC) of Energy

The definition of LPC of wind energy was taken from a DOWEC report (Zaaijer, 2000). LPC is defined as “the cost price of production per unit of energy, expressed in actualized nominal money”. The LPC is given below in Equation 5.1 and is the primary parameter that will be used to determine the difference between the two-bladed turbine and the three-bladed turbine. (The decommissioning costs have been neglected in this equation).

$$LPC = \frac{C}{a_n \cdot AEY} + \frac{C_{O\&M,y}}{AEY} \quad \text{Equation 5.1}$$

LPC – Levelised Production Cost [€/kW-hr]

C – Investment costs [€]

AEY – annual energy yield [kW-hr/year]

$C_{O\&M,y}$ – annual operation and maintenance cost [€]

a_n – annuity factor defined by $a_n = \frac{1 - \left(\frac{1}{1+r}\right)^{T'}}{r}$

r – Real interest rate

T' – Economic lifetime of the wind farm [years]

Annuity factor was fixed considering a real interest rate of 5% and a 20 year economic lifetime for the wind turbine. Interest accumulated during the construction period was ignored. So annuity factor was calculated as 12.4.

The AEY will be calculated from the wind distribution at site and the power curve of the designed turbine. For the AEY calculation mechanical and electrical losses are neglected. For the cost estimation of the turbine components the following procedure was adopted: First the cost breakup and mass breakup up of the components of a typical 5MW turbine was obtained using a cost and scaling model. From these two parameters the cost per unit mass of each component was derived. Cost for turbine maintenance was obtained per turbine. Cost for turbine installation was obtained per unit time. This was the primary objective of this chapter. The chapters following this will deal with rotor, support structure design and installation procedures of the two-bladed and three-bladed concepts. From these chapters the masses (or time, depending on the case) of the rotor, support structure and other elements will be obtained and upon multiplying this with the cost per unit mass (or cost/unit time) obtained, the cost of each element can be found. Cost differences between the concepts in maintenance aspects will be derived from a concept study on maintenance aspects of large-scale offshore wind farms (van Bussel and Zaaier, 2001). Differences in the duration of installation will be derived from present day installation data available. With this, the total investment cost and annual O&M cost can be obtained and fed into Equation 5.1 to obtain the LPC.

5.2 Cost and Scaling Model

The component cost and mass break up developed for this project was based largely on the NREL cost model (Fingersh, et al, 2006). The NREL model is based on a 50 MW onshore wind farm. The baseline turbine used is a land-based, three-bladed, upwind, pitch controlled, active yaw, variable speed wind turbine with a rating of 1.5 MW. The tower is tubular and made of steel.

To model the offshore wind farm most of the components within the (offshore) turbine have been modeled in the same way as for the land based turbine except for a cost increase of 13.5% on all components (Fingersh, et al, 2006). This is the marinization component which factors in the special paints and coatings needed to increase the survivability of turbine components in a marine environment. The NREL offshore cost model is based on a 500 MW wind farm using one hundred and sixty seven 3MW wind turbines with an array spacing of 7D by 7D, where D is the rotor diameter. The NREL offshore wind farm is situated 8 kilometers from shore in a water depth of 10m. The NREL cost and scaling models for the support structure, offshore electrical network and installation have been modified to suit these conditions. NREL states that these models are very rough and research into newer models are underway and will be presented when ready.

5.2.1 Suitability of the NREL model for the selected wind farm

From the information presented above it is evident that for NREL's cost model to be used in a suitably accurate manner, the size of the wind farm chosen for this report must closely match the size of the NREL offshore wind farm.

The NREL cost model gives the cost of the components of the wind turbine and turbine installation as a function of the rotor diameter or the turbine rating. The operation and maintenance costs were given as a function of the annual energy yield (AEY). While the model serves well for the costs of the components of the wind turbine itself, it may not serve well to determine the installation costs, the offshore operation and maintenance costs and the power collection costs for wind farm parameters other than what was specified for the NREL model. This is because the installation, operation and maintenance and the power collection costs are more sensitive to the number of turbines in the wind farm than to the turbine rating or rotor diameter or AEY. Therefore it is important to ensure that the chosen size of the wind farm does not affect these above mentioned parameters.

5.2.2 Cost of Offshore Electrical Network

The Offshore Electrical Network as stated earlier is composed of power collection and power transmission. The cost for this component depends on wind farm layout, distance from shore, the number of turbines and the rating of the turbine. Because a large amount of power is being transmitted over a distance of 70km (wind farm to shore), an offshore transformer station was used.

The NREL model calculates the cost of power collection (mostly the electrical undersea cables) and then divided it among the 167 turbines so that each turbine's contribution to the power collection costs can be estimated. The offshore transformer station costs and power transmission costs are also split between the 167 turbines. This results in a scaling factor (a number, essentially) which can be multiplied by (one) turbine's rating to get its (the turbine's) share of the offshore electrical network costs. However this scaling factor is heavily dependent on NREL specified farm parameters i.e. a distance of 8km from shore and an array spacing of 7D. Therefore, a new scaling factor needs to be obtained for use in this project.

From Figure 5-1 it is seen that the electrical offshore network cost varies in a linear fashion as distance to shore changes if the number of turbines and the turbine rating is kept constant (the cost depicted in the figure is not as important as the trend of the cost line).

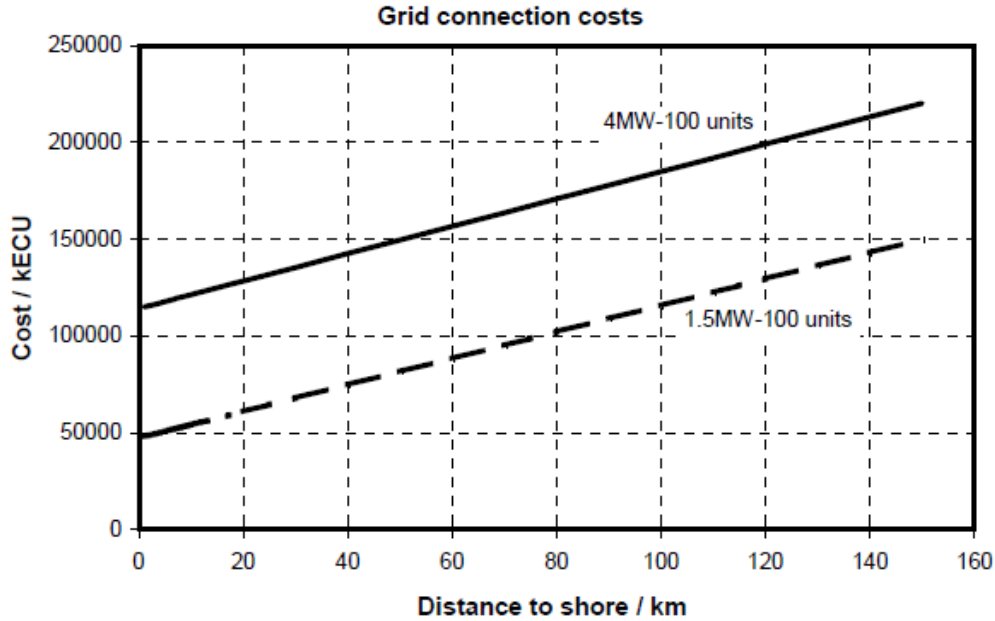


Figure 5-1: Offshore grid connection cost as a function of the distance to shore and the turbine rating (Cockerill et al, 1997)

Since the NREL model is designed for a 500 MW wind farm (i.e. the same amount of power that the wind farms in this report will be producing) the costs of the offshore substation is assumed to be suitably captured by the NREL scaling constant. Additionally, because of the identical total power output it is assumed that the change in the number of turbines do not play a role in the new scaling factor. The array spacing is a function of the rotor diameter and its effect is therefore captured by the existing NREL model. This leads to the conclusion that the cost increase will be primarily due to the power transmission costs from the offshore substation at the wind farm to shore. Based on these assumptions Figure 5-2 (below) was constructed and shows the cost of the Offshore Electrical Network at the site chosen for this report (70km from shore). The method used to construct the figure is as follows:

- The offshore electrical network costs of a one hundred 5MW turbines at a site 8km from the shore (distance of NREL farm) was obtained using the NREL model.
- The slope of the line was obtained from Figure 5-1.
- The above two parameters was put into the equation of a line to obtain the intercept.
- Thus a line equation with x and y as unknowns was obtained.
- This equation was again solved for a distance of 70km from shore to obtain the offshore electrical network costs for the site used in this report.

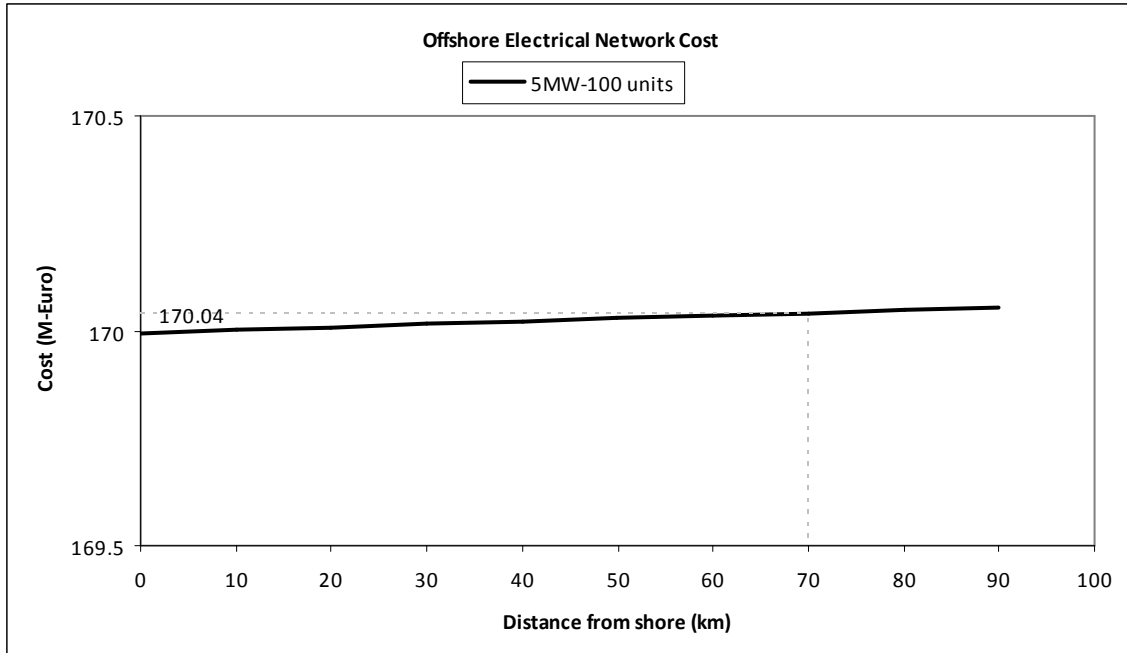


Figure 5-2: Offshore electrical network cost for the wind farm

5.2.3 Cost of Turbine components per unit mass

From the NREL model the cost and mass breakdowns of each component and the cost of the systems and procedures were obtained. Most scaling relationships were derived in terms of the rotor diameter (which in this report is fixed at 126m) and turbine rating (5MW). For the actual scaling relationships refer to the NREL cost and scaling model (Fingerish et al, 2006).

From the model the investment cost was found to be 1754 €/kW. The contribution of each component/procedure to the investment cost was obtained. See column 2 and 3 of Table 5-1. Then, the mass contribution per kW was calculated. See column 4 and 5 of Table 5-1. The masses were obtained from the NREL model. From column 3 and column 5 the cost contribution per unit mass was calculated. See column 6.

Table 5-1: Cost per kg of each component/procedure per turbine

Cost	Euro (million)	Euro/kW	kg	kg/kW	Euro/kg
Blades (three-blades)	0.95	188.3	71629.2	14.3	13.2
Rigid Hub	0.16	31.3	30213.4	6	5.2
Teetering Hub					9.4
Pitch mechanism & bearings (three-blades)	0.24	47.5	13526	2.7	17.6
Gearbox (3-stage planetary spur)	0.89	177.3	37998.6	7.6	23.3
Generator (high speed generator)	0.42	84.0	16690.3	3.3	25.5
Yaw drive & bearing	0.15	29.5	13152	2.6	11.3
Nacelle	1.65	328.9	166790.6	33.4	9.8
Support Structure	1.95	387.9	1000000	200	1.9
Installation (three-bladed)	0.65	129.3	-	-	-
Offshore Electrical Network	1.70	340	-	-	-
Total	8.80	1754	-	-	-

The following should be kept in mind while assimilating the information presented:

- The 'baseline' blade scaling relations (for mass and cost) were used from the NREL model as no carbon was used for the blade. The blade was assumed to be manufactured entirely of glass fiber.
- The current version of the NREL model is dated December 2006 and this is what was used in the cost analysis of this report. Most of the information presented in the NREL model was based on the RE Power 5MW turbine. The NREL turbine had a tower top mass of approximately 350 tons. The components shown in Table 5-1 (except for the rotor) do not represent the entire mass at the tower top but only the components for which information could be found (and that are relevant for this report). For calculation purposes a tower top mass of 350 tons was treated as the baseline. From the NREL cost model a tower top mass of 290 tons was obtained. So to obtain the baseline tower top mass, 60 tons was added to the nacelle mass. This mass difference arises because masses of certain components (e.g. transformer) were not accounted for.
- The hub in the NREL cost model is a rigid hub. Since a teetering hub is used for the two-bladed turbine its cost was obtained from the WindPACT Turbine Rotor Design study (Malcolm and Hansen, 2002). The WindPACT report states that the teetering hub weighs slightly less than the three-bladed rigid hub, but in this report the mass of the teetering hub was assumed to be equal to that of the three-bladed rigid hub. The difference in cost per kg between the two-hubs was a factor 1.8 which is what is seen in Table 5-1.

While it was important to obtain realistic values of the costs of different components, the focus in the report was on the difference in these costs for the different concepts. The cost/kg for all the components shown in the previous section can be used to

determine the investment cost for the two-bladed and three-bladed turbines. However, cost of procedures like installation and O&M may not be suitably captured as the number of blades on the turbine changes. Therefore these two procedures are examined separately in the next two sections to see if the change in concept produces a change in cost and if this is found to be the case a suitable method to accurately capture their contribution to the LPC will be determined.

5.2.4 Cost of Installation

Installation costs will depend on the hub height (which is a function of the rotor diameter) and the number of turbines in the farm. The NREL model for installation captures the cost as a function of the turbine rating. This implies that rotor diameter and thus hub height are factored into the installation costs. It may be argued that as the hub height increases, the cost of installation changes drastically and therefore may not be accurately represented by the NREL model. See Figure 5-3. From this figure, it can be seen that as the hub height goes above 85m there is a step change in the day rate. It should be noted that this figure uses data that was available before 2001. At that time specialized turbine installation vessels did not exist. So, this data most likely consisted of the day rates of different vessels each of which possessed a hoisting crane.

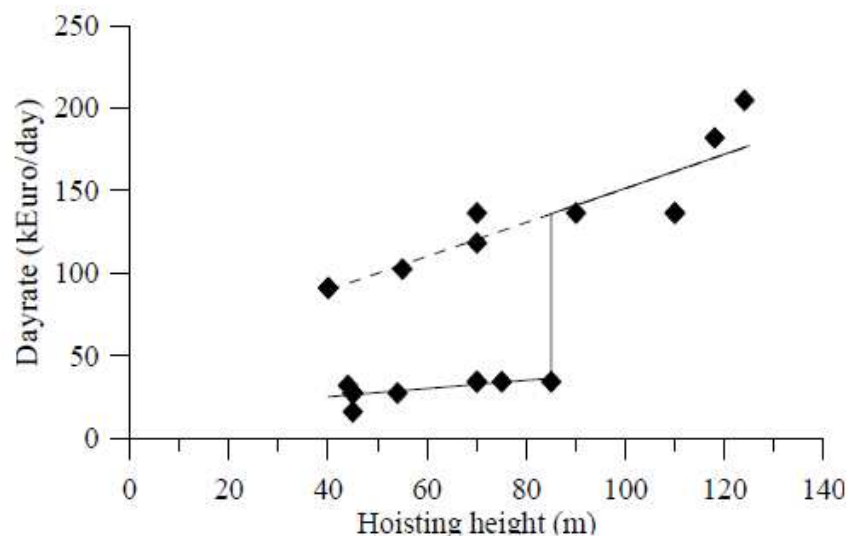


Figure 5-3: Installation cost as a function of hoisting height (Source: G.J.W. van Bussel and Zaaier, 2001)

Driven by need, specialized turbine installation vessels appeared after 2001. These vessels (Sea Energy, Sea Power) were used extensively to install offshore turbines with a rating of 2 to 3 MW. Although they are capable of lifting up to 400 tons they have a limited hoisting height. The main boom lengths of these cranes are around 60-70m (www.a2sea.com, 2010). Innovative solutions like that employed for the Thornton Bank wind farm can be used to overcome this. Here a tower was installed on a barge (the Buzzard) and the hoisting crane was installed atop the tower. With this modification, the required hub height was reached without using a more expensive installation vessel.



Figure 5-4: Turbine installation at the Thornton Bank wind farm using the modified Buzzard

From this, it will be assumed that the NREL model suitably captures the cost associated with the increase in hoisting height i.e. no step change in day rates will be accounted for. The installation costs are also a function of the number of turbines. See Figure 5-5 below shows that higher the number of turbines to be installed, lower will be the installation cost. (Again, the cost depicted in the figure is not as important as the trend of the cost line). As seen from the figure the installation costs decreases with increase in number of wind turbines and levels off after a certain number of wind turbines have been installed. There is no drastic cost decrease as the number of installed turbines increases from 100 to 300.

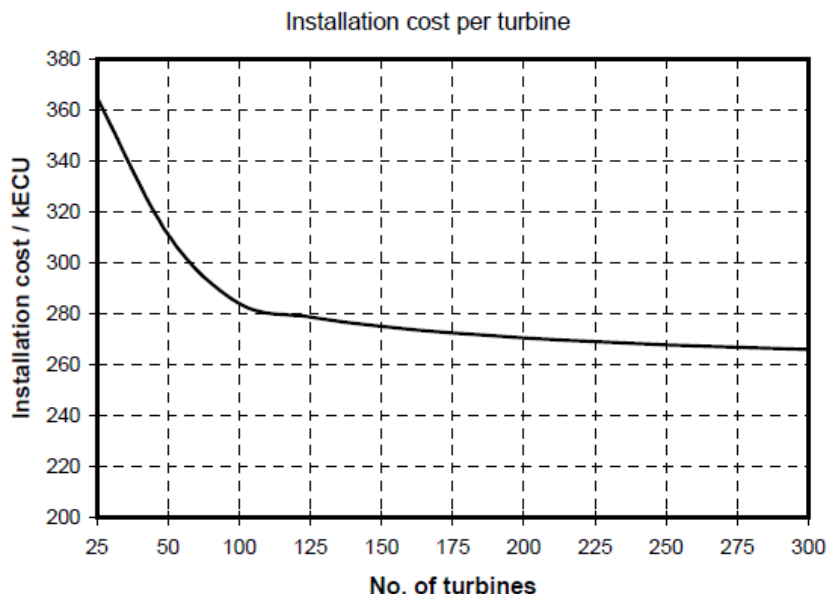


Figure 5-5: Installation cost as a function of the number of wind turbines (Cockerill et al, 1997)

Therefore it would be safe to estimate that the cost of installation/per turbine (obtained from the NREL model) in a wind farm of one hundred and sixty seven 3MW turbines (the NREL wind farm) is not significantly different from cost of installation/per turbine in a wind farm of one hundred 5MW turbines.

From this it was decided that the NREL cost model for the installation did not have to be modified to apply it for the wind farms in this report. The NREL cost model gives the installation cost of a three-bladed 5MW reference turbine and thus cannot be used to differentiate between the two-bladed and three-bladed concept. So, it was decided to obtain the installation cost of the turbine per hour, since it is expected that the installation time of each concept is different.

From the NREL cost model the installation cost of one 5MW turbine is €646500 (from Table 5-1). To determine the difference in installation costs between the three-bladed and two-bladed turbine, the following procedure was used. First the total time required to install a 5MW offshore three-bladed turbine will be obtained from literature. The installation cost of €646500 will be divided by this time to get the turbine installation cost per hour. Next the installation time-split of a 5MW three-bladed and a 5MW two-bladed offshore turbine will be determined from available sources. This quantity will be multiplied by the turbine installation cost per hour to obtain the installation costs of both concepts. See Table 5-2.

Table 5-2: Installation costs

Turbine Installation cost per hour	A <i>(€ 646500/hours required to install 5MW 3-bladed turbine)</i>	€/hour
Turbine	Installation time (hours)	Installation cost (€)
100 Three-bladed turbines	B <i>(From available sources)</i>	A X B
100 Two-bladed turbine	C <i>(From available sources)</i>	A X C

This method assumes that the same equipment is used to install both concepts and that the weather conditions at site do not change during the installation of all the turbines in the farm. See Chapter 8 for the final costs obtained.

5.2.5 Cost of Operation and Maintenance

The NREL cost model (and most other literature available) estimates the operation and maintenance costs per turbine as a function of its annual energy yield. NREL indicates that the model is rudimentary and that actual O&M costs can vary between different wind farms employing the same wind turbine based on different factors such as wind farm size, tower height, etc (Fingersh, et al, 2006). So, for this report it was decided to obtain actual O&M costs from a DOWEC O&M study (Zaaijer, 2003). From this study, the

'improved baseline' offshore wind farm was used. It consists of 80 three-bladed wind turbines of 6MW rating at a distance of 50km from shore. The maintenance crew is permanently stationed on the offshore transformer platform. The availability of the wind farm is 97% and the O&M cost for the entire wind farm is 14.4 million Euro per year. Dividing this by the number of turbines yields 0.18 million Euro per turbine per year. The contributions to the annual O&M cost per turbine are shown in Figure 5-6.

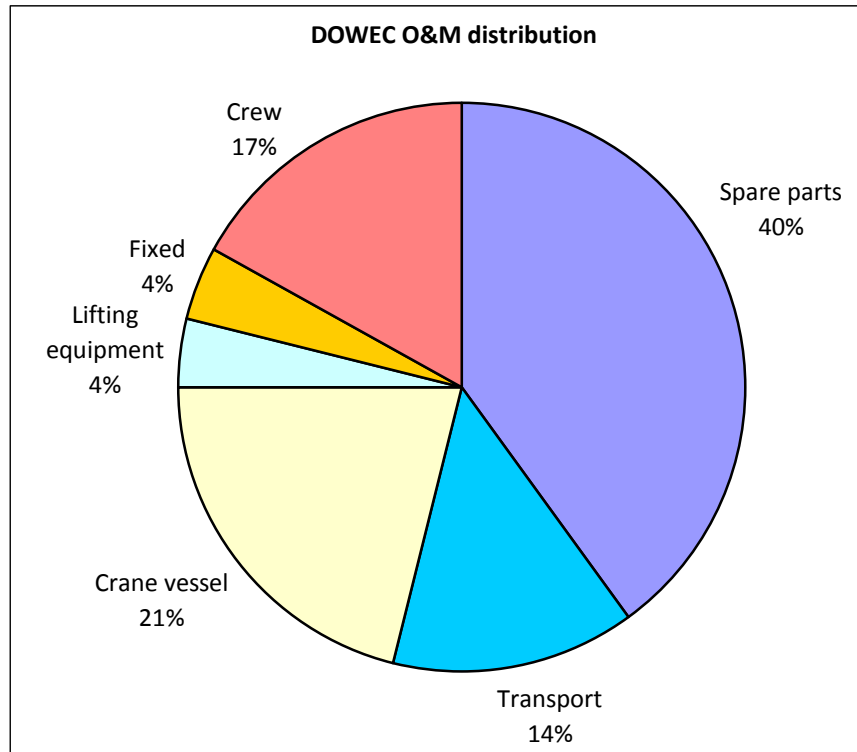


Figure 5-6: Annual O&M cost breakdown per turbine

The DOWEC turbine has a rating of 6MW but the turbines used in this wind farm have a rating of 5MW. It will be assumed that this difference in turbine rating does not change the O&M cost. In the figure, 'Fixed' refers to the cost incurred for permanent occupation of a monitoring station. 'Transport' refers to the transport of the repair crew from their accommodation on the transformer platform to the turbine that needs maintenance. 'Lifting equipment' refers to the cranes present in the wind farm. The other terms are self explanatory. From this, it can be inferred that almost all elements in the figure retain the same percentage of costs per wind turbine (when comparing the DOWEC wind farm with the wind farm of this report). The only elements that may not retain their percentage of costs per turbine are the crane vessel, because it needs to come from the harbour for any heavy lift maintenance activity and the cost of spare parts which scales with the turbine cost.

In the case of the wind farm in this report the crane vessel has to travel 70km rather than the 50km specified in the DOWEC study. Because the bulk of this cost is associated with the time taken for the hoisting and repair/replacement operation, this report

assumes that the cost associated with the extra 20km that the crane vessel needs to travel can be neglected. At this point in the report, it will also be assumed that the cost of spare parts of the two-bladed turbine and the three-bladed turbine will be the same. The results of the calculation of the investment costs of the turbines will determine if this assumption is valid or not.

Thus the cost of O&M was obtained as 0.18 million Euro per turbine per year X 100 turbines = 18 million Euro for the wind farm per year. From the above assumptions it follows that this cost applies to both concepts.

It can also be noted that there was no effort taken to weigh the advantages and disadvantages of this particular maintenance strategy i.e. repair crew being accommodated on the transformer platform. This strategy was simply applied to the wind farms employing both turbine concepts because, as stated earlier, this report only seeks to differentiate between two concepts.

Data for component failures was taken from G.J.W. van Bussel and Zaaier, 2001. This paper was a study on relative reductions of failures of different turbine components with emphasis on future offshore wind turbines. The data was based on land based three-bladed wind turbines that experienced coastal wind conditions which was the most useful data available at the time. Determining the actual failure frequencies of the components of the two-bladed and three-bladed turbine was not in the scope of this report. Therefore the failure frequencies of the components of the two-bladed and three-bladed turbine were extrapolated from the data and are presented below in Table 5-3.

Table 5-3: Failure frequencies of the two-bladed and three-bladed turbine

Component	Offshore Failure frequency (failures/year)	
	3-Bladed	2-Bladed
Shaft and Bearings	0.02	0.02
Brake	0.05	0.05
Generator	0.05	0.05
Parking Brake	0.05	0.05
Electric	0.1	0.1
Blade	0.11	0.07
Yaw System	0.15	0.15
Pitch Mechanism	0.14	0.09
Gearbox	0.15	0.15
Inverter	0.16	0.16
Control	0.17	0.17
Total	1.15	1.06

From the table it can be seen that the number of failures per year for the two-bladed turbine are lesser. But the teetering hubs failures of the two-bladed turbine are not seen in this table. From the same study, the yearly cumulative failure frequencies of the

different concepts studied are reproduced below in Figure 5-7. Out of all the concepts shown, the robust turbine and the stall teeter turbine are two-bladed turbines.

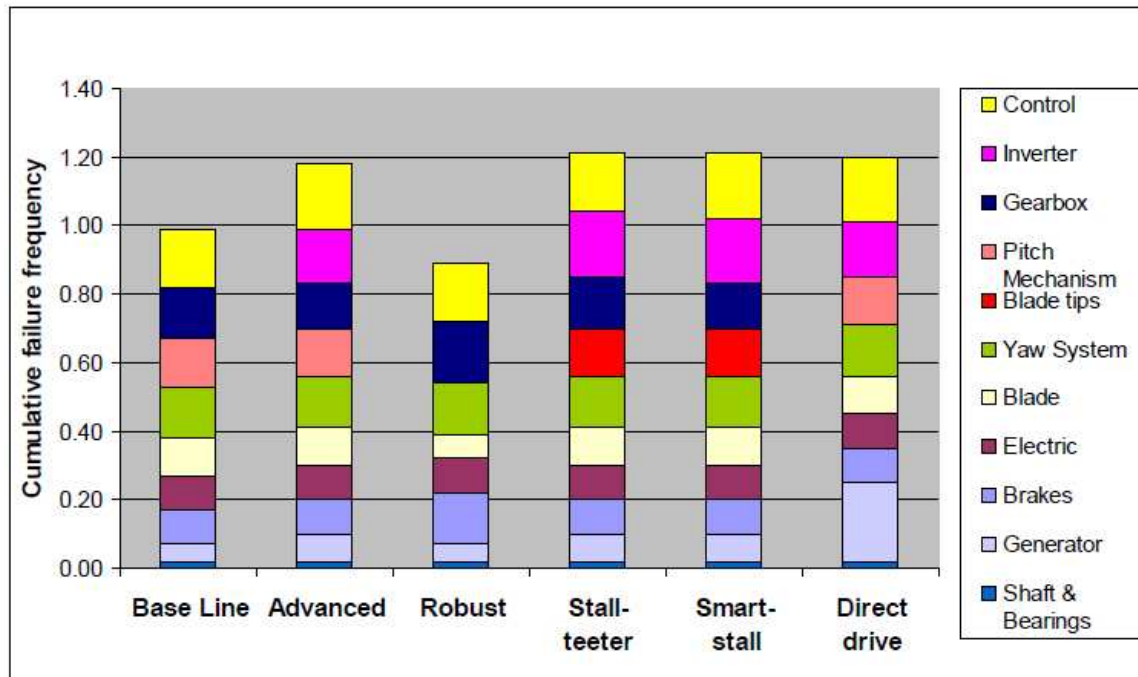


Figure 5-7: Yearly cumulative failure frequencies (Source: van Bussel and Zaaier, 2001)

On visual inspection of the contributions of blade failures, it can be noted that the blade failures of the stall teeter concept are more or less equal to the blade failures of the baseline concept. From this it was concluded that failures in the teetering hub were incorporated into blade failure and that the blade failure rates of the three-bladed turbine are equal to the blade + hub failure rates of the two-bladed turbine.

From this information, the only conceivable advantage (in terms of maintenance) of the two-bladed concept is the lower pitch mechanism failures. This small difference lead to one extra pitch mechanism failure for the three-bladed turbine when compared with the two-bladed turbine (over the course of 20 years). Thus, it was decided to keep the availability of both turbines the same which is a reasonable assumption. This means that both turbines are affected by failure equally and both turbines function for the same amount of time for their whole lifetimes.

5.3 Final Note

The information in this cost model was obtained from various sources. As such, the numbers presented in this model may not accurately match industry figures. However, for this report the numbers and figures obtained were sufficient as this thesis only seeks to demonstrate the differences in the LPC between a 5MW two-bladed and a 5MW three-bladed turbine.

In this chapter only the annual maintenance cost and the electrical offshore network cost was fixed. All remaining quantities were determined as a function of the mass or, in the case of Installation, as a function of time required for installation.

6 Design Tip Speed Ratio

This chapter discusses the choice of the design tip speed ratio (λ_{design}). The relation between power coefficient and λ_{design} , and blade geometry and λ_{design} is briefly discussed. Although λ_{design} has a bearing on the machine cost, the primary basis of its selection was aerodynamic performance. The choice of λ_{design} plays a role in certain other factors (like support structure, gearbox, etc). This chapter concludes with the finally chosen λ_{design} value along with some λ_{design} values of present day offshore wind turbines.

6.1 Definition

The tip speed ratio (λ) is defined as the ratio of the tangential velocity of the blade tip to the speed of the wind. See Equation 6.1.

$$\lambda = \frac{\Omega \cdot R_{\text{tip}}}{U_o} \quad \text{Equation 6.1}$$

U_o – Wind speed [m/s]

Ω – Rotor rotational speed [rad/s]

R_{tip} – Distance of the blade tip from the hub [m]

The design tip speed ratio in this report is defined as the λ at which the blade twist and chord were designed.

6.2 Influence of Design tip speed ratio on certain parameters

This section discusses the influences λ_{design} has on parameters such as power coefficient, blade geometry, aerodynamics, support structure, gearbox and some practical aspects like aerodynamic noise, pile driving and blade erosion.

6.2.1 Blade Geometry and Design tip speed ratio

An important consequence of the choice of λ_{design} is the effect it has on the rotor blade geometry. To estimate the rotor geometry the blade element theory or strip theory is commonly used. The swept area of the rotor is divided into annuli and it is assumed that these annuli do not influence each other. Each blade element is formed with the chord of the airfoil section at each annulus and the width of the annulus. Figure 6-1 shows the cross section of an airfoil with the different angles and the vectors involved.

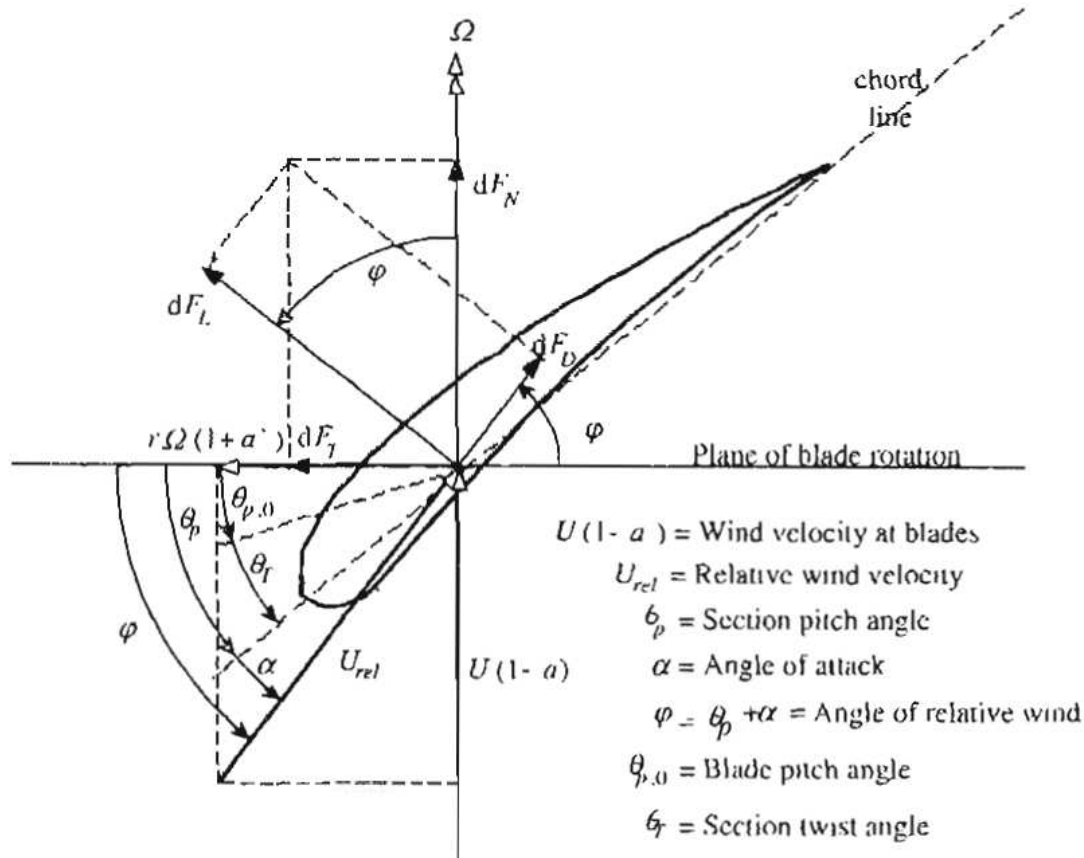


Figure 6-1: Airfoil geometry with forces acting on it (Manwell et al, 2006)

Definition of terms (besides those already defined in Figure 6-1)

dF_N – Axial (thrust) force per blade element moment [N]

dF_L – Lift force per blade element [N]

dF_D – Drag force per blade element [N]

dF_T – Tangential force per blade element [N]

r – Distance of the airfoil section from the hub [m]

c – Chord of the blade element [m]

dr – Width of the blade element /annulus (perpendicular to the plane of the paper) [m]

a – Axial induction factor

a' – Tangential induction factor

Using the λ_{design} in the momentum theory the axial and tangential velocity for the different axial and tangential induction factors can be estimated. Based on this, the section inflow angle (φ) can be calculated. See Equation 6.2 and Equation 6.3. The optimal angle of attack (α) can be fixed based on the C_l of the airfoil corresponding to $(C_l/C_d)_{max}$ (C_l is the lift coefficient and C_d is the drag coefficient). This leads to the calculation of the section twist angle (θ_T) and the section pitch angle (θ_p). The section chord can also be obtained using a mathematical formula. See Equation 6.4. These

equations are simplified forms but are quite sufficient to obtain first order blade geometry.

$$\lambda_r = \frac{r}{R_{tip}} \lambda \quad \text{Equation 6.2}$$

$$\phi = \tan^{-1} \left((1-a) \cdot \frac{1}{\lambda_r} \right) \quad \text{Equation 6.3}$$

$$c = \frac{8\pi r}{BC_{l,design}} (\sin \phi \tan \phi) \frac{a}{1-a} \quad \text{Equation 6.4}$$

λ_r – Section speed ratio

c – Chord of the section [m]

r – Distance of the airfoil section from the hub [m]

ϕ – Section inflow angle [rad]

B – Number of blades

$C_{l,design}$ – Chosen Lift coefficient of the airfoil.

Equation 6.3 and Equation 6.4 is for the situation without wake rotation. From this the relation between the section chord, λ_{design} and number of blades can be seen. The combination of the momentum theory and the blade element theory is referred to as the Blade Element Momentum theory (BEM).

6.2.2 Power Coefficient and Design tip speed ratio

The power coefficient (C_p) of the rotor is a function of λ_{design} . C_p is defined as the ratio of the amount of power extracted by the rotor to the amount of power available in the wind. The maximum power that can be theoretically obtained corresponds to the Betz limit, and that corresponds to a power coefficient of approximately 0.6. The C_p - λ_{design} curves of turbines with 3, 2 and 1 blade(s) can be seen in Figure 6-2. It shows the Betz limit and the reasons why this theoretical C_p cannot be reached in reality. These losses are discussed in the following section. Another piece of information that the figure gives is the relation between λ_{design} and the number of blades on the turbine for a certain C_p . From this it can be seen that choice of λ_{design} has a direct bearing on the power extraction capabilities of the two-bladed and the three-bladed rotor.

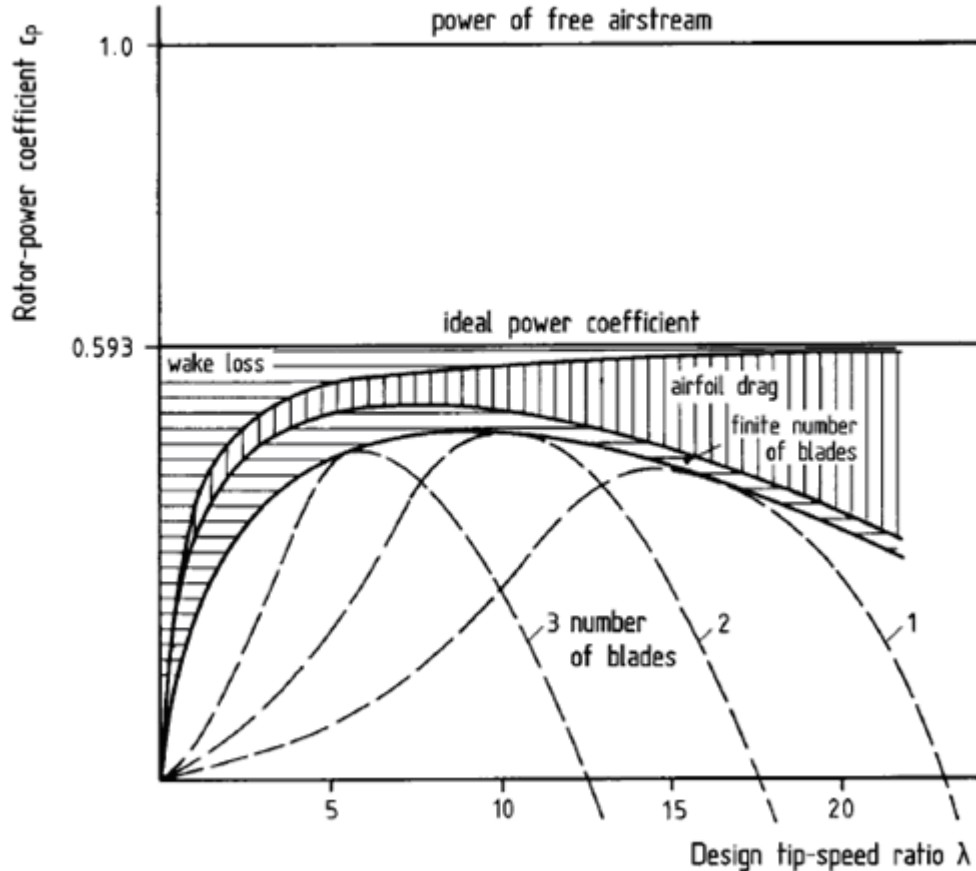


Figure 6-2: Power coefficient Vs λ_{design} for 3, 2 and 1 blade(s) (Hau, 2006)

6.2.3 Aerodynamic considerations stemming from Design tip speed ratio

It is apparent that λ_{design} can be set as an independent variable based on which a number of blade designs can be obtained and analyzed. However, incorporating this in tandem with treating the axial induction factor as an independent variable is beyond the scope of this report. So, λ_{design} was chosen, based primarily on obtaining the highest C_p .

As the concept changes (number of blades and λ_{design}) the rotor power coefficient will also change. The discussion on difference in aerodynamic performance between the two-bladed and three-bladed rotors was taken from Snel which is based on classical blade element momentum theory (Snel, N.D). Three aerodynamic loss mechanisms can be identified:

- Losses due to profile drag
- Losses due to non-uniformity of induction in the rotor plane
- Losses due to wake swirl

These losses prevent the rotor from attaining the Betz optimum power coefficient and are discussed below. They are all given in the form of a multiplier of $C_{p,\text{Betz}}$.

6.2.3.1 Losses due to profile drag

First the importance of the aerodynamic profile will be briefly explained. Depending on flow conditions at the airfoil and the loading on the airfoil there are a number of

requirements that an airfoil must satisfy before it can be selected. However these will not be dealt with here. In this section only the C_l/C_d ratio will be discussed. These are properties of the airfoil which depend on the airfoil profile. To obtain a high rotor power coefficient, α is chosen such that it corresponds to the point on the C_l - α curve where C_l/C_d ratio is the highest. Figure 6-3 shows the polars for Reynolds number corresponding to rated wind speed at the blade tip of the NREL 5MW reference turbine. The figure shows the C_l/C_d and C_l variation with α . In this case the maximum C_l/C_d ratio is 180. Further inboard, structural requirements dictate that airfoils with larger thicknesses are used. Inboard airfoils have a lower C_l/C_d ratio (approximately 70-80 near the blade root).

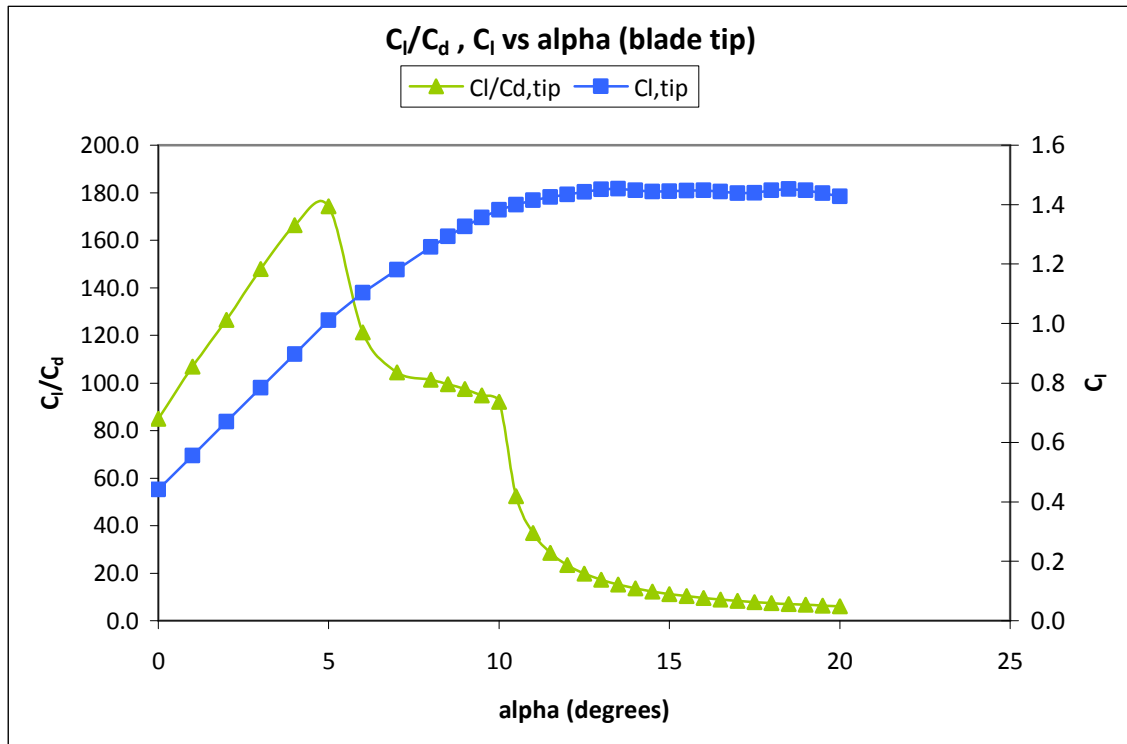


Figure 6-3: C_l/C_d and C_l polar's for a NACA 6464 airfoil used at the blade tip of the 5MW NREL reference turbine

C_l and C_d translate to lift force and drag force respectively and the influence of these on the rotor thrust force and torque developed can be seen in Equation 6.5 and Equation 6.6 respectively.

$$dF_N = B \frac{1}{2} \rho U_{rel}^2 (C_l \cos \varphi + C_d \sin \varphi) c \cdot dr \quad \text{Equation 6.5}$$

$$dQ = B \cdot r \cdot dF_T = B \frac{1}{2} \rho U_{rel}^2 (C_l \sin \varphi - C_d \cos \varphi) r \cdot c \cdot dr \quad \text{Equation 6.6}$$

dQ – Torque generated per blade element [N-m]

Integrating these equations over the rotor gives the total thrust on the rotor and torque generated by the rotor. The importance of minimizing C_d in these equations can easily be seen.

Now coming back to profile losses, Figure 6-4 can be used to show the influence of drag and the influence of the number of blades on C_p .

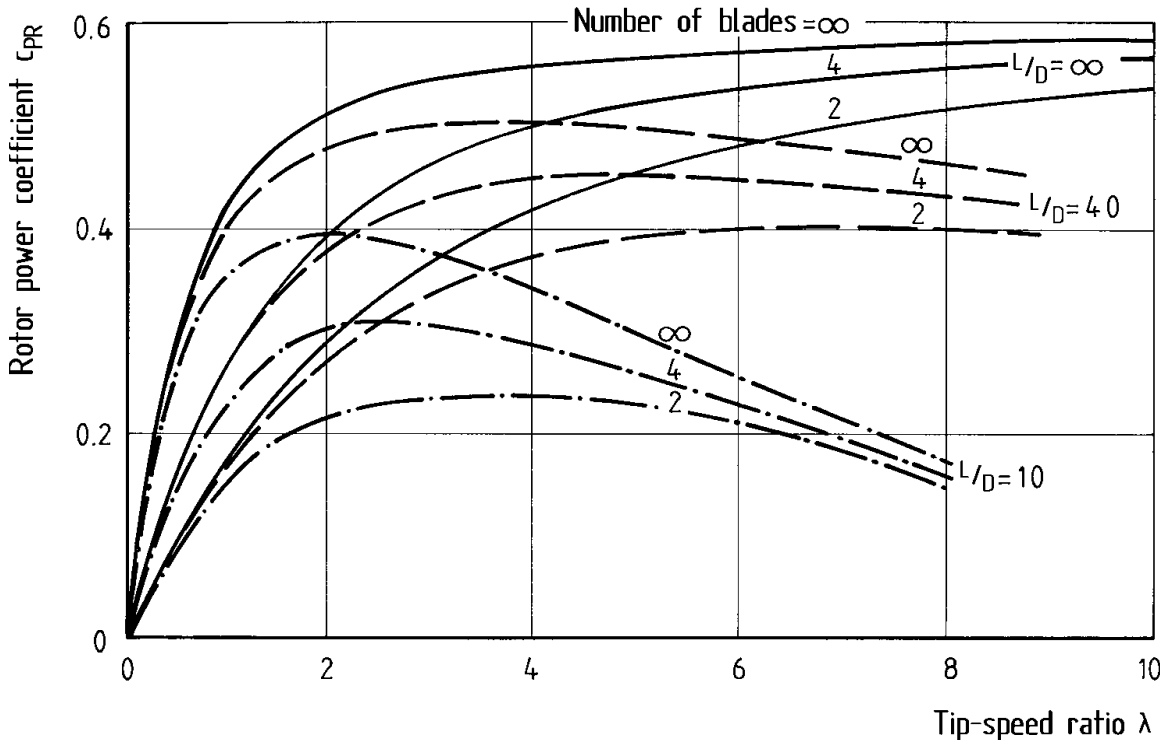


Figure 6-4: Influence of C_l/C_d and number of blades on C_p (Hau, 2006). [In the figure $L=C_l$ and $D=C_d$]

As the effect of increasing drag decreases the C_l/C_d ratio, C_p drops. This effect is more pronounced when the C_l/C_d ratio is between 10 and 40 (in the figure) while it is not so obvious for C_l/C_d ratios between 40 and infinity.

Thus, the losses due to profile drag of the airfoil translate to a loss in energy extraction which can be represented by Equation 6.7.

$$\text{Energy loss factor due to drag} = \lambda_{design} \cdot \frac{C_d}{C_l} \quad \text{Equation 6.7}$$

Snell, N.D.

6.2.3.2 Losses due non-uniformity of induction in the rotor plane

Axial induction factor is defined as the ratio of the reduced velocity at the rotor to the free stream velocity. See Equation 6.8.

$$a = \frac{U - U_r}{U} \quad \text{Equation 6.8}$$

U_r – Wind velocity at rotor [m/s]

U – Free stream wind velocity [m/s]

Using the momentum theory C_p can be reduced to: $C_p=4a(1-a)^2$. Finding the maxima of C_p yields the Betz limit i.e. $C_{p,Betz}\approx 0.593$ and this occurs when $a=1/3$. However, the momentum theory models the rotor as a disc (in other words: a rotor with infinite number of blades) and assumes that all the fluid elements in the plane of the disc interact with the disc, imparting its momentum to the disc. In reality, because of the finite number of blades on the rotor not all fluid elements interact equally with the disc. To model this loss, Prandtl's correction is generally used. Prandtl approximated the trailing vortices as discs which move with wake velocity. The free stream velocity meets the discs travelling with wake velocity at the disc edges. Fluid elements of the free stream weave in and out between successive discs. The wider apart the discs the deeper the fluid elements from the free stream penetrate, thus implying less uniform velocities for larger distances between the discs.

This loss factor for small values of the loss is approximated by Equation 6.9.

$$\text{Energy loss factor due to non uniformity of induction} = \frac{0.84}{B\lambda_{design}} \quad \text{Equation 6.9}$$

Snell, N.D.

The distance between the discs is proportional to $(1/B\lambda_{design})$. Thus, the losses decrease with increasing number of blades and increasing λ_{design} .

6.2.3.3 Losses due to wake swirl

Some researchers (Snell, N.D.) approximate that these losses can be ignored.

6.2.3.4 λ_{design} for highest aerodynamic efficiency

Using the information from sections 6.2.3.1, 6.2.3.2 and 6.2.3.3 the total loss factor is calculated as follows:

$$\text{Total loss factor} = \lambda_{design} \cdot \frac{C_d}{C_l} + \frac{0.84}{B\lambda_{design}} \quad \text{Equation 6.10}$$

For λ_{design} corresponding to highest aerodynamic efficiency these losses need to be minimized. Therefore minimizing Equation 6.10, λ_{design} is obtained as

$$\lambda_{design} = \sqrt{\frac{0.84}{B} \cdot \frac{C_l}{C_d}} \quad \text{Equation 6.11}$$

If C_l/C_d is assumed to be constant for both concepts, it can be seen from Equation 6.11, that the tip speed ratio of a two-bladed rotor is always 1.22 times higher than that of the three-bladed rotor.

6.2.4 Structural design considerations stemming from Design tip speed ratio

The economic considerations discussed here pertain to the support structure, the gearbox and the rotor blades.

6.2.4.1 Support Structure

The design of the support structure is based on its natural frequency. While designing the support structure it should be ensured that the natural frequency of the support structure does not lie in the 1-P region or the N-P region of the rotor (where N is the number of blades). The 1-P regions and the N-P regions are determined by rotor rotational speed and the number of blades. If the natural frequency of the support structure lies in these regions resonance will occur resulting in large fatigue damage. The 1-P and 3-P regions of the NREL three-bladed turbine at rated wind speed are shown below in Figure 6-5 with a wave spectrum included as well. Most support structures are designed so that they lie in the soft-stiff region. If λ_{design} increases (while U_0 remains the same), the rotor operating regions shift to the right.

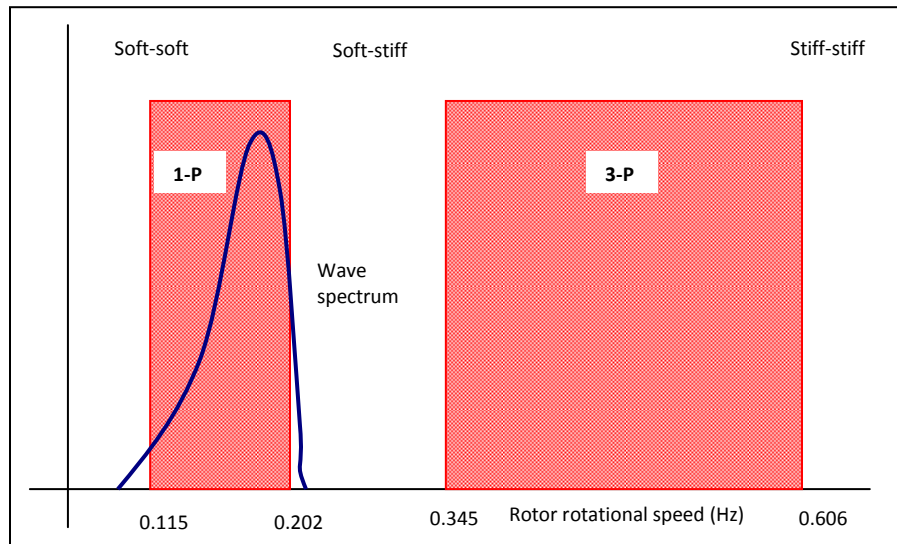


Figure 6-5: 1-P and 3-P regions with wave spectrum

Using a simple model the natural frequency of the support structure can be analyzed. See Figure 6-6, Equation 6.12 and Equation 6.13.

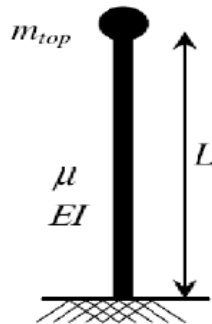


Figure 6-6: Simple model for the monopile

$$f_{nat} \cong \frac{3.04}{4\pi^2} \frac{E_{steel} I}{(M_{top} + 0.227 \mu L) L^3} \quad \text{Equation 6.12}$$

f_{nat} – Natural frequency of the support structure [Hz]

E_{steel} – Young's modulus (of steel) [N/m²]

M_{top} – Mass of the nacelle and rotor [kg]

μ – Mass per unit length of the monopile [kg/m]

L – Length of the monopile [m]

I – Moment of inertia of the monopile cross section [m⁴]

$$I = \frac{\pi}{64} (D_o^4 - D_i^4) \quad \text{Equation 6.13}$$

D_o – Outer diameter of the monopile [m]

D_i – Inner diameter of the monopile [m]

From this, it is evident that as λ_{design} increases, for the natural frequency of the support structure to remain in the soft-stiff region, the diameter of the support structure must increase. This means an increase in steel usage and therefore a higher cost.

6.2.4.2 Gearbox

Gearbox mass is expected to decrease as λ_{design} increases. This is due to two reasons. First, as λ_{design} increases, lesser torque is developed for the same power transmitted from the rotor to the generator. So, the gearbox is designed for this lesser torque and therefore lesser material is used. Secondly, as λ_{design} increases the overall transmission ratio of the gearbox decreases. This again implies lesser material usage. This lesser material usage translates to lower gearbox weight and lower tower top mass.

6.2.4.3 Rotor blades

A higher λ_{design} means more slender blades. This means lesser material usage and therefore lesser cost and lower rotor weight. An added advantage is that slender blades are generally more flexible and this property leads to 'shedding' of aerodynamic loads on the rotor. Therefore lesser loads are transferred to the drive train (Jamieson, 2009). However, a flexible blade is more likely to hit the tower. These effects, though, are not so easy to quantify at this stage.

6.2.5 Practical considerations stemming from Design tip speed ratio

The practical considerations discussed here pertain to aerodynamic noise, pile driving and blade erosion.

6.2.5.1 Aerodynamic Noise

The aerodynamic noise generated by the turbine is almost proportional to the fifth power of the tip speed (Burton, et al, 2001). Standards have been set up to govern wind turbine noise on land leading to a reduction of λ_{design} for land based turbines. Although it can be argued that aerodynamic noise does not affect the design of offshore turbines it

is quite probable that there is a limit on the noise generated. However, in this report this will not be considered as a limit on the design and thus will not be discussed further.

6.2.5.2 *Pile Driving*

In section 6.2.4.1, it was noted that as λ_{design} increases the diameter of the support structure increases. The widest pile that has been driven, to date, has a diameter of 5.2m (Menck, 2010). This was done using an adapter for existing hammers. Menck indicates that the 6m (diameter) barrier is being breached. With this in mind, it would be unwise to disqualify a higher λ_{design} simply because of the unavailability of pile driving equipment. Therefore on the same lines of aerodynamic noise generation, this will not be considered as a limit and will not be discussed further. It should be noted that a higher pile diameter leads to higher energy requirements for pile driving and perhaps will result in a higher installation cost.

6.2.5.3 *Blade Erosion*

Blade erosion is a problem for most turbines and this becomes pronounced at higher tip speeds. Factors responsible for erosion at an offshore site include frozen particles and liquid droplets (rain drops and salt spray). Blade erosion leads to a drop in the power coefficient besides leading to shorter blade life. While technologies exist for erosion protection, it was beyond the scope of this report to study the difference in erosion as λ changed and then translate that to a cost increase. Therefore blade erosion will also not be considered as a detriment to choosing λ_{design} .

6.2.6 Today's Offshore Turbines

The three major offshore wind turbines of 5MW range used presently are the REPower 5M turbine, the Bard 5.0 and the Areva M5000. Out of these the Bard 5.0 has a tip speed ratio of 8 which was the highest among the three (Bard-offshore, 2010). The Bard 5.0 also has the largest blade mass, 29.5 tons. The M5000 on the other hand has a blade mass of 16.5 tons and a tip speed ratio of about 6.5. The RePower 5M also has similar values for turbine blade mass and tip speed ratio. This mass increase of the Bard 5.0 may seem contrary to the fact that high λ_{design} leads to slender blades, but this is due to the difference in material used for the blades. REPower and Areva incorporate carbon fibres in their blades while the Bard turbine uses only GFRP (de Vries, 2007). Another fact about the Bard 5.0 was that a λ of 9 to 9.5 was avoided because this leads to reduced wear of the blade tips (GL Beaufort 6, 2008).

6.3 Summary of selection parameters for λ_{design}

From the preceding sections Table 6-1 was constructed. It indicates which factors were used and which factors were neglected.

Table 6-1: Summary of selection parameters of λ_{design}

Parameter	Primary Consideration	Secondary Consideration	Not Considered
Rotor Aerodynamic Efficiency	Yes	-	-
Support Structure	-	Yes	-
Gearbox	-	Yes	-
Rotor Blades	-	Yes	-
Aerodynamic Noise	-	-	Ignored
Pile Driving	-	-	Ignored
Blade Erosion	-	-	Important but was not quantified

6.4 Selection of λ_{design}

Based on the above information a value for λ_{design} was chosen. A wind speed of 11m/s was considered for the selection of λ_{design} .

- The natural frequency of the support structure cannot be allowed to go below 0.25 Hz because wave spectrums show that the energy of waves is highest below this frequency (See Figure 3-6). The 1-P region should then be lower than 0.25Hz. Assuming that the upper bound of the 1-P region is kept at 0.2Hz, this frequency corresponds to a λ_{design} of 7. From Figure 6-4 it can be seen that for C_l/C_d between 40 and infinity and for a finite number of blades, C_p change is minimal as λ_{design} changes between 3 and 7. This implies that there is no aerodynamic advantage in reducing λ_{design} below 7. Thus the lower limit of λ_{design} was fixed at 7.
- Next, a λ_{design} range of 7 to 12 was chosen and C_l/C_d values were obtained for an airfoil section which is located at a position corresponding to $r/R_{\text{tip}}=0.85$ using XFOIL. R_{tip} as stated in Chapter 2 is 61.5m. The DU180 airfoil was chosen because it represents the airfoil used at the outboard section of the blade. The polars obtained are shown below in Figure 6-7.
- Table 6-2 below shows the Reynolds numbers corresponding to λ_{design} . The polar indicates that as Reynolds number increases the design C_l/C_d ratio increases but after a Reynolds number of 14 million there is a drop in the design C_l/C_d ratio. This is the point where the prevailing effect of drag comes into play. From this it was concluded that choosing a λ_{design} greater than 10 (which corresponds to a Reynolds number of 14.5 million) leads to drag effects starting to cause a drop in the C_l/C_d ratio. So the upper limit of λ_{design} was fixed at 10.

Table 6-2: Reynolds numbers corresponding to λ_{design}

λ_{design}	Reynolds number
7	10.2 million
8	11.6 million
9	13.1 million

10	14.5 million
11	15.9 million
12	17.4 million

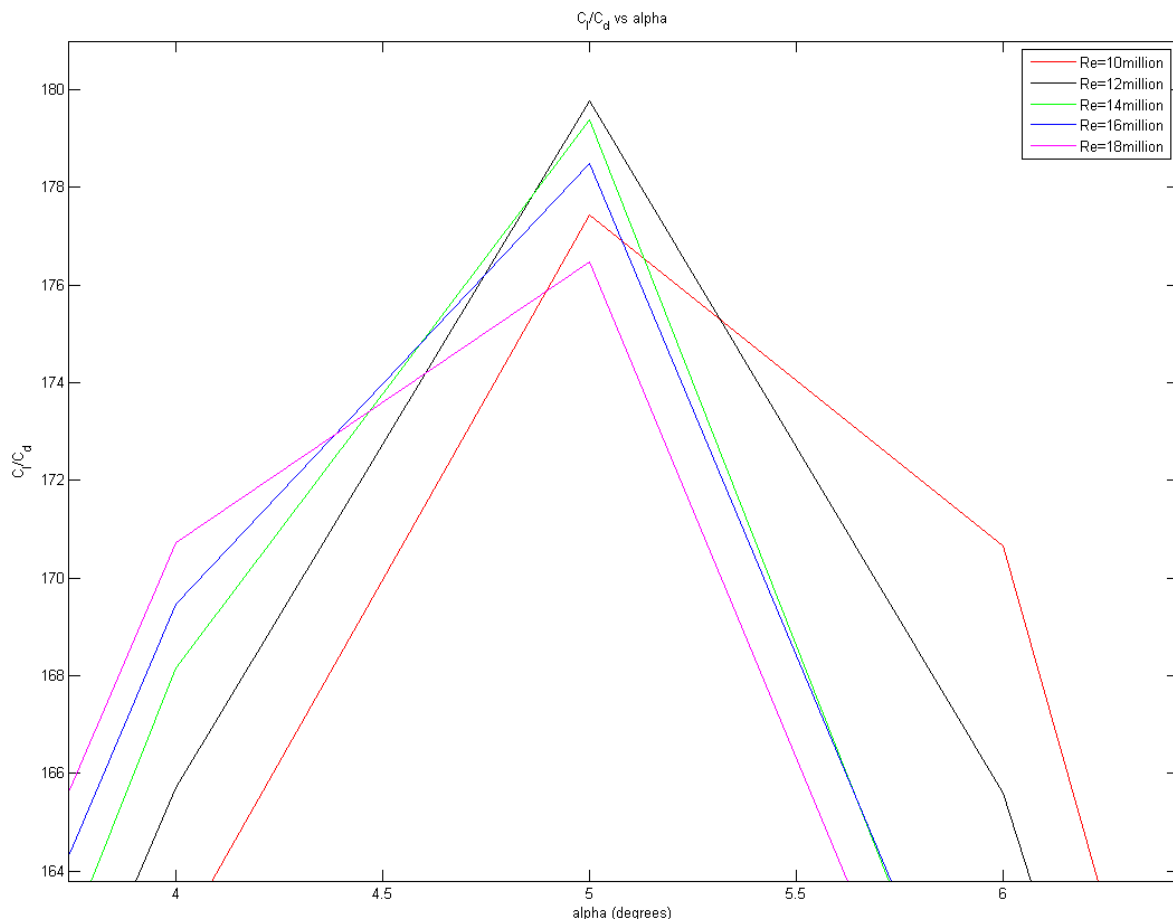
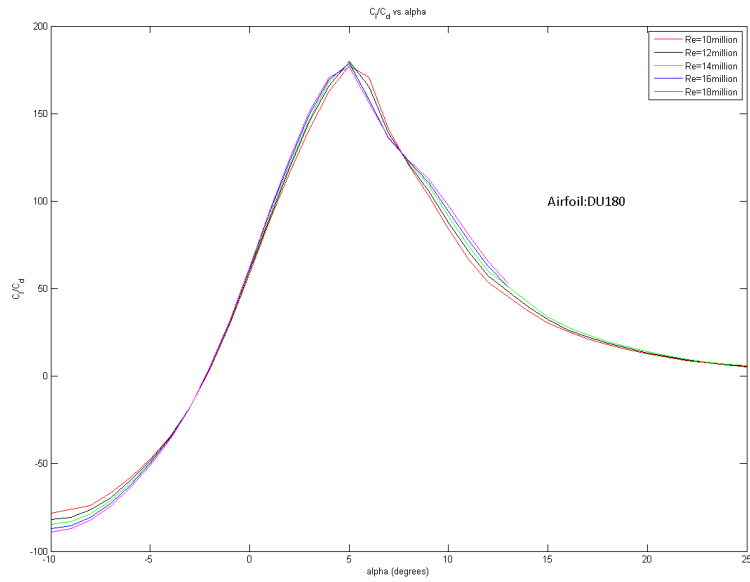


Figure 6-7: C_l/C_d of the DU-180 (Above) and Close up of the max C_l/C_d values (below)

- Now from Figure 6-7 it is observed that the highest C_l/C_d ratios are between 179 and 180. These correspond to Reynolds numbers between 12 million and 14 million and a Mach number of 0.24 (which occurs at the chosen airfoil section). This corresponds to a λ_{design} between 8.25 and 9.75. From this it is clear that the λ_{design} 's of both concepts must remain in this envelope.
- Using the knowledge that λ_{design} of the two-bladed concept must be 1.22 times higher than the three-bladed concept, λ_{design} of the two-bladed concept becomes 10.07 if λ_{design} of the three-bladed concept is set at 8.25. A λ_{design} of 10 corresponds to a Reynolds number of 14.5 million and since this lies outside the envelope, a λ_{design} of 9.8 was selected which yielded a Reynolds number of 14 million.
- These values were chosen because of the result of Equation 6.11. It is clear however that choosing a λ_{design} of 9.8 for the three-bladed concept is also perfectly feasible. The advantages of a higher λ_{design} for the three-bladed turbine would mean blades with lower chords and a lower transmission ratio for the gearbox implying cost savings. Therefore another case for the three-bladed turbine was chosen i.e. with a λ_{design} of 9.8.
- The finally chosen values for λ_{design} are shown in Table 6-3.

Table 6-3: Finally assigned λ_{design} to the 2-bladed and 3-bladed turbines

λ_{design}, 3-bladed	8.3
λ_{design}, 2-bladed	9.8
λ_{design}, 3-bladed (ii)	9.8

7 Component Design and Installation Procedure

7.1 Rotor Design

The initial step in rotor design is the selection of airfoils for different sections of the blades. XFOIL was used to determine the lift and drag coefficients of the airfoils chosen. Following this, the rotors of the two-bladed and three-bladed turbine were designed using the chord and twist equations from the previous chapter. For the analysis in this report, wake rotation was neglected. The blades thus obtained were analysed using a BEM code developed to obtain the thrust and torque which were used to calculate the power generated and the bending moments on the blades. The corrections used in the BEM theory are also outlined in this chapter. The internal structure of the airfoils was chosen based on literature available and materials were also chosen for the internal structure based on data available. The rotors designed were analysed for fatigue using Bladed 3.80.

7.1.1 Airfoil selection and properties

There are a large number of airfoils used for wind turbines. These are mainly from DUWIND (the Netherlands), NREL (USA) and Risø (Denmark). Analysing all airfoils, obtaining their C_l and C_d and coming to a conclusion as to which one was the best suited was not in the scope of this report. Therefore it was decided to base the selection of the airfoils on the NREL reference turbine (which in turn was based on the DOWEC). The relative span wise positions of the different airfoils on the blade were kept the same as that of the airfoils on the NREL blade. The DU airfoil co-ordinates (required for input to XFOIL) were available.

The distribution of the chosen airfoils is shown below in Table 7-1.

Table 7-1: Airfoil Distribution

Airfoil Distribution				
Blade section	Distance from hub (m)		Airfoil	Airfoil length along blade (m)
	From	To		
1	blade root	8.2	Cylinder	8.2
2	8.2	13.325	DU 00-W2-401	5.125
3	13.325	21.525	DU 00-W2-350	8.2
4	21.525	25.625	DU 97-W-300	4.1
5	25.625	33.825	DU 91-W2-250	8.2
6	33.825	42.025	DU 00-W-212	8.2
7 (i)	42.025	52.275	DU 95-W-180	10.25
7 (ii)	52.275	61.5		9.225

7.1.1.1 2D Airfoil aerodynamic properties

Using the NREL reference turbine the Reynolds number variation was obtained over the length of the blade. Figure 7-1 shows this variation for the NREL rotor rotating at 13.8 rpm (which corresponds to a λ_{design} of 8.3) at a wind speed of 11m/s. Similarly the Mach number variation across the length of the blade was calculated and plotted. See Figure 7-2.

These differences in Reynolds numbers and Mach numbers can be expected for the rotors designed for this thesis as well (Paul, 2010) and therefore the C_l 's and C_d 's along the blade length were obtained according to their performance at these Reynolds and Mach numbers. Strictly speaking, the Reynolds numbers would change as the chord of each section of each designed blade changed (as axial induction factor is varied). But for this project this effect on the change in the C_l 's and C_d 's was neglected.

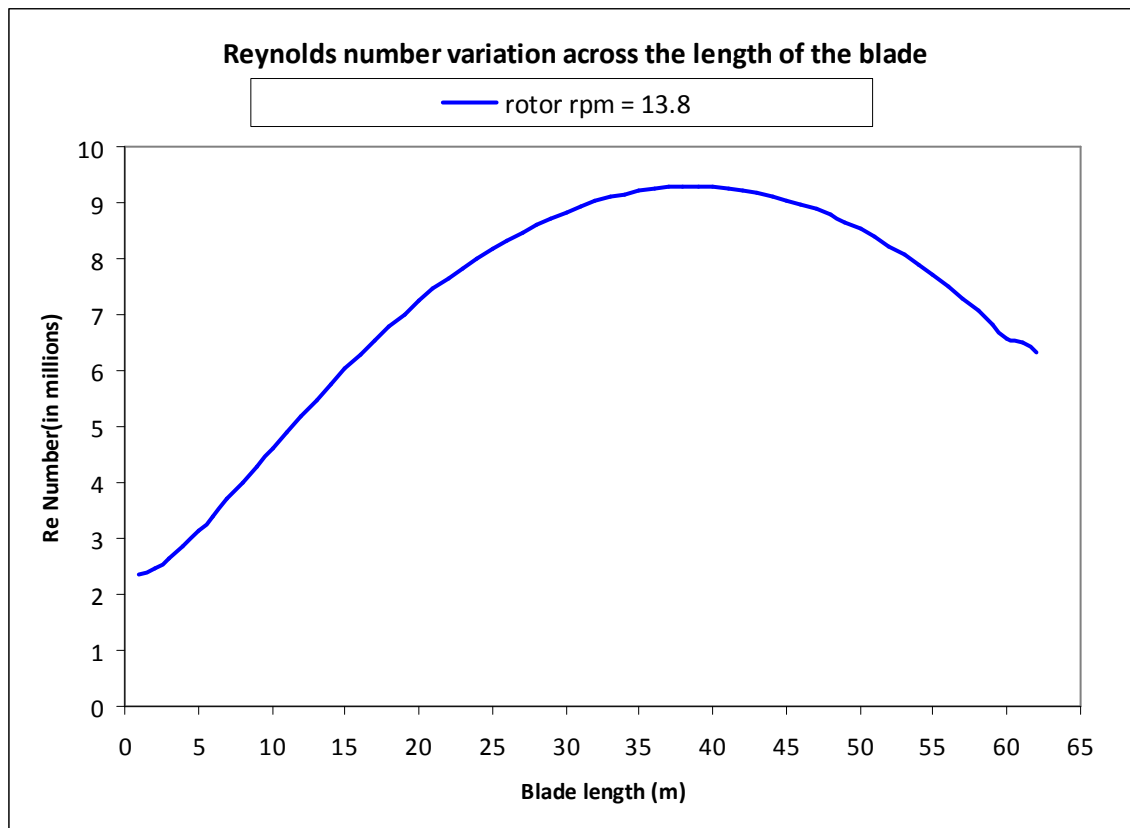


Figure 7-1: Reynolds number variation across the length of the blade. The NREL 5MW reference turbine was used for this figure.

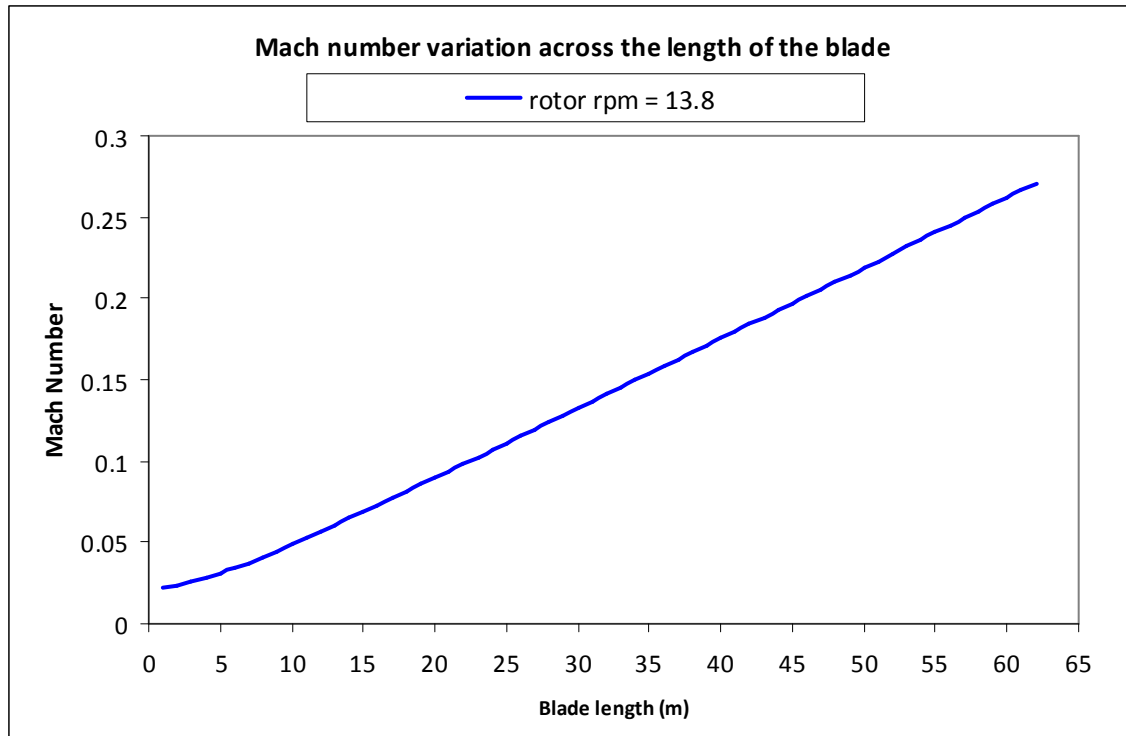


Figure 7-2: Mach number variation across the length of the blade. The NREL 5MW reference turbine was used for this figure.

Notes:

- Blade section 8 of the NREL model has the NACA 6464 airfoil. In this report, the NACA 6464 airfoil was replaced with the DU 93-W-180 due to unavailability of the NACA 6464 co-ordinates. The DU 93-W-180 has a slight camber and can be used for operation near the blade tip.
- The airfoil length along the blade for section 7 was split into two parts, one of length 10.25m and the other of length 9.225m, and the polars were obtained for each part for different Reynolds and mach numbers.

The procedure to determine the C_l and C_d 's is as follows: For each blade section (see Table 7-1) the Reynolds number and Mach number were obtained (from Figure 7-1 and Figure 7-2 respectively). These were input into XFOIL along with the airfoil co-ordinates to obtain the 2-D C_l and C_d 's. A sensitivity analysis was carried out to see if the Reynolds number and Mach number change over the length of each blade section had a large effect on the C_l 's and C_d 's. One such example is shown below in Figure 7-3 and Figure 7-4. From the analysis it was concluded that for the range of Reynolds considered the C_l/C_d ratios and the C_l values were the highest for the highest Reynolds numbers. Mach numbers also played a role in increasing the C_l/C_d ratios and the C_l values, although this increase was not as significant as the increase due to the change in Reynolds numbers. To obtain the C_l and C_d 's for further analysis the Reynolds number and Mach number at midpoint of each blade section was used.

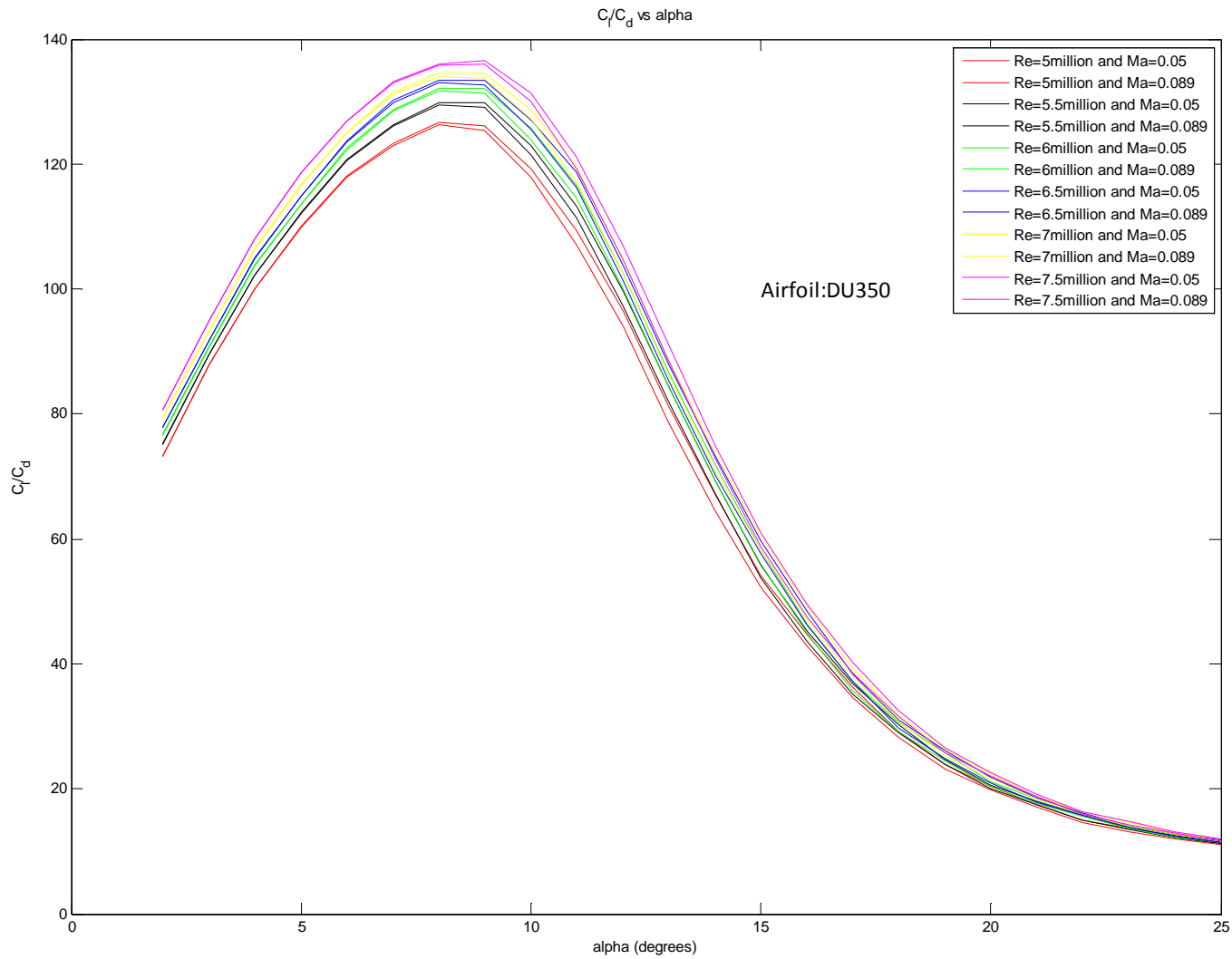


Figure 7-3: Change in C_l/C_d with change in Re and Mach number

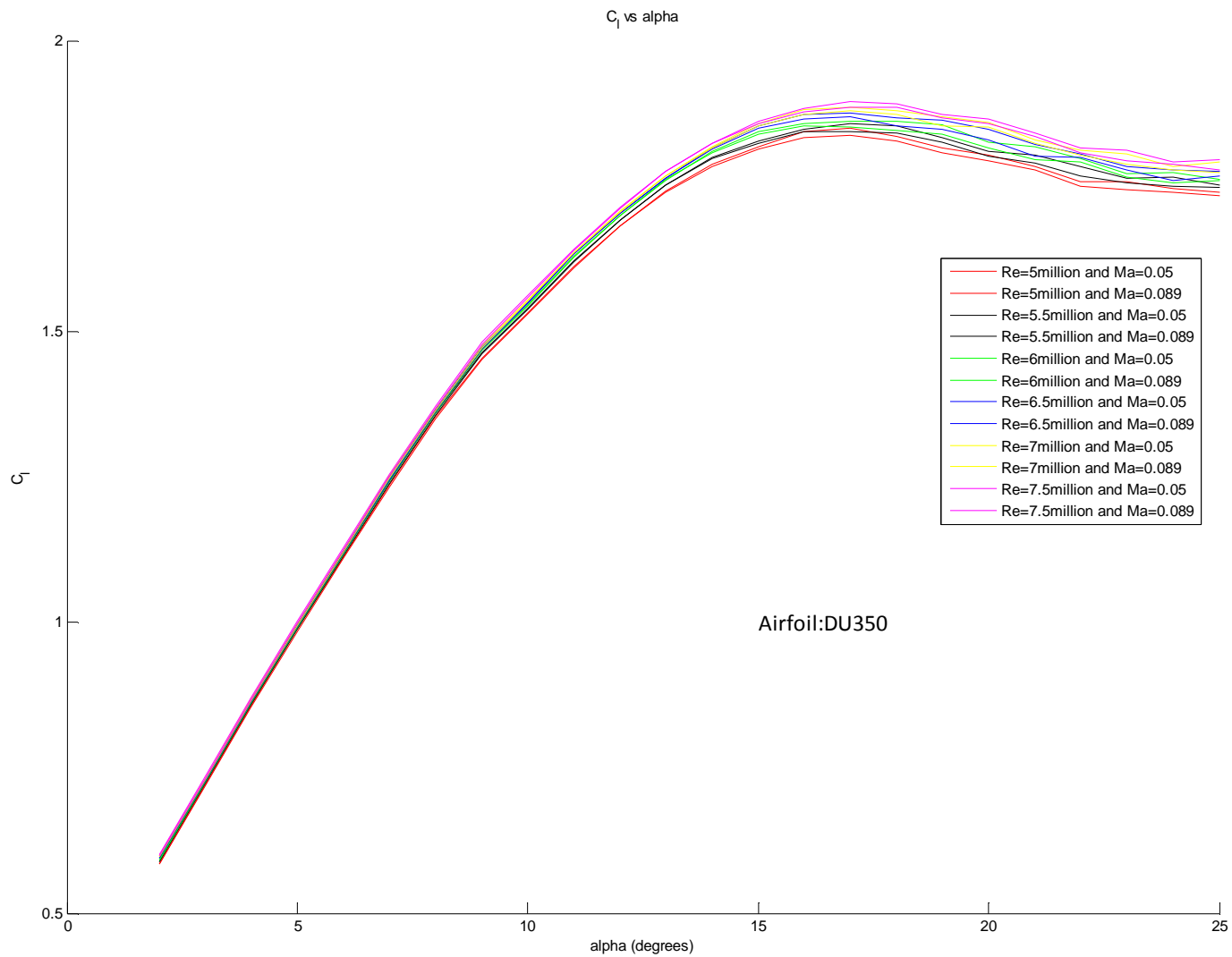


Figure 7-4: Change in C_l with change in Re and Mach number

7.1.1.2 Stall Delay

Stall delay is the phenomenon wherein observed lift coefficients at inboard sections of the rotating blade are significantly higher than the maximum possible lift coefficients obtained from two-dimensional static tests. This effect is the larger near the blade root and reduces along the length of the blade. See Figure 7-5. For a more thorough discussion on stall delay refer to Chapter 3 of the *Wind Energy Handbook*.

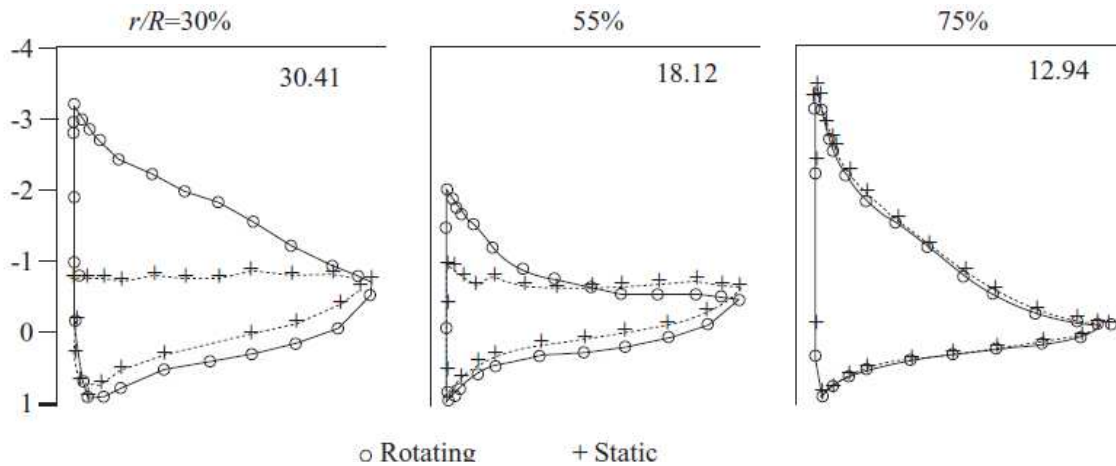


Figure 7-5: Pressure measurements at different stations along the span for a rotating blade and a non-rotating (static) blade. The numbers at the top of each case indicate the angle of attack. [Source: Burton, et al, 2001]

Since stall delay leads to higher C_l 's the measured rotor power will be larger than what will be predicted if 2-D C_l 's are used. A number of methods are available to obtain the C_l and C_d of the airfoils in the region when $\alpha > \alpha_s$. Here, the Viterna-Corrigan method was used because of its simplicity and because it yields sufficiently accurate results (Viterna and Corrigan, 1981). The factor that affects stall delay is the aspect ratio i.e. the ratio of the blade length to the chord. An aspect ratio of 25 was assumed for both concepts. The airfoil properties were not corrected for any other effects.

7.1.2 Chord and Twist Selection

The twist and chord of the blades were selected using Equation 6.3 and Equation 6.4 respectively. These equations are for the analysis with the wake rotation neglected. The maximum allowable chord and twist of the blade are limited by manufacturing requirements. To date, the blade with the largest chord, 5.94m, belongs to the Bard Offshore 5.0 (de Vries, 2007). For twist, information was available only for the NREL 5 MW turbine and it has a maximum twist of 13.308° . Therefore, for this report the maximum allowable chord will be set at 6m and the maximum allowable twist will be set at 13° .

7.1.3 Blade Element Momentum theory

The Blade Element Momentum (BEM) theory was used primarily because of its simplicity and the speed involved in obtaining the results coupled with the fact that the theory gives reasonably accurate results. For a detailed discussion of the theory refer to Chapter 3 of the *Wind Energy handbook* (Burton, et al, 2001) or Chapter 3 of *Wind Energy Explained* (Manwell, et al, 2006). A number of assumptions and some corrections are used to get accurate results when the theory does not suffice. The assumptions used are as follows:

- The wind velocity over the rotor swept area is assumed to be uniform. This means that shear and yaw effects are ignored.
- The rotor blades are split into a number of strips and it is assumed that these strips can be analysed independent of each other
- Tower shadow is ignored.
- The flow is assumed to be steady i.e. unsteady flow effects were not taken into account.

The wind turbine rotor was modelled using the BEM theory according to the procedure in Chapter 3 of the *Wind Energy Explained*. The 61.5 m long blade was split into 60 annuli with each annulus having a width of 1.025m.

The corrections used in the BEM theory are presented in the next two sections:

7.1.3.1 Glauert's correction for heavily loaded rotors

Beyond the axial induction factor 'a' of 0.33 the momentum theory is no longer valid. It was empirically determined that the thrust values are much higher than what the theory predicts. See Figure 7-6. In the region where $a > 0.33$, Glauert's correction was used to obtain realistic values for the thrust.

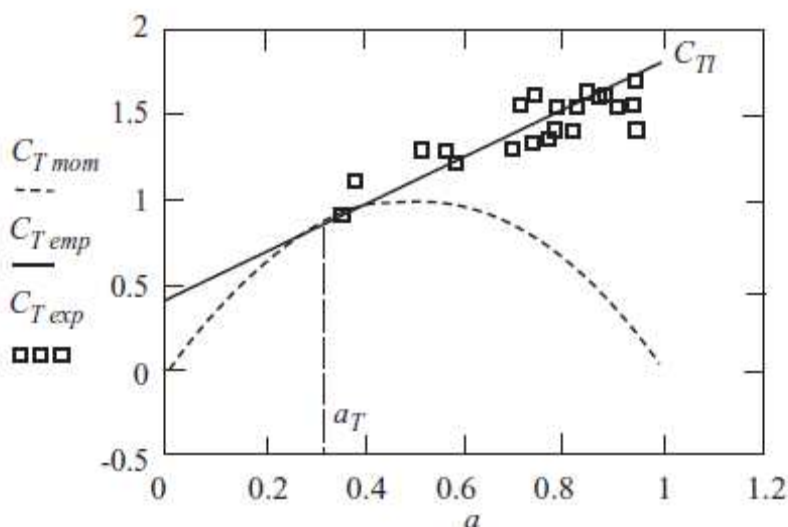


Figure 7-6: Empirical correction for rotor thrust [Source: Burton, et al, 2001]

The correction is given in Equation 7.1.

$$\begin{aligned}
C_T &= 4a(1-a) \text{ for } a \leq \frac{1}{3} \\
C_T &= 4a(1-F_G a) \text{ for } a > \frac{1}{3} \\
\text{where } F_G &= \frac{5-3a}{4}
\end{aligned}$$

Equation 7.1

C_T – Thrust coefficient
 a – axial induction factor
 F_G – the correction factor

7.1.3.2 Prandtl's correction for tip loss

During the operating of the wind turbine, the tip vortex causes very high values of 'a' near the blade tips. This leads to low ϕ values and therefore low generated torque and therefore low power generation. This loss is particularly relevant to this project because the number of blades on the rotor plays a part. To model the tip loss, Prandtl's correction was used. This is a simple approximation and yields sufficiently accurate results. For more details on Prandtl's correction refer to Chapter 3 of the *Wind Energy Handbook*.

The tip loss correction is incorporated into the equation for wind velocity at the rotor as shown in Equation 7.2.

$$U_r = U_o (1 - a F_{tip}(r_i))$$

Equation 7.2

U_r – wind velocity at the rotor [m/s]
 U_o – Free stream wind velocity [m/s]
 a – axial induction factor and

$$F_{tip}(r_i) = (2/\pi) \cos^{-1} \left[\exp \left(- \left\{ \frac{(B/2)[1-(r_i/R)]}{(r_i/R) \sin \phi} \right\} \right) \right]$$

Equation 7.3

Manwell, et al, 2006

B – Number of blades
 r_i – Distance of the annulus i from the hub [m]
 R – Blade length [m]
 ϕ – Inflow angle [rad]

It can be seen from this simplified form that the number of blades play a role in determining the tip loss. Figure 7-7 shows the tip loss factor for a three-bladed and a two-bladed turbine designed for this report. (It should be noted that these blades were designed for the optimal induction factor of 0.33 and design with respect to tip loss was not considered). The axial induction factors for each section are calculated iteratively based on these equations and the final values are also shown in Figure 7-7. The axial induction factors of both turbines are almost identical up till $r/R = 0.9$. After this point, the axial induction factor of the two-bladed turbine is farther away from the optimal axial induction factor of 0.33 than the axial induction factor of the three-bladed turbine. Axial induction factors in this range indicate that the rotor is not extracting the optimal

amount of energy from the wind. This will lead to the two-bladed turbine producing lesser power than the three-bladed turbine.

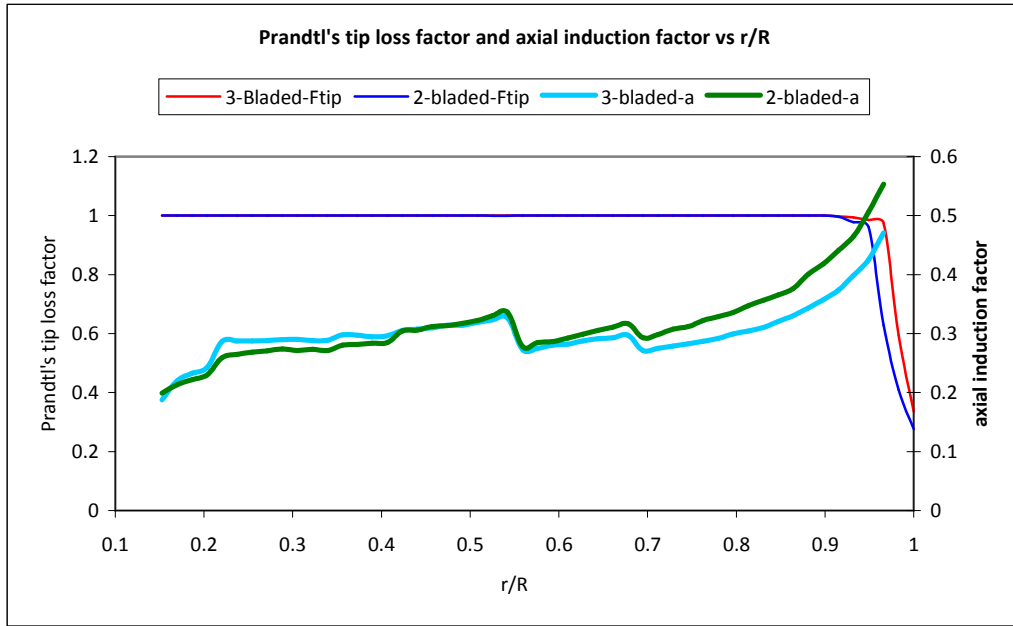


Figure 7-7: Span-wise variation of Prandtl's tip loss correction and the axial induction factor

These were the only modifications included with the BEM code to determine the power generated by the turbine and the thrust loading on the rotor. This method was not intended to serve as a precise calculation tool but serves sufficiently to determine the differences in loading and power generated between the two-bladed and the three-bladed concepts.

7.1.4 Internal structure of the airfoil

The internal structure of each airfoil was chosen to consist of spar caps and shear webs as shown in Figure 7-8.

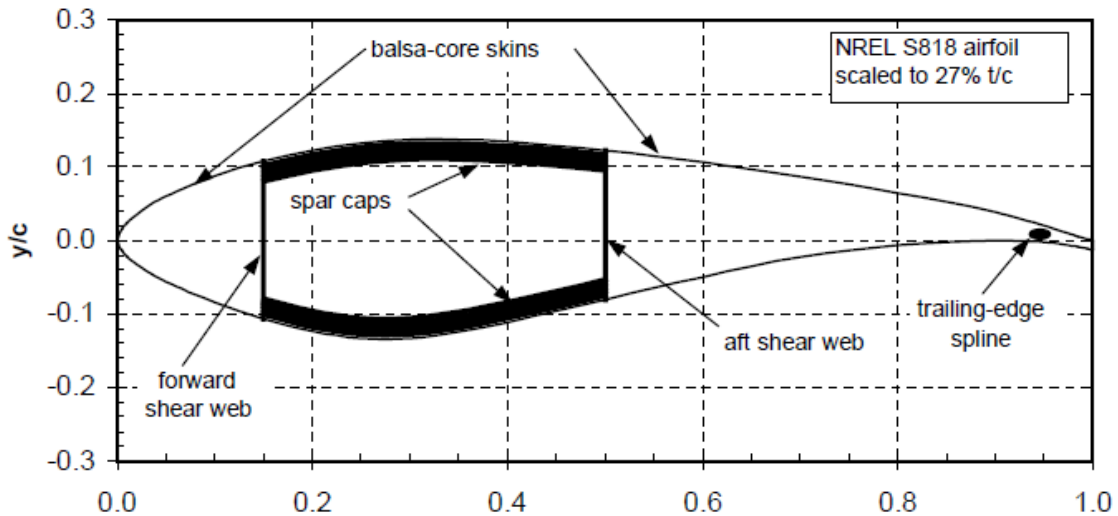


Figure 7-8: NREL S818 airfoil internal structure

The dimensions of the spar caps and the shear webs need to be determined after a buckling and fatigue analysis on them is performed and the shell must be designed to withstand torsional moment. A buckling and torsional analysis to determine the dimensions of the load carrying elements of the airfoil was not in the scope of this report. Only a fatigue analysis was performed. The airfoil skin, spar cap and shear web dimensions of the NREL 5MW reference turbine were used as reference values. The skin, spar cap, and shear web dimensions of the NREL 5 MW reference turbine are shown below in Figure 7-9. These were made a function of the chord times maximum lift coefficient ($c \cdot Cl_{max}$) of each blade section (for the NREL turbine) i.e.

$$\text{dimension}_{\text{design}} = \frac{(c \cdot Cl_{max})_{\text{design}}}{(c \cdot Cl_{max})_{\text{NREL}}} \times \text{dimension}_{\text{NREL}}$$

The parameter $Cl_{max} \cdot c$ is referred to as "Maximum static operation loads" and serves as an indicator for the highest static loads (van Rooij, 2003). Thus, for the different blades designed starting values for the thicknesses of the spar cap, shear web and shell were obtained. The final structure and stiffness distribution will be changed if the fatigue analysis shows that strength is insufficient.

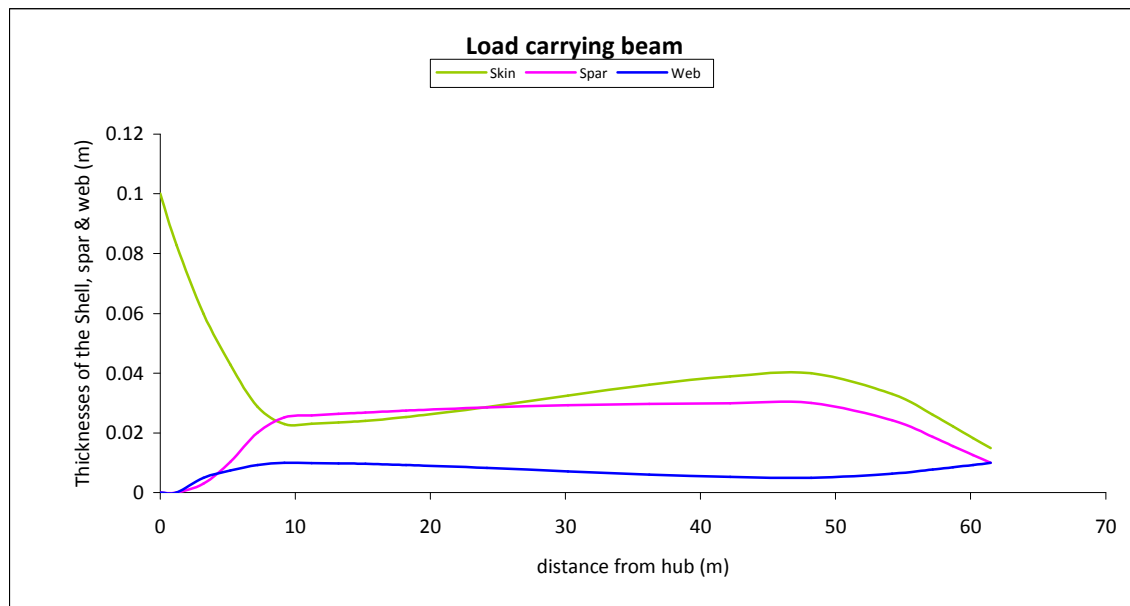


Figure 7-9: Dimensions of the airfoil shell, spar cap and web of the NREL 5MW reference turbine blade

The number of divisions for the structural analysis is the same as that used for the BEM code, i.e. sixty. For simplicity, it was assumed that there was no variation in the thicknesses of the shell, spar cap and shear webs for each structural element. This is not strictly true, but for this report, the assumption does not affect the comparison between the two-bladed and the three-bladed concept.

The spar caps and shear webs were modelled from the geometry of the airfoil (i.e. the x and y co-ordinates which define the profile), using simple co-ordinate geometry formulae. An example of one such structural cross section is shown in Figure 7-10.

Because of co-ordinate geometry based modelling the calculated second moment of area due to contributions of each element may not be accurate (for example, where the shear web meets the spar cap). It can also be seen that the thickness of each shear web is not uniform. This again is due to the co-ordinate geometry based modelling. However these differences do not play a critical role when differentiating between the two-bladed and the three-bladed case and were ignored.

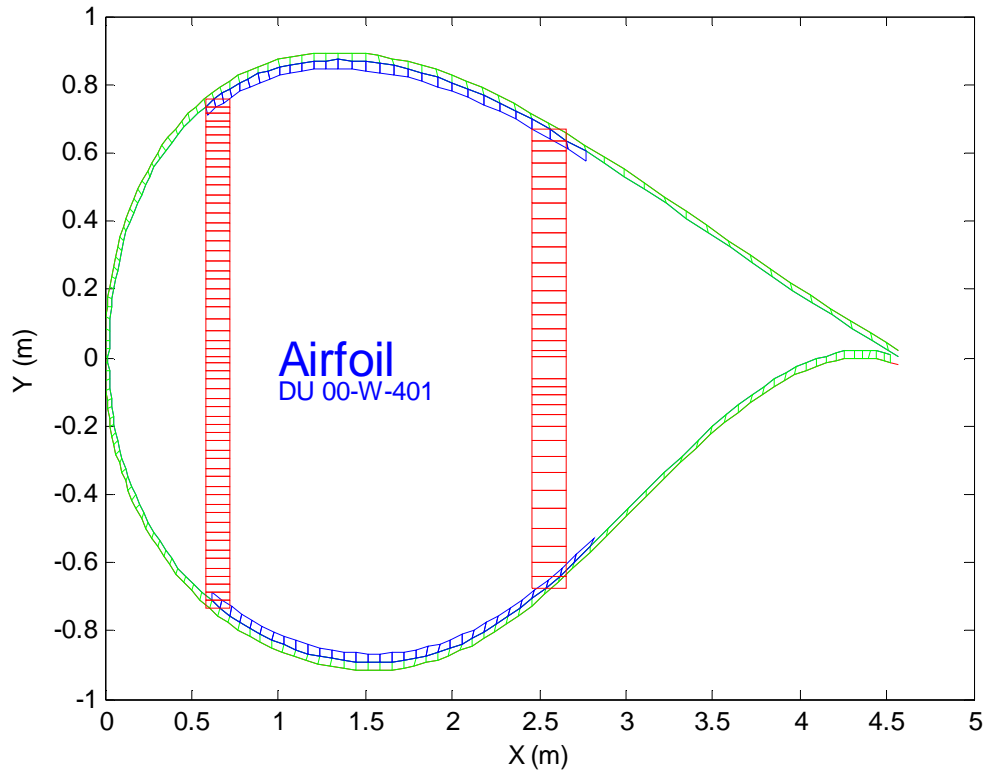


Figure 7-10: Cross section of the DU-401 airfoil

The spar caps extended from 12.5% of the chord to 60% of the chord for each airfoil. The shear webs were placed near the beginning and near the end of the spar caps. See Figure 7-10.

7.1.5 Material Selection

The materials were chosen from the Optimat database (Optimat, 2006). For a detailed list of all the materials, the different tests performed, the geometries adopted for the materials, the different 'R' ratios for the tests and finally the properties of the materials refer to the database itself. (Note: R is the ratio of the minimum stress to the maximum stress). In this report all material properties were based on tests conducted for $R=-1$, meaning that the stress cycles have a mean value of 0.

7.1.5.1 *Airfoil skin*

The skin provides the required aerodynamic shape of the airfoil. The skin is subjected to a pressure distribution due to the airflow and also because of the blade bending

moment. Torsional loading due to the pitching moment of the blade is also an important parameter in skin design. So to stiffen the shell, panels are used. These panels are typically 'sandwiches' made of composite material and a balsa wood core. For the stiffness analysis the properties of the balsa core and composite material with multidirectional fibers was considered. The panels comprised of 2/3rd of balsa core and 1/3rd of MD-2 (Lund and Johansen, N.D.).

7.1.5.2 Spar Caps

During turbine operation the blades bend downwind. Due to wind shear the loading on the blade is not uniform. This leads to the spar caps of the airfoil experiencing cycles of compression and tension. These loads occur along the length of the blade. So for the spar caps, laminates with unidirectional fibers are chosen, with the fibers along the length of the blade. From the Optimat database UD-2 was chosen for the spar caps. The points for the S-N curve for UD-2 are shown below in Figure 7-11.

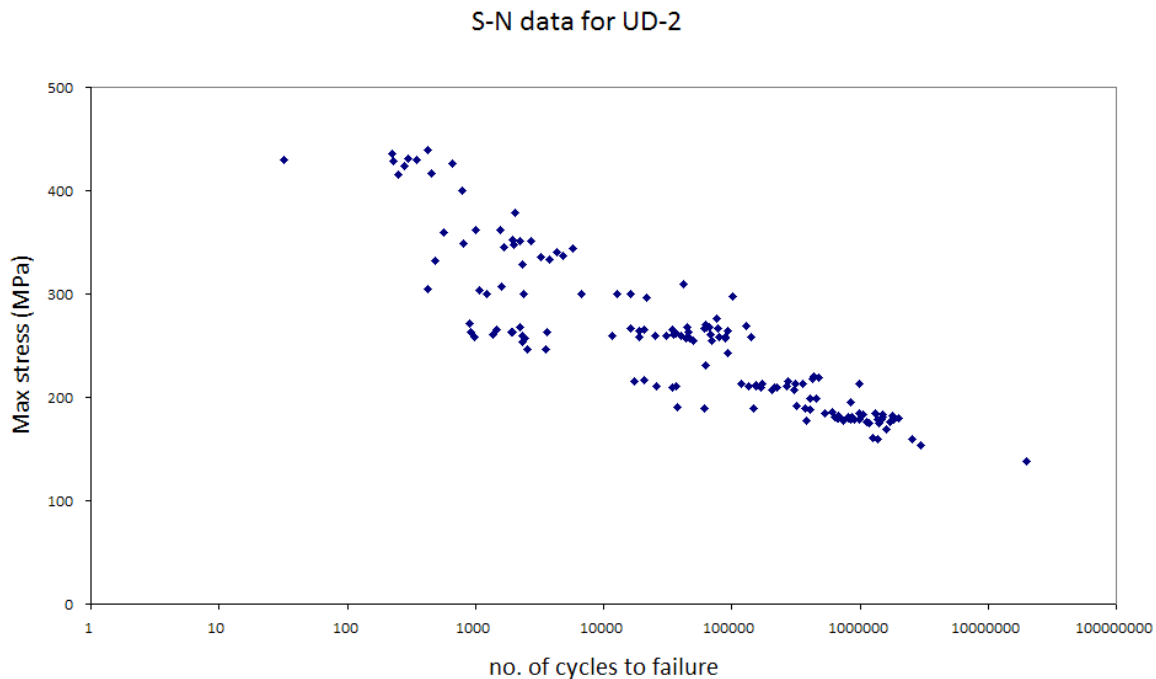


Figure 7-11: S-N curve of UD-2 (Optimat database, 2006)

7.1.5.3 Shear Webs

During turbine operation as the spar caps absorb the load it is essential that they remain in their position relative to the entire blade. To ensure this, shear webs are used. As the blade bends and because the spar caps need to remain in their position, the webs experience a shear load. To deal with this loading, multidirectional fibers are used in the construction of the shear webs. From the Optimat database MD-2 was chosen for the shear webs. The points for the S-N curve for MD-2 are shown below in Figure 7-12.

S-N data for MD-2

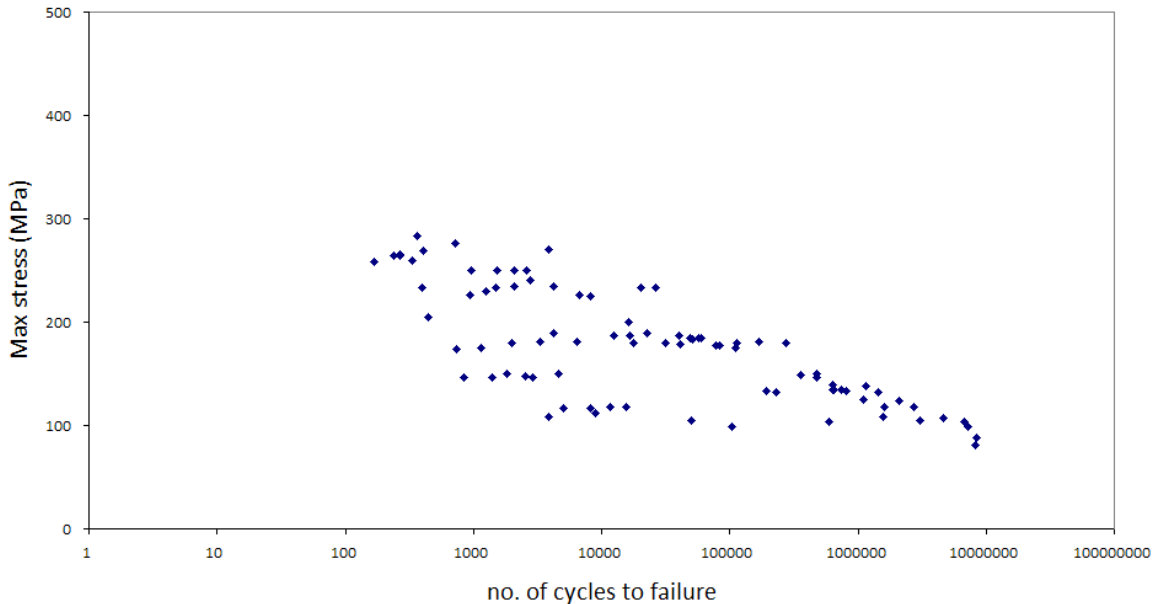


Figure 7-12: S-N curve of MD-2 (Optimat database, 2006)

The properties of the materials are shown below in Table 7-2.

Table 7-2: Material Selection (Source: Optimat (2006) and Auszac.com (2007))

	Material	Ultimate tensile strength (MPa)	Ultimate compressive strength (MPa)	Young's Modulus (GPa)	Density (kg/m ³)
Shell	Balsa wood	19.9	12.1	1.28	163
Spar Cap	UD-2	39.2	39.0	39	1950
Shear Web	MD-2	27.0	27.0	29	1910

7.2 Nacelle

In this section the change in the masses of the components in the nacelle as a consequence of the change in concept will be discussed. The components discussed are as follows:

- Generator
- Gearbox
- Hub (Rigid and Teetering)
- Pitch mechanism
- Yaw Drive and bearing

Other components like the low speed shaft, main bearings, main frame, nacelle cover, etc, will also experience a change in mass as the concept changes, but it was assumed that the change in these masses are very small and therefore can be neglected. The nacelle itself has a length of 18m and its height and breadth are equal to 6m. These dimensions were taken from the REPower 5MW turbine's nacelle (de Vries, 2009).

7.2.1 Generator

As stated in Chapter 2, the generator used is a DFIG with an operating speed range of 600 to 1100 rpm. The three-bladed and the two-bladed concepts will have the same generator and thus no difference in generator mass is envisioned as the number of blades change. The generator mass will be modelled according to the NREL equation. See Equation 7.4.

$$Mass = 6.47 \times Machine_rating^{0.9223} \quad \text{Equation 7.4}$$

(Fingersh, et al, 2006)

7.2.2 Gearbox

The gearbox is a combination of two planetary stages and a spur gear stage. The mass of the gearbox will change as the operating torque changes and as gearbox transmission ratio changes. Both operating torque and transmission ratio are a function of λ_{design} .

7.2.2.1 *Mass as a function of main shaft torque*

The mass is modeled according to the NREL scaling model. The relation is given below in Equation 7.5 where the main shaft torque is in kNm and the mass in kg.

$$Mass = 4 \times 70.94 \times Main_shaft_torque^{0.759} \quad \text{Equation 7.5}$$

(Fingersh, et al, 2006)

7.2.2.2 *Mass as a function of transmission ratio*

The change in mass as transmission ratio changed was modeled with simple relations. Using the information that the maximum step up ratio is 1:6 per stage, the gear ratio of the last stage (spur gear stage) is calculated for a rated wind speed of 11m/s. See Table 7-3. The spur gear and generator shaft can be visualized using Figure 7-13.

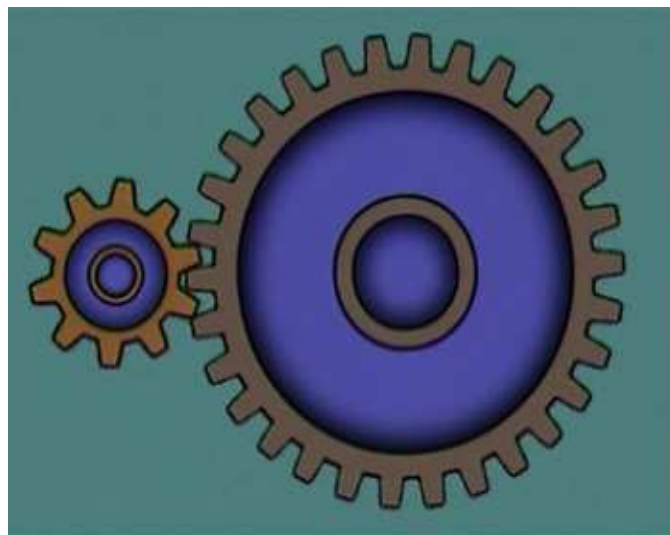


Figure 7-13: Driven gear on the generator shaft (Left) and driving gear i.e. the spur gear (Right)

Table 7-3: Spur Gear Speed ratio estimation

	$\lambda_{\text{design}}=8.3$	$\lambda_{\text{design}}=9.8$
Rated wind speed (m/s)	11	
Rotor rotational speed (rpm)	13.8	16.3
Speed in Gearbox Stage I (rpm)	83	98
Speed in Gearbox Stage II (rpm)	498.2	588.2
Rated Generator shaft speed (rpm)	1000	
Step up ratio between generator shaft and the spur gear	2	1.7

Based on simple gear relations it is known that the spur gear diameter is inversely proportional to its rotational speed. If it is assumed that the spur gears of the gearboxes of both turbines have the same thickness and the gear diameter of the generator shaft does not change, the mass of each spur gear can be estimated as a function of the spur gear diameter and eventually as a function of the spur gear rotational speed. See Equation 7.6, Equation 7.7 and Equation 7.8.

$$D_{\text{spur}} = \frac{1}{N_{\text{spur}}} \quad \text{Equation 7.6}$$

$$\text{Mass}_{\text{spur}} = \rho_{\text{steel}} \times \frac{\pi D_{\text{spur}}^2}{4} \quad \text{Equation 7.7}$$

$$\text{Mass}_{\text{spur}} = \rho_{\text{steel}} \times \frac{\pi}{4 N_{\text{spur}}^2} \quad \text{Equation 7.8}$$

D_{spur} – Diameter of the spur gear [m]

N_{spur} – Ratio between generator shaft speed and spur gear speed

$\text{Mass}_{\text{spur}}$ – Mass of the spur gear [kg]

ρ_{steel} – steel density (assumed for the spur gear) [kg/m^3]

Equation 7.8 gives a mass of 1500 kg when the transmission ratio is 1.7 and 1800kg when the transmission ratio is 2. These numbers are exaggerated because a unit thickness was assumed for the spur gear. In reality the thicknesses will be lesser. From this it was concluded that the change in spur gear size did not significantly impact the gearbox mass when compared to the change in gearbox mass due to the difference in main shaft torque. Therefore this aspect was neglected for all future analyses and only change in gearbox mass due to change in main shaft torque was considered.

7.2.3 Hub

As stated in Chapter 5, there is a slight difference in mass between the teetering hub of the two-bladed turbine and the rigid hub of the three-bladed turbine. But this difference will be neglected and it will be assumed that both hubs have the same mass. Equation 7.9 will be used to model the mass of the hub.

$$Mass_{hub} = \frac{1}{B} [0.954 \times total_blade_mass + 5680.3] \quad \text{Equation 7.9}$$

(Fingersh, et al, 2006)

7.2.4 Pitch mechanism

The mass of the pitch mechanism will be modelled using a relation from the NREL scaling model and is a function of the blade mass and number of blades. See Equation 7.10.

$$Mass_{pitch_system} = \frac{1}{B} ([0.1295 \times total_blade_mass + 491.31] \times 1.328 + 555) \quad \text{Equation 7.10}$$

(Fingersh, et al, 2006)

Pitch system mass and total blade mass are expressed in kg.

7.2.5 Yaw System

The yaw drive and bearing will be designed for the moment encountered at the yaw bearing at the rated wind speed of the turbine. A relation from the NREL scaling model will be used to model the mass of the yaw system. See Equation 7.11.

$$Mass_{yaw_system} = 0.0152 \times \left(\frac{peak_moment}{bearing_diameter} - 36 \right)^{1.489} \quad \text{Equation 7.11}$$

(Fingersh, et al, 2006)

Yaw system mass is expressed in kg, the peak moment in kNm and bearing diameter in m. The flapwise root bending moment at the rated wind speed will be considered for the peak moment and bearing diameter will be taken as the diameter of the tower section at the tower top.

7.3 **Support Structure Design**

The design of the support structure is initially governed by natural frequency requirements and is carried out using the Rayleigh method for stepped towers. After the support structure outer diameter is fixed buckling checks will be performed to ensure that the wall thickness chosen was adequate. The pile penetration depth is fixed using the Foundation Pile Analysis Tool. After the tower is designed it will be analysed using Bladed 3.80 and if required its dimensions will be modified based on the fatigue analysis.

7.3.1 Design based on Natural Frequency

The support structure is designed with the view that the support structure consisted of a monopile of uniform diameter up till the platform. From the platform upwards the tower consisted of sections with decreasing diameter with the smallest diameter at the tower top which is 4m. Each section had a height of 1m. The transition piece was not modelled. From Chapter 3 the length of the support structure was obtained. The natural frequency of the tower was calculated using the method from the Opti-Owecs project. See Equation 7.12.

$$T_t^2 = \frac{4\pi^2(M_{top} + m_{eq}L)L^3}{3EI_{eq}} \left[\frac{48}{\pi^4} + \frac{3EI_{eq}}{K_{rot}L} + \frac{3EI_{eq}}{K_{lat}L^3} \right] \quad \text{Equation 7.12}$$

(Source: Opti-Owecs, 1996)

T_t – natural Period [s]

M_{top} – Tower top mass [kg]

E – Young’s modulus of steel [210 GPa]

L – Length of support structure from seabed to hub height [m]

K_{rot} – Rotational stiffness of the soil [Nm/rad]

K_{lat} – Lateral stiffness of the soil [N/m]

The determination of K_{rot} and K_{lat} is explained in section 7.3.3. The natural frequency in Hz is given by $1/T_t$. The definitions of m_{eq} and I_{eq} are given below in Equation 7.13 and Equation 7.14. Also see Figure 7-14.

$$m_{eq} = \frac{\sum_{j=1}^n m_j l_j \left(1 - \cos\left(\frac{\pi x_j}{2L}\right) \right)^2}{L} \quad \text{Equation 7.13}$$

$$I_{eq} = \frac{\sum_{j=1}^n I_j l_j \cos^2\left(\frac{\pi x_j}{2L}\right)}{L} \quad \text{Equation 7.14}$$

(Source: Opti-Owecs, 1996)

m_j – Mass of section j [kg]

l_j – Length of section j [m]

x_j – Distance of midpoint of section j to the seabed [m]

L – Support structure length [L]

I_j – Second moment of area of section j [m⁴]

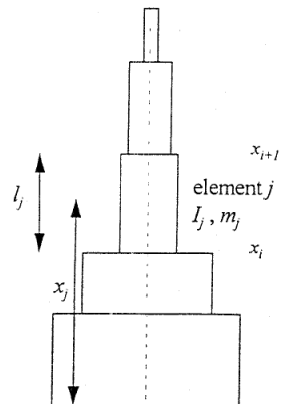


Figure 7-14: Stepped tower (Source: Opti-Owecs, 1996).

The support structures will be designed such that their natural frequencies fall in the soft-stiff region i.e. in between the 1-P and the N-P regions. Since the λ_{design} of the two-

bladed and three-bladed turbines are fixed at 9.8 and 8.3 respectively and because of the change in the number of blades, the 1-P and N-P regions will be different for both concepts.

7.3.2 Scour

No scour protection was considered for the wind farms. Instead the support structure was designed taking scour into account. The DOWEC project stated that the difference in cost between a monopile with scour protection and a heavier monopile with no scour protection was not significant for the 6MW turbine (Oud, 2002). The depth of the scour hole was taken as 2.5 times the base diameter of the pile (GL IV-2 2004).

7.3.3 Pile Penetration and Soil Stiffness

To determine the pile penetration depth the Foundation Pile Analysis Tool was used. As input the soil parameters from Chapter 3 and the thrust force on the rotor at rated wind speed was used. The aerodynamic and hydrodynamic loading on the support structure was ignored. The thrust force was multiplied by a factor 1.5 to simulate a gust at rated wind speed. The length of the pile must be enough such that it can transfer all the loads to the soil and thus prevent structure displacement at the seabed level and at the end of the pile. The max permissible allowable displacement was chosen as 0.12m at the seabed and 0.02m at the end of the pile (de Vries and van der Tempel, 2007). The foundation properties are modelled by a lateral spring (with stiffness K_{lat}) and a rotational spring (with stiffness K_{rot}) at the seabed level as shown in Figure 7-15. The spring constants were obtained from the Foundation Pile Analysis Tool. These were input in to Equation 7.12 to obtain the natural frequency of the support structure.

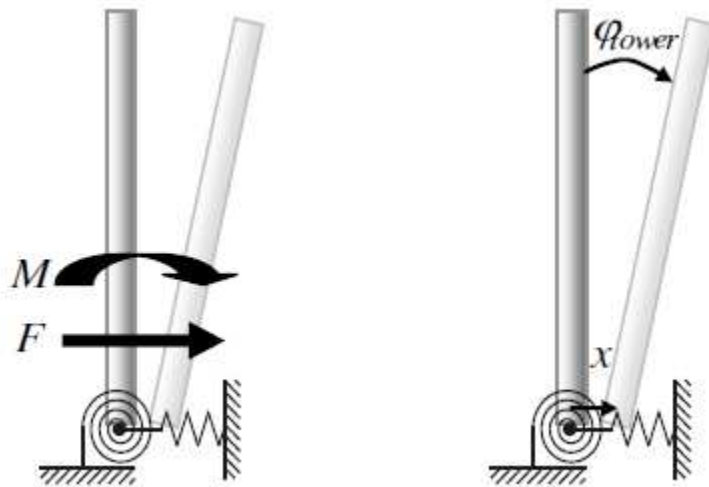


Figure 7-15: Foundation properties represented by rotational and linear springs. x =lateral displacement, ϕ_{tower} =rotational displacement (Source: van der Tempel, 2006)

7.3.4 Buckling checks

Bar buckling and shell buckling checks were carried out according to GL standards (GL IV-2, 2004).

7.3.4.1 *Bar buckling*

Bar buckling checks were carried out for the structure as a result of it being subjected to axial compressive loads due to tower top mass + support structure mass and bending moment due to rotor thrust. The buckling checks were carried out at the seabed level because this is where the maximum loading occurs. For the support structure to have been satisfactorily designed for bar buckling Equation 7.15 must be satisfied.

$$\frac{N_d}{\kappa N_p} + \frac{\beta_m M_d}{M_p} + \Delta n \leq 1$$

Equation 7.15

(Source: GL IV-2, 2004)

N_d – Axial compressive load [N]

N_p – Plastic compression resistance [N]

κ – Reduction factor

β_m – moment coefficient

M_d – Bending moment [N-m]

M_p – Plastic resistance moment [N-m]

The axial compressive load and the bending moment was obtained from the design process while the other parameters in the equation were determined using the procedures given in GL IV-2.

7.3.4.2 *Shell buckling*

Shell buckling checks were carried out on the support structure at the seabed level as a result of it being subjected to axial compressive loads and pressure loading. For the pressure loading the fifty year maximum wave height was considered. It was assumed that the water inside the pile is at the LAT. The difference in water levels inside and outside the pile will give rise to differential pressure loading which leads to circumferential stresses. For the support structure to have been satisfactorily designed for shell buckling Equation 7.16 must be satisfied.

$$\left(\frac{\sigma_x}{\sigma_{xu}} \right)^{1.25} + \left(\frac{\sigma_\phi}{\sigma_{\phi u}} \right)^{1.25} \leq 1$$

Equation 7.16

(Source: GL IV-2, 2004)

σ_x – Axial compressive stress [N/m²]

σ_{xu} – Ultimate buckling stress for axial compressive stress [N/m²]

σ_ϕ – Circumferential stress due to pressure [N/m²]

$\sigma_{\phi u}$ – Ultimate buckling stress for circumferential stress [N/m²]

The axial compressive stress and the circumferential stress due to pressure was obtained from the design process while the other parameters in the equation were determined using the procedures given in GL IV-2.

7.3.5 S-N curve

The support structure is made up of steel plates which have been rolled into cylinders and welded at the joints longitudinally. Then these hollow cylinders are welded together along the circumference to form the support structure. Due to the wind and wave loading on the turbine and support structure, failure begins at the welds. To perform the fatigue analysis the S-N curve for the welds was required and it was obtained from the GL standards (GL IV-2 2004). The equations to determine the S-N curve are shown below in Equation 7.17 and Equation 7.18.

$$\log(N) = 6.69897 + mQ \quad \text{Equation 7.17}$$

$$Q = \log\left(\frac{\Delta\sigma_R}{\Delta\sigma}\right) - \frac{0.39794}{m_o} \quad \text{Equation 7.18}$$

(Source: GL IV-2, 2004)

N – Number of cycles to fatigue failure

m – Inverse slope of S-N curve

m=m_o for Q≤0

m=2m_o-1 for Q>0

Δσ_R – fatigue strength reference value of S-N curve at 2 million cycles of stress range [N/mm²]; 100 for tubular joints

Δσ – Stress range [N/mm²]

m_o – inverse slope of S-N curve; 3 for welded joints

For the welds below the platform a corrosion factor of 1.25 was applied according to the GL standards. Thus Δσ_R in Equation 7.18 becomes 100X1.25=125. The S-N curves were constructed according to the information presented above and are shown below in Figure 7-16.

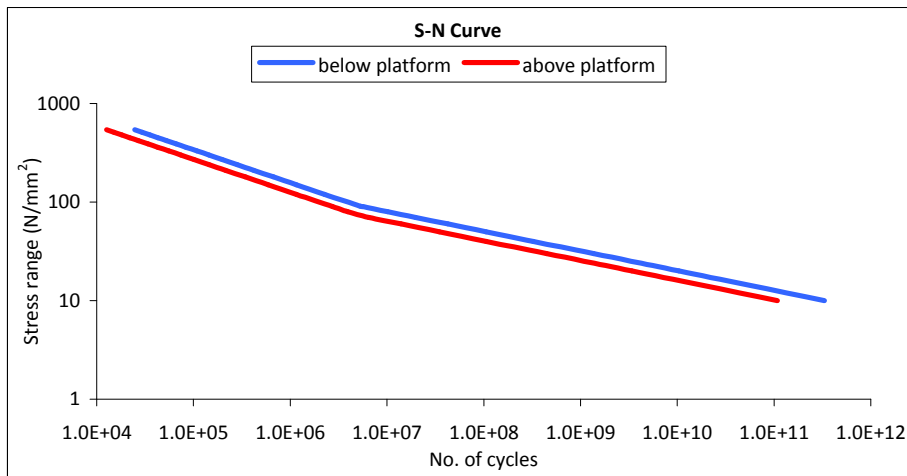


Figure 7-16: S-N curve for the monopile welds

7.4 Fatigue Analysis of the Blades and Support structure

The fatigue analysis of the blades and support structure was done using Bladed 3.80. The rotor and support structure obtained after the initial design process, their respective material properties (S-N curves) and the sea states was input into Bladed. The lifetime of the wind turbine was chosen as 20 years. Since the spar cap takes most of the loading it will be the primary focus of the fatigue analysis of the blade. For the support structure the welds will be the primary focus of the fatigue analysis. A damage equivalent load greater than 1 meant that the component being analyzed is not adequately designed for fatigue. For the blades the spar cap thickness was increased and the simulation was rerun. For the support structure the diameter to thickness ratio was increased and the simulation was rerun. This was repeated until damage was found to be lesser than 1.

7.5 Installation Procedure

There are a number of installation procedures which are employed in the industry. These include transporting and installing the fully assembled rotor (Figure 7-17: Left), transporting and installing the fully assembled wind turbine (Figure 7-17: Right) and the bunny ear method i.e. transporting and installing the nacelle + two rotor blades as one unit (Figure 7-18). Due to the availability of specialized offshore turbine installation equipment, the installation costs will not be treated as a function of the turbine weight and hub height, rather, it will be a function of the time required for installation.

Most modern 5MW turbines are installed with the rotor pre-assembled on shore. Examples of such wind farms are the Thornton Bank and Alpha Ventus. The bunny ear method was used for the Horns Rev project which comprised eighty turbines with turbine rating of 2 MW. As of this time, only the Beatrice wind farm has installed turbines fully assembled. Because this method is not common and because of the delay that the Beatrice wind farm installation encountered, this installation method was not considered here.



Figure 7-17: Installation with rotor fully assembled (Left). Installation with the wind turbine fully assembled (Right).



Figure 7-18: Bunny Ear method

Three installation methods were identified using information from an offshore wind turbine installation company (www.a2sea.com). These are; the bunny ear method, the

single blade lift method and the complete rotor lift method. The advantages and disadvantages are discussed below in Table 7-4.

Table 7-4: Turbine Installation methods: Pros and cons (Nedergaard, 2008)

Installation method	Advantages	Disadvantages
Bunny ear method	<ol style="list-style-type: none"> 1. Easy to handle 2. Efficient with limited harbor facilities 3. Narrow port entrances possible 4. Known and proven methodology 	<ol style="list-style-type: none"> 1. Precise work to fit last blade
Single blade lift method	<ol style="list-style-type: none"> 1. Both vertical and horizontal blade fits possible 	<ol style="list-style-type: none"> 1. Time consuming: longest offshore time
Complete rotor lift method	<ol style="list-style-type: none"> 1. Known and proven methodology 	<ol style="list-style-type: none"> 1. Very dependent on wind conditions at site 2. Large harbor facilities required to pre-install large number of rotors 3. Large harbor cranes required

From this it was concluded that the complete rotor-nacelle assembly lift method was most suited for the two-bladed turbine and for the three-bladed turbine, the complete rotor lift method was chosen based on the present trend in the industry for 5MW offshore turbines.

Figure 7-19 shows the component breakup for the installation for the turbines.

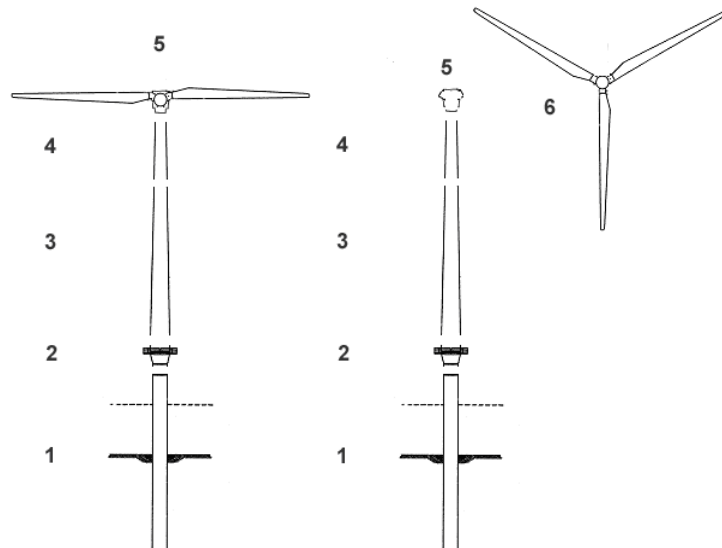


Figure 7-19: Component break up for installation. Rotor-nacelle assembly lift method: 2-bladed (Left) and complete rotor lift method: 3-bladed (Right)

Data for installation times for turbines with monopile type support structures were available for turbines in the 2-3 MW range (Gerdes, et al, N.D., www.hornsrev.dk, N.D.). From these sources it was estimated that the required time for installing one turbine along with its electrical connections is approximately 6 days. Installation data for 5MW turbines was available for the Alfa Ventus wind farm (www.alpha-ventus.de) and the Thornton bank wind farm (www.c-power.be). From these sources the installation time for one turbine in the Thornton bank wind farm was 35 days and for one turbine in Alfa Ventus was 17 days. This was primarily due to the distance of the farm from the shore because of which electrical infrastructure installation took up the bulk of the time (5 months for the Thornton bank project) and the fact that these activities did not occur together. Even if they did occur together, the time taken would have reduced to 30 days per turbine for the Thornton bank wind farm.

Coming to the turbine, the Thornton bank wind farm needed 11.5 days per wind turbine (excluding the support structure) while the Horns Rev wind farm only required 2 days per wind turbine (excluding the support structure). This was because in Horns Rev four tower + turbine installations were accomplished before the installation vessel headed back to port for more turbine components.

In the Thornton bank wind farm two jack-up vessels were used to install one wind turbine, after which the vessel transporting the rotor returned to port to get the next rotor.

Since the wind farms in this project utilized turbines the same size as that of the Thornton Bank project, it was decided to follow a similar installation procedure as that of the Thornton Bank wind farm. However, 11.5 days was considered inappropriate and instead the time taken to install the tower and nacelle-rotor assembly was based on the Horns Rev installation time i.e. two days.

The assumptions used for the installation are:

- One vessel will be used for the turbine installation
- The vessel will possess the ability to drive the monopile and the ability to install the tower, nacelle and the pre-assembled rotor.
- The vessel will have enough space on board to store two tower sections, the nacelle and the pre-assembled rotor.
- One jack up barge will be used to transport the above mentioned turbine components from port to site.
- The accessibility of the site remains the same during the installation of all turbines.

The assumed installation procedure is as follows:

First the monopile and transition piece of all turbines will be installed i.e. components 1 and 2 (see Figure 7-19). For this the installation vessel will remain at site while the transport barge delivers the required number of monopiles and transition pieces as and when the need arises.

After all monopiles and transition pieces of all turbines are installed, the tower, nacelle and rotor will be installed i.e. components 3 to 6 (see Figure 7-19). The transport barge will transport one set of components 3 to 6 to the site and jack itself up. The installation vessel which is already at the site will transfer the components from the transport barge

to itself. When the transfer is complete the installation vessel will begin installing the components and the transport barge will go back to port to pick up the components for the next turbine. When turbine installation is complete the installation vessel will move to the site of the next turbine to await the transport barge.

8 Implementation and Results

This chapter describes the implementation of the design process which was described in earlier chapters. Only one design iteration is presented here, namely the three-bladed turbine with an induction factor of 0.33 and $\lambda_{\text{design}}=8.3$. After the implementation the results of the entire iterative design process will be presented.

8.1 Rotor

As mentioned earlier the rotor was designed with a stepwise variation in the axial induction factor. The change in axial induction factor has a cascading effect. First the blade chord and twist distribution would change, leading to a different amount of material usage. This blade dimension change would affect the power generated and this therefore the AEY. The change in rotor weight changes the tower top mass and this along with the change in rotor loading has an effect on the support structure.

8.1.1 Blade dimensions

The blade dimensions were obtained using the basic equations from Chapter 6. As an example, chord and twist distributions for a three-bladed turbine ($\lambda_{\text{design}}=8.3$) with a design axial induction factor of 0.33 at each section are shown below in Figure 8-1. The optimal values in the figures are those obtained from the basic blade design equations. From the figure the effect of the different C_t 's can be seen. The abrupt changes in the chord and twist distributions show where the airfoil changes along the blade. For ease of manufacturing, linear forms of the optimal distributions were chosen. These are also shown in the figures.

The final chord and twist distributions for different induction factors are shown in Figure 8-2 for the three-bladed turbine. The inboard sections of the blade have been chamfered so that it meets the cylindrical blade root which has a diameter of 3.5m (for blade designs where it is needed) and the chord values at the blade tips have been reduced to 0.3. The twist has been brought to zero near the blade tips. The largest twist for each blade is at the section closest to the cylindrical section of the blade root.

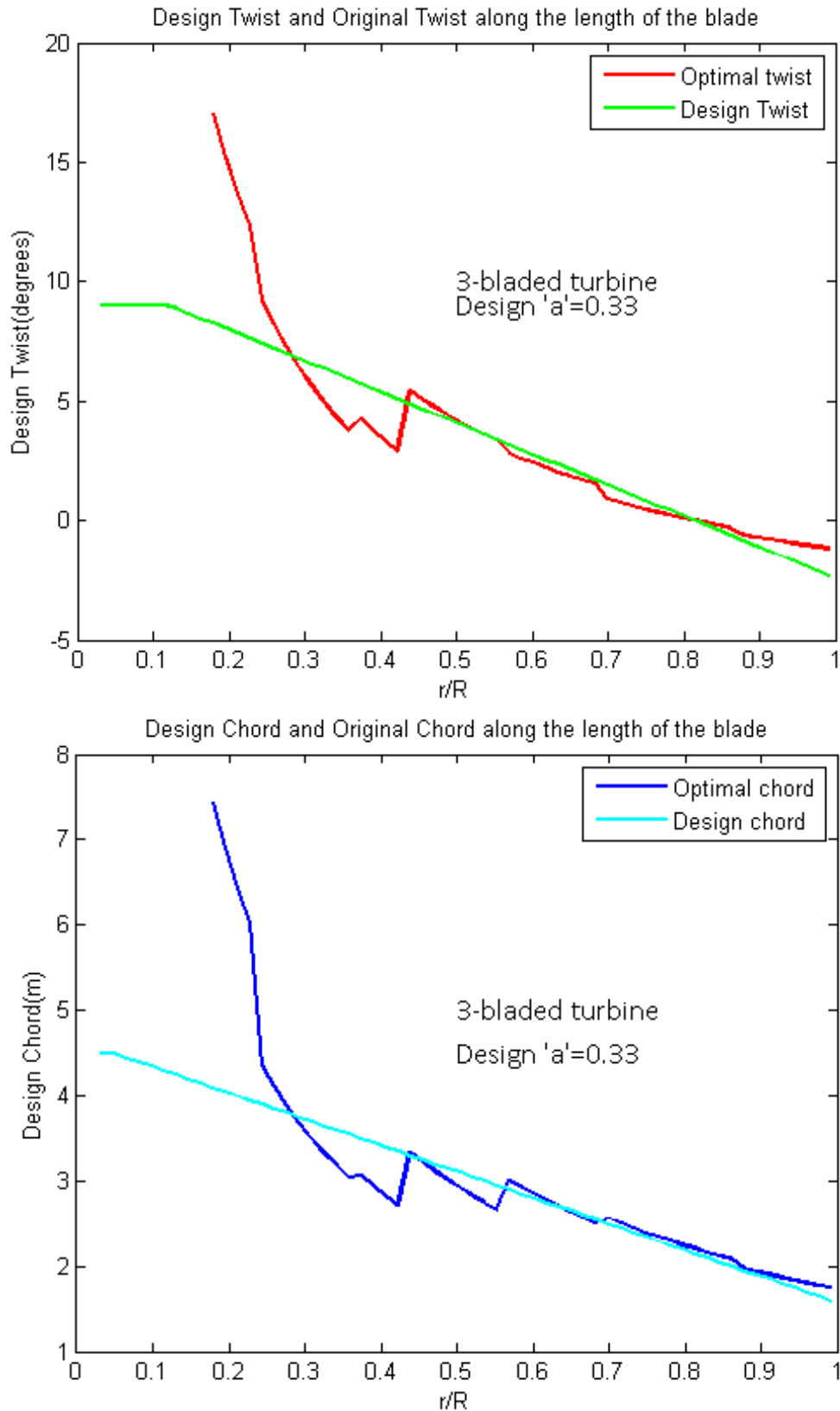


Figure 8-1: Optimal linearised twist and Design twist (Above), Optimal linearised chord and Design Chord (Below)

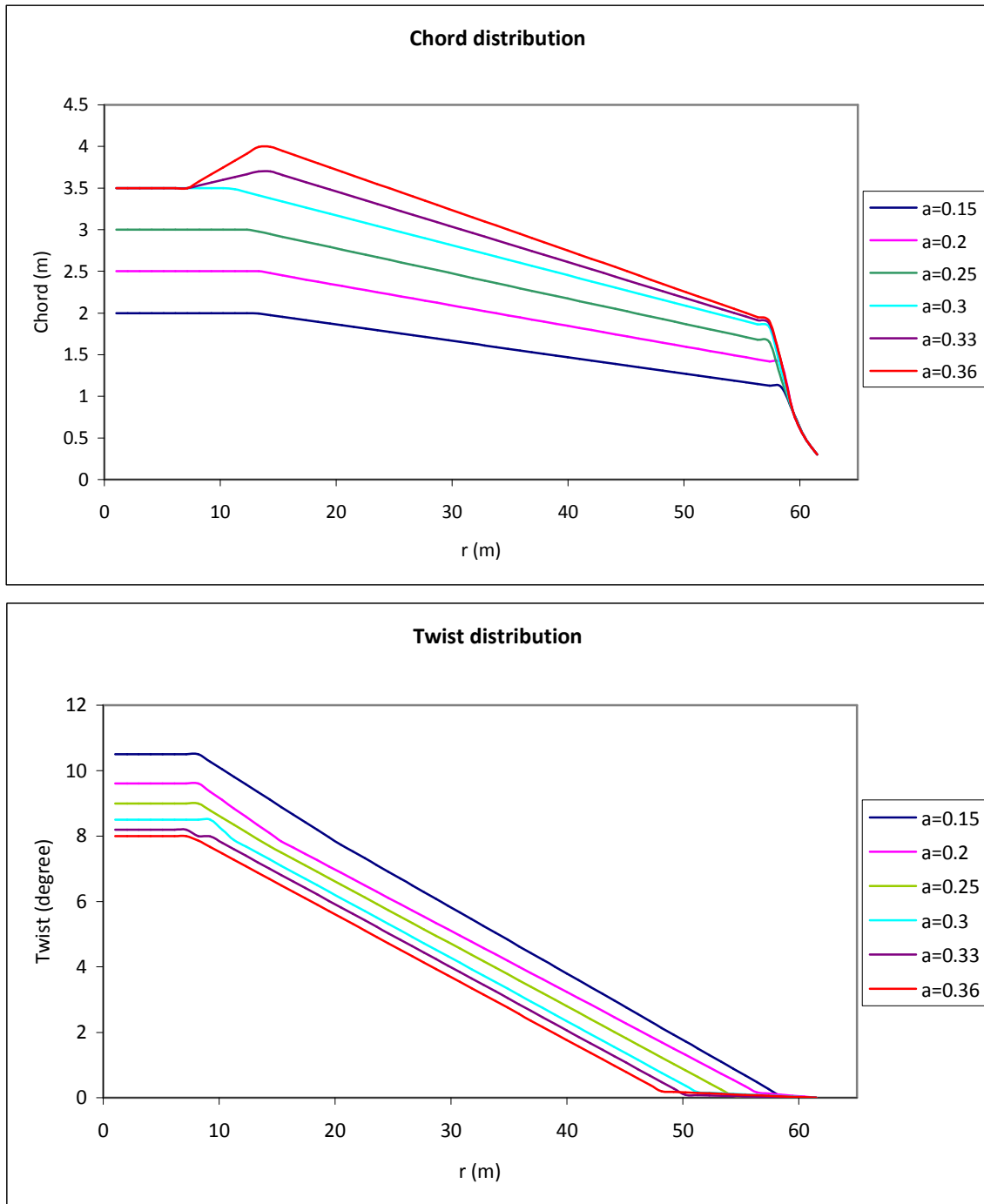


Figure 8-2: Chord (above) and Twist (below) distributions for the three-bladed turbine with $\lambda_{\text{design}}=8.3$ for different 'a' values

8.1.2 Blade Strength and Mass

Blades must be primarily designed for fatigue as they experience a large number of stress cycles during their 20 year life time. In addition to this, blades should be able to resist ultimate loads and finally the stiffness of the blade must be enough to prevent a

blade-tower strike. Based on these requirements the flapwise and edgewise second moments of inertia and stiffness were calculated using the initial dimensions obtained in Chapter 7, and is shown below in Figure 8-3 and Figure 8-4 respectively.

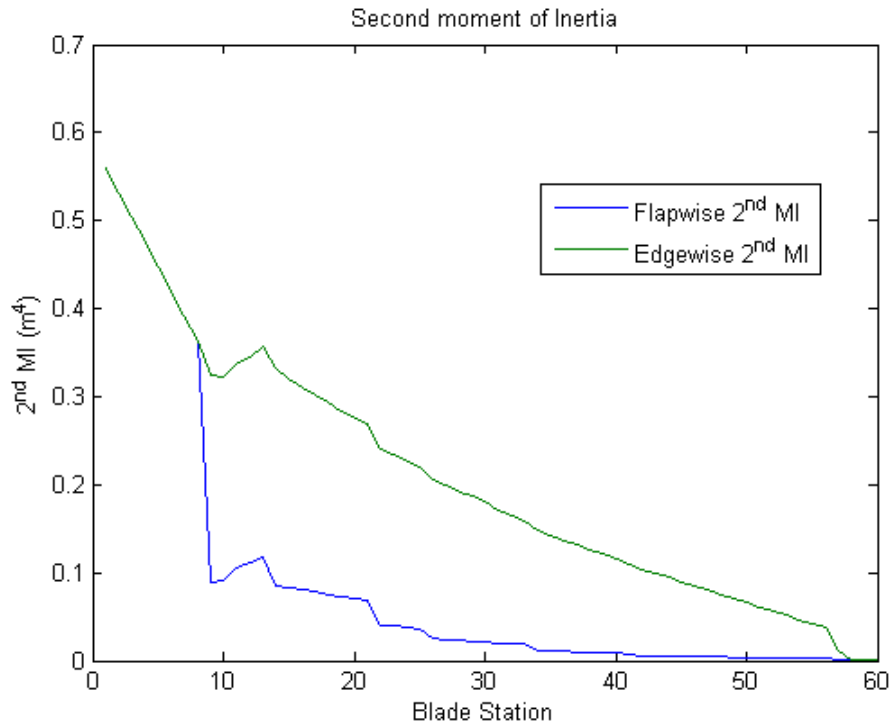


Figure 8-3: Second moment of area distribution (3-bladed, $\lambda_{design}=8.3$, $a=0.33$)

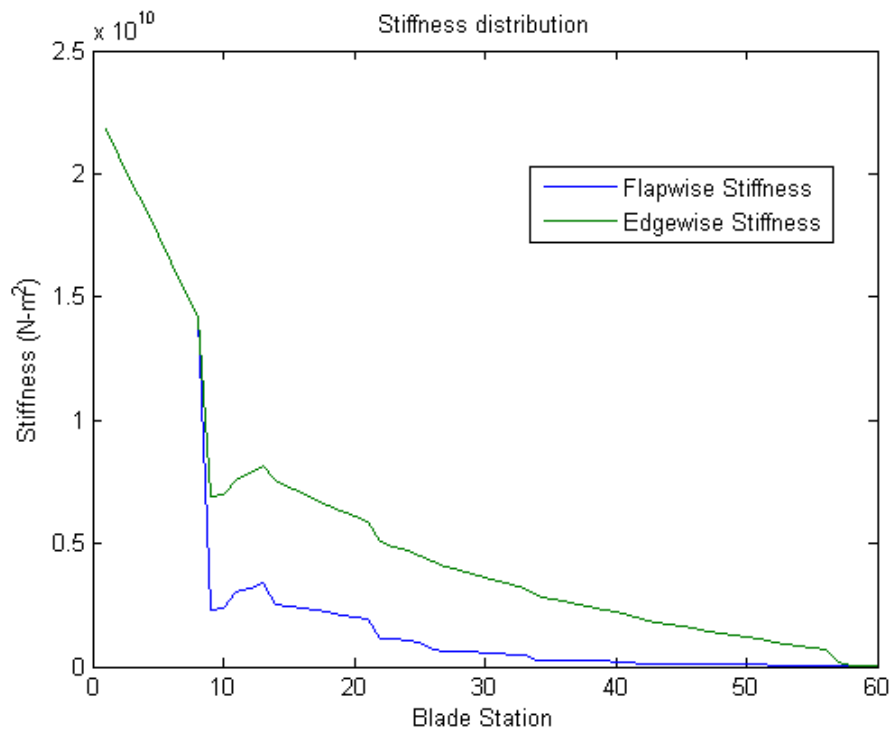


Figure 8-4: Stiffness distribution (3-bladed, $\lambda_{design}=8.3$, $a=0.33$)

The mass distribution of each element within the blade is shown below in Figure 8-5 and the total mass distribution of the blade is shown in Figure 8-6.

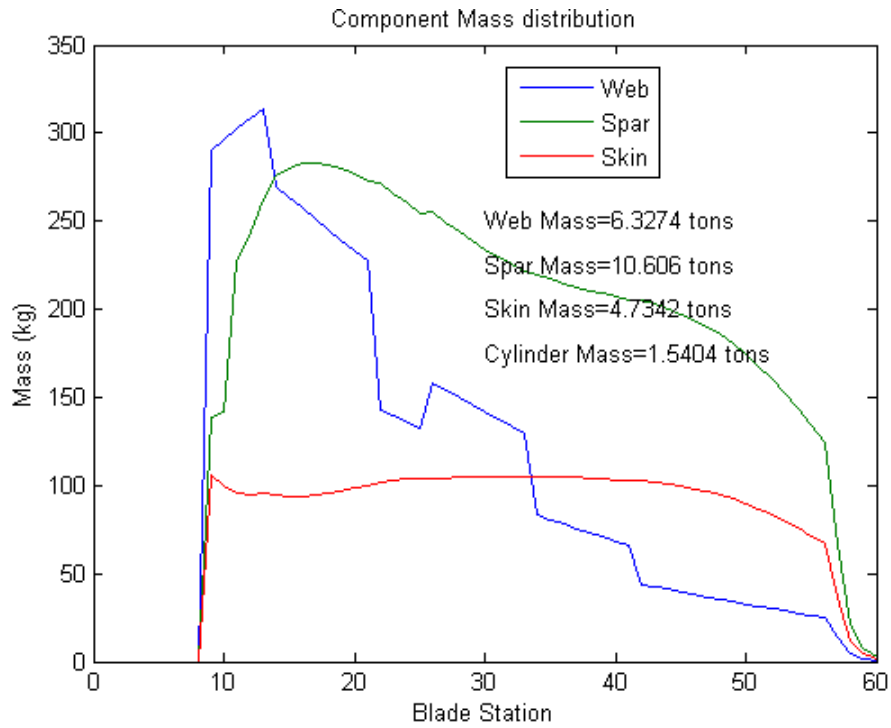


Figure 8-5: Mass distribution of each component (3-bladed, $\lambda_{design}=8.3$, $a=0.33$)

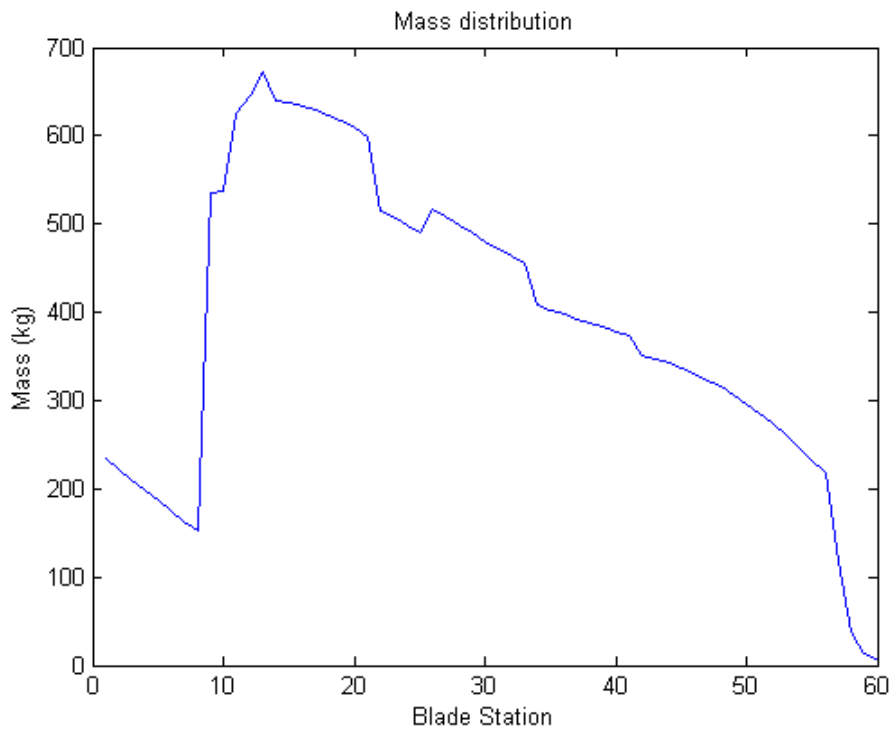


Figure 8-6: Total mass distribution (3-bladed, $\lambda_{design}=8.3$, $a=0.33$)

8.1.3 Rated Wind Speed

The rated wind speed for turbine operation is determined from the BEM code. As the axial induction factor was varied between 0.15 and 0.36, the rated wind speed of the turbine varied from 12.1 to 11 m/s for the three-bladed turbine with $\lambda_{\text{design}}=8.3$. Since the blades were designed for one λ_{design} this means that the rotational speed of the rotor also varied.

8.1.4 Design and Operating curves from the BEM code

The chord and twist distributions thus obtained along with the airfoil polars obtained from Chapter 7 constitute the blade. The blade was analysed to obtain the power generated and the axial thrust on the rotor. As an example a three-bladed rotor ($\lambda_{\text{design}}=8.3$) was used with a design axial induction factor of 0.33. See Appendix I for a set of design and operating curves for this example rotor.

8.1.5 Blade verification checks

Flapwise bending moment is the dominant contributor towards blade loading. Figure 8-7 shows the flapwise bending moment at different span locations along the length of the blade. The bending moments at the root are the highest and they decrease along the length of the blade.

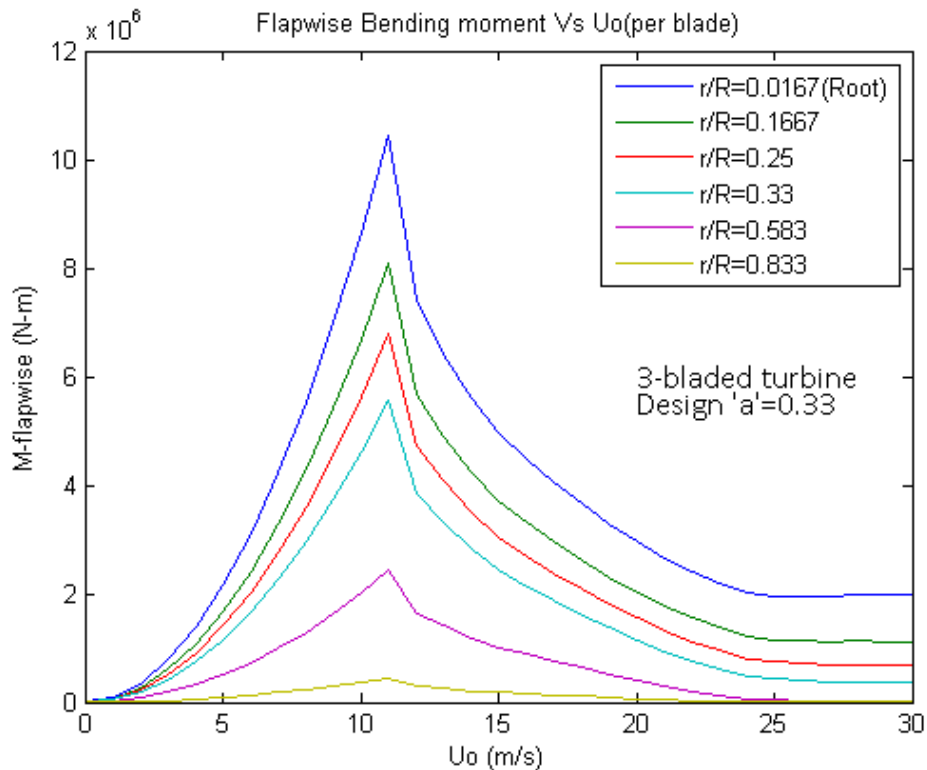


Figure 8-7: Flapwise bending moment at different span locations

8.1.5.1 Blade Deflection

From Bladed 3.80 the deflection of the blade tip was obtained. In this example the largest deflection of 5.25m occurs at a wind velocity of 13.61 m/s i.e. at sea state 8. The blade tower clearance is calculated below. See Figure 8-8 and Table 8-1.

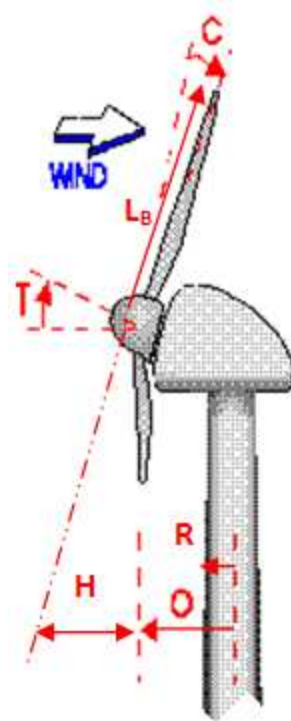


Figure 8-8: Determining blade tower clearance

Table 8-1: Determining blade tower clearance

Parameter	Abr.	Value	Source
Blade length	L_B	61.5 m	Chapter 2
Cone angle	C	2°	NREL reference turbine
Tilt angle	T	5.5°	NREL reference turbine
Total angle	-	7.5°	$C+T$
Horizontal distance	H	8 m	$=L_B \times \sin(C+T)$
Overhang	O	5m	NREL reference turbine
Tower radius	R	3.35m	Chapter 8
Blade tower clearance	-	9.5m	$=H+O-R$

The blade tower clearance in this example meets the minimum requirements to prevent a tower strike for the maximum blade tip deflection. If the blade tower clearance can be reduced, then costs can be reduced because the overhang and the tilt angle can be reduced. However, quantifying these cost reductions is not in the scope of this report. Changing the blade stiffness to save mass while maintaining the minimum requirements

for blade-tower clearance can be done, but it was thought better to wait for the results of the fatigue analysis before attempting this.

8.1.5.2 Ultimate Loads

From Bladed, the largest combined flapwise and edgewise root bending moment was obtained. The stress at the root section due to this bending moment was calculated as 37.5 Mpa. This is much lower than the ultimate stress of the hollow circular section material which is 550 MPa (Optimat, 2006).

8.1.5.3 Blade Fatigue

The fatigue analysis was done using Bladed. The dimensions of the internal structure of the airfoil and the hollow cylindrical section at the blade root were modified suitably to withstand fatigue damage during the turbines 20 year operational life.

The blade mass was found to be around 26.4 tons.

8.2 Nacelle

The masses of the components in the nacelle were found using the NREL scaling relations. These individual masses of each component were translated into money using the quantities determined in Chapter 5. The total mass which was found to be 341 tons (including the rotor) was used in the design of the support structure. See Table 8-4 for masses of the nacelle components obtained for all iterations.

8.3 Support Structure

The procedure to design the support structure was outlined in the previous chapter. Some of the results are discussed in this section.

8.3.1 Foundation Pile

Using the Foundation Pile Analysis Tool it was estimated that a pile length of 35m was needed to ensure that the toe kick was less than 0.02m. With this pile length pile deflections at the sea bed did not cross 0.1m. The pile diameter is the same as the base diameter of the tower (which was finally selected as 6.7m.)

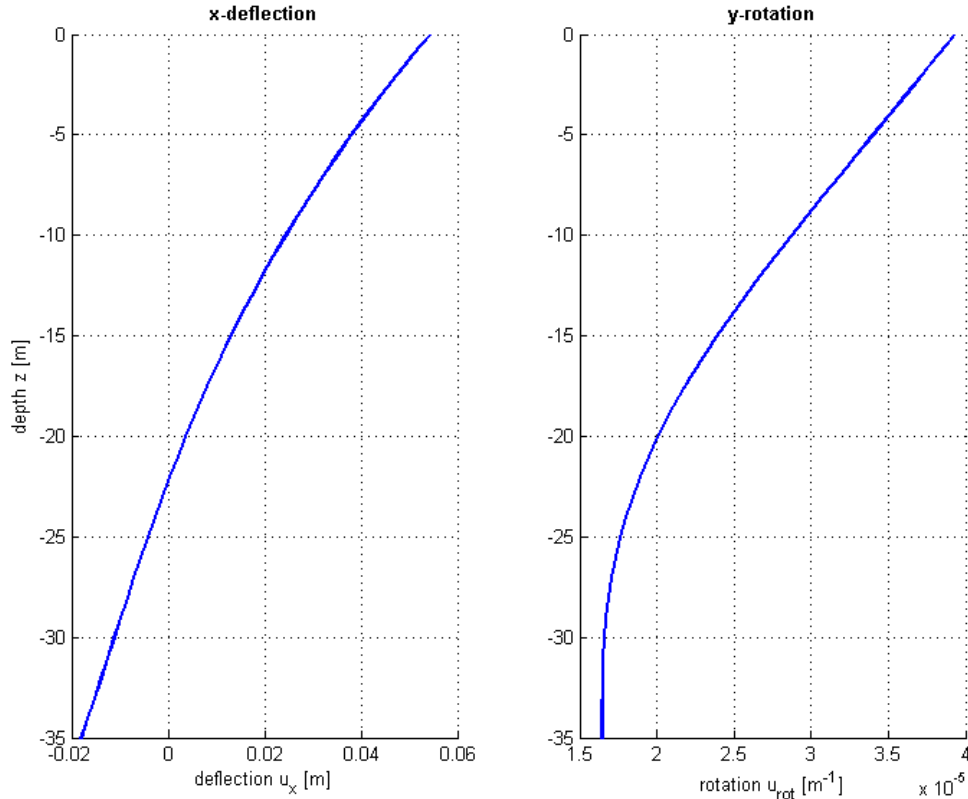


Figure 8-9: Lateral and rotational pile deflections at the seabed and at the pile toe

With this pile length the rotational and lateral stiffness played a role to ensure that the support structure's natural frequency stayed above the 1-P region. The mass of steel used for this foundation pile is 274 tons. The translational and rotational stiffness was found to be 19.5×10^6 N/m and 3.29×10^{12} Nm/rad.

8.3.2 Tower

Preliminary tower designs based on the natural frequency analysis indicated that the required outer diameter of the tower base was around 5.5m with a wall thickness of 7cm. Bar and shell buckling checks showed that the support structure would not fail due to buckling. However the primary design driver in this case was fatigue because of the wind and wave conditions of the chosen site. Fatigue of the support structure is highest at the seabed level because of the combined effect of wind and wave loading resulting in a fluctuating bending moment at the seabed level. Fatigue at the mean sea level (splash zone) is also high due to wave impact on the support structure. Fatigue on the tower is relatively lower. Maintaining the outer diameter of the tower at 5.5m and increasing the wall thickness to design for fatigue resulted in uneconomical steel usage. So, the outer diameter was increased as well. In this example, a support structure with base diameter of 6.7 and a tower top diameter of 4m was designed (shown below in Figure 8-10). A constant diameter was maintained for the tower from seabed level to the platform level. From the platform to the tower top the diameter decreased linearly. The thickness of the pile at seabed level was 13.5 cm (corresponds to a

diameter/thickness ratio of 50) which was found sufficient to overcome fatigue failure. The calculated natural frequency of the tower is 0.3 Hz and the mass of steel used for the tower was found to be 1685 tons.

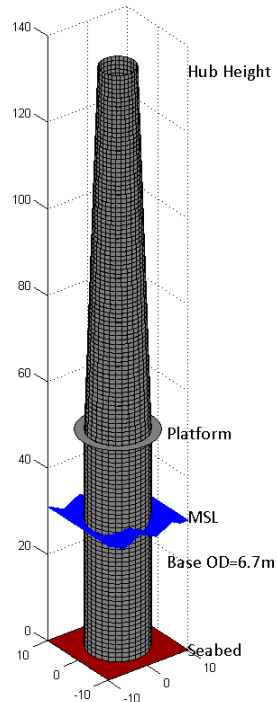


Figure 8-10: Support structure with base diameter of 6.7m

8.4 Installation

The time split for component installation was based on a time lapsed video of an onshore 1.5 MW wind turbine installation at NREL (www.youtube.com). This was compared with other available time lapsed videos of turbine installation to confirm that the time periods obtained were accurate enough. Based on this and the information from Chapter 7, a breakup of time required for the installation procedure for each turbine was found. See Table 8-2. These figures may not be extremely accurate but sufficed for the purposes of this report.

Table 8-2: Time Breakup for Installation Procedures

Component	Working time (hrs)		Source
	2-bladed	3-bladed	
Component 1	6	6	www.prinsesamaliawindpark.eu/
Component 2	2	2	assumed
Component 3	7.81	7.81	NREL installation video
Component 4	10.05	10.05	NREL installation video
Component 5	18.98	18.98	NREL installation video
Component 6	-	11.16	NREL installation video
Total	44.9	56	

Since the turbine considered for the NREL cost model was a three-bladed 5MW turbine the cost per turbine is 646500 €. The total time taken to install one three-bladed turbine is 56 hours. Therefore the cost per hour is $646500/56=11545$ €. The costs are shown below in Table 8-3.

Table 8-3: Installation costs

Installation cost	11545	€/hour
Turbine	Installation time (hours)	Installation cost (€)
100 Three-bladed turbines	$100 \times 56 = 5600$	64650000
100 Two-bladed turbines	$100 \times 44.9 = 4490$	51835446

8.5 Results

This completed one design iteration. The mass distributions were obtained and using the quantities from Chapter 5, the investment cost was obtained. From this the LPC of energy was obtained. Design iterations were carried out for all cases when the axial induction factor was changed and the LPC of energy was obtained for all cases. The results are discussed below for the rotor, nacelle and support structure. Table 8-4 shows the tabulated results for all iterations and finally the LPC's for all the iterations are shown.

From the investment cost calculated it was concluded that the cost of spare parts will not play a significant role in the operation and maintenance costs as the concept changes. Therefore the assumption made earlier regarding the cost of spare parts was valid.

8.5.1 Rotor

With the implementation of the BEM code, it was noticed that as the induction factors increased, C_p increased; until it reached its highest value (around 0.52) which

corresponded to induction factors between 0.3 and 0.36. See Figure 8-11. (This is the example of the three-bladed turbine with $\lambda_{design}=8.3$).

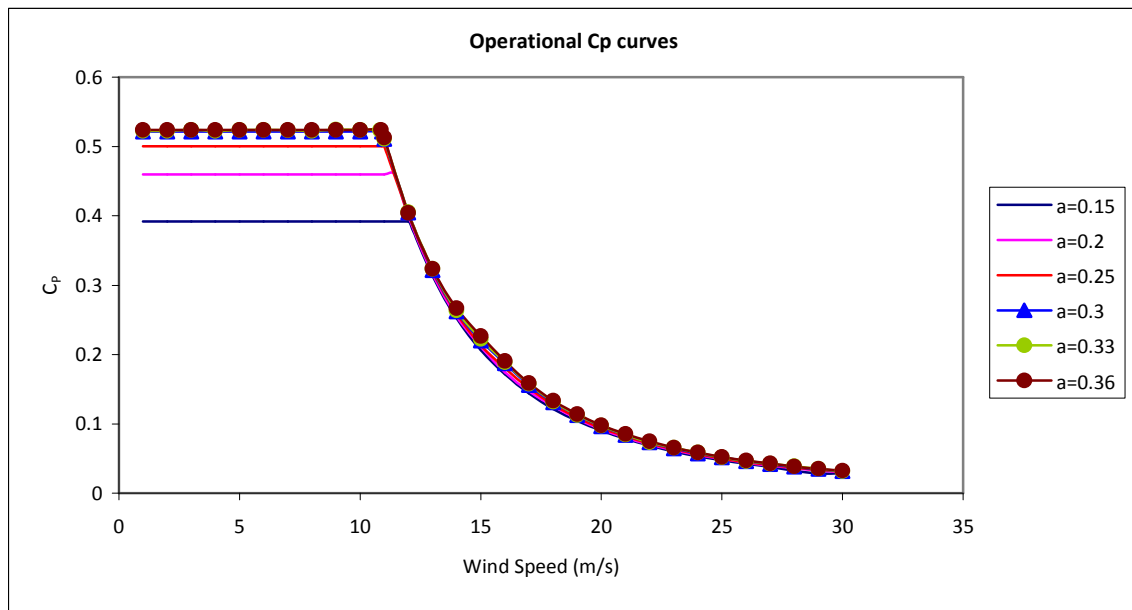


Figure 8-11: C_p vs Wind Speed as 'a' changed

The corresponding C_T versus wind speed curves are shown below in Figure 8-12. It can be seen that the thrust coefficient continues to increase as the design induction factor increases. This means that designing for induction factors higher than 0.33 leads to higher loads on the rotor while yielding no additional power than what it produces at design ' a '=0.33.

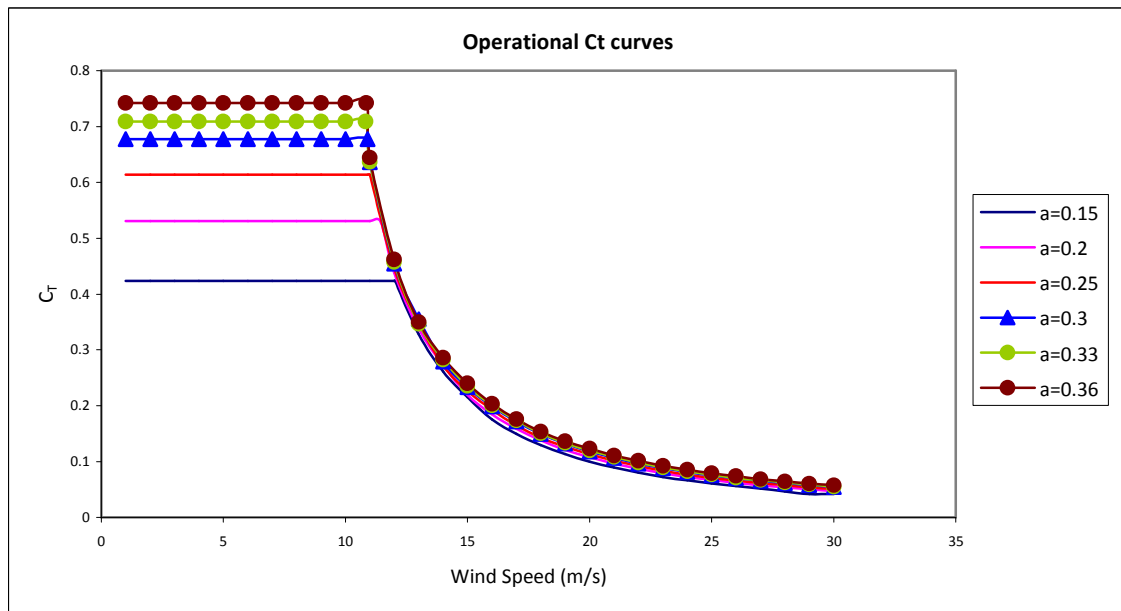


Figure 8-12: C_T vs Wind Speed as 'a' changed

The rotor costs of the two-bladed turbine were found to be cheaper than that of the three-bladed turbine. See Figure 8-13. This was as expected. Another result of the fatigue analysis was that blades with design induction factors lesser than 0.25 could be designed only with an uneconomical use of material. This is because lower induction factors meant lower chords and this led to lower blade strength. Fatigue analyses indicated that the strength was insufficient and hence the blade internal structure needed more material. Plotting those values did not allow the variations for design induction factors greater than 0.25 to be observed clearly and therefore they are omitted from the final result.

The rotor costs of the three-bladed turbine with a $\lambda_{\text{design}}=9.8$ after induction values of 0.33 were slightly lesser than the rotor costs of the two-bladed turbine. As the chord increased (when $a>0.3$) it was found that strength calculated was sufficient to withstand fatigue and it was not required to use more material in the blade. For the three-bladed turbine with $\lambda_{\text{design}}=9.8$, it was not possible to design reasonably economical rotors for induction factors lesser than 0.3.

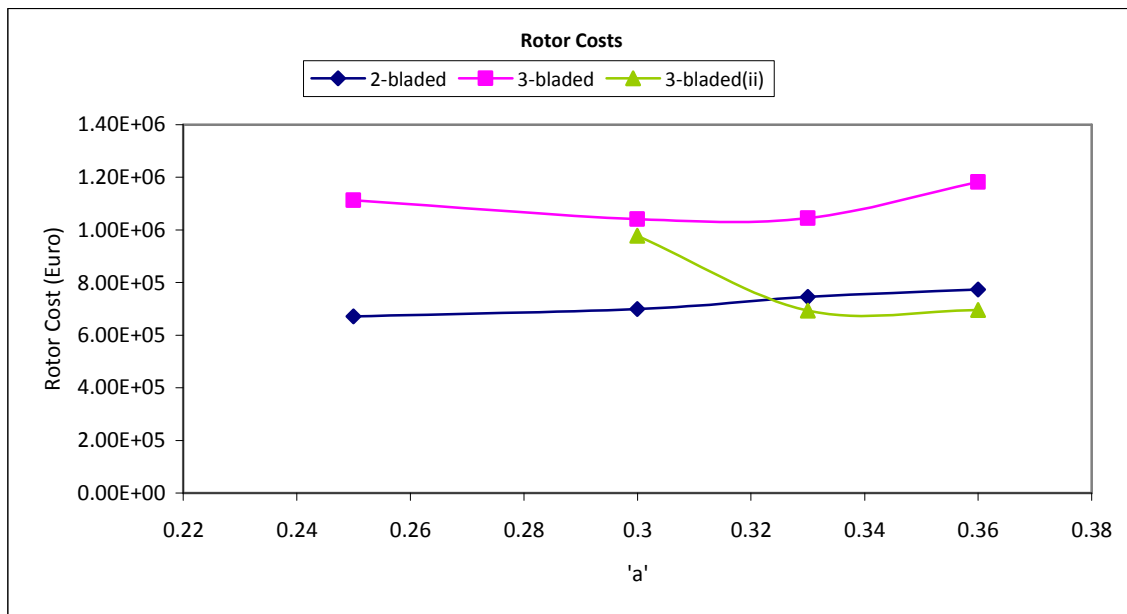


Figure 8-13: Rotor Costs as 'a' changes

The AEY of the three-bladed rotors was higher than that of the two-bladed rotor. See Figure 8-14.

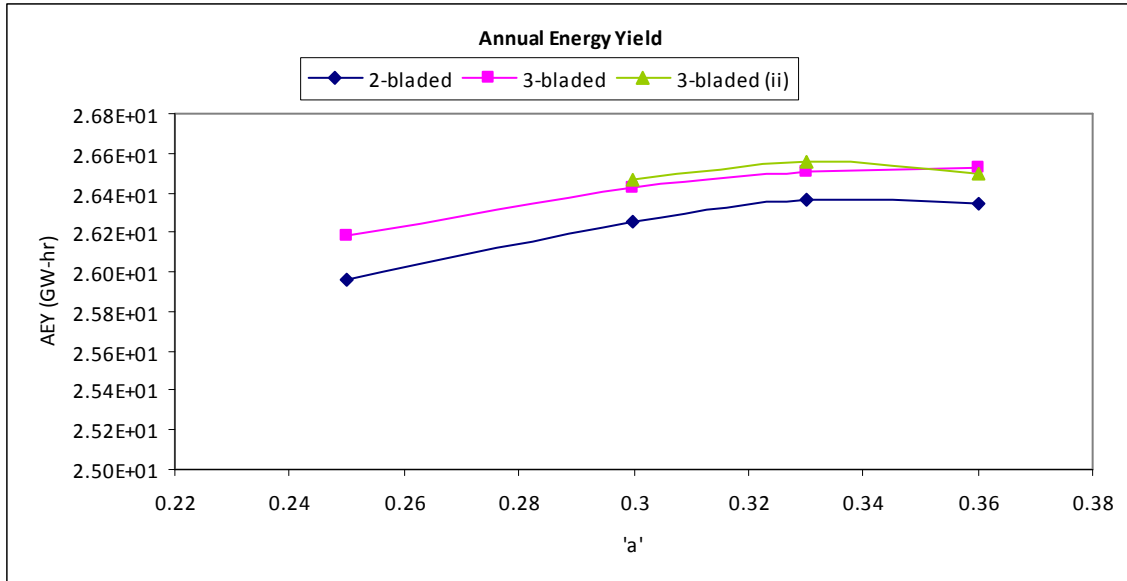


Figure 8-14: AEY as induction factor changed

8.5.2 Nacelle

In the nacelle a change in mass was observed. The tower top mass is shown in Figure 8-15. A large difference in mass between the two-bladed turbine and the three-bladed turbine with $\lambda_{\text{design}}=8.3$ was not observed, even though the gearbox mass of the two-bladed turbine is lesser than the three-bladed turbine with $\lambda_{\text{design}}=8.3$. This is because the equation used to model the yaw drive mass is a function of the blade root bending moment and this leads to the mass of the yaw drive of the two-bladed making up for the lesser weight of the gearbox. On the other hand the tower top mass of the three-bladed turbine with $\lambda_{\text{design}}=9.8$, after 'a' values of 0.3 was lower than the tower top mass of the other two turbines. This is mostly because of the lower rotor mass.

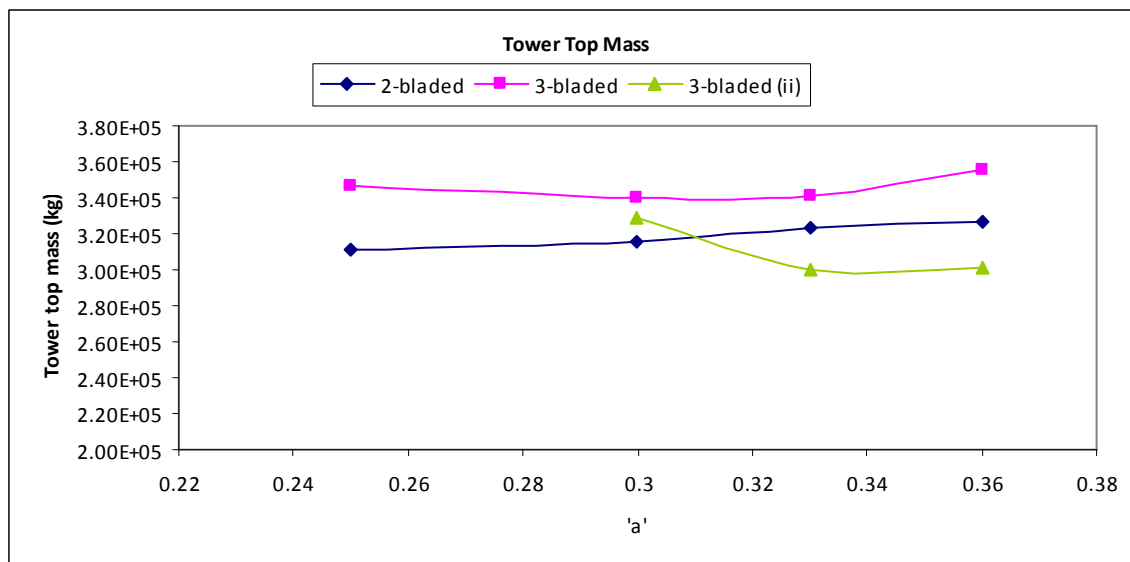


Figure 8-15: Tower top mass as 'a' changes

8.5.3 Support Structure

The support structure contributed to the larger LPC of the two-bladed turbine. Because of the small soft-stiff region in between the 1-P and the 2-P regions it was difficult to design a monopile type support structure which satisfied both natural frequency requirements and fatigue damage requirements. On the other hand, for three-bladed turbines, it was possible to find a suitable outer diameter for the support structure and a suitable inner diameter such that both fatigue and natural frequency requirements were satisfied.

The 1-P and N-P regions for the three-bladed turbine and the two-bladed turbine are shown in Figure 8-16 and Figure 8-17 respectively.

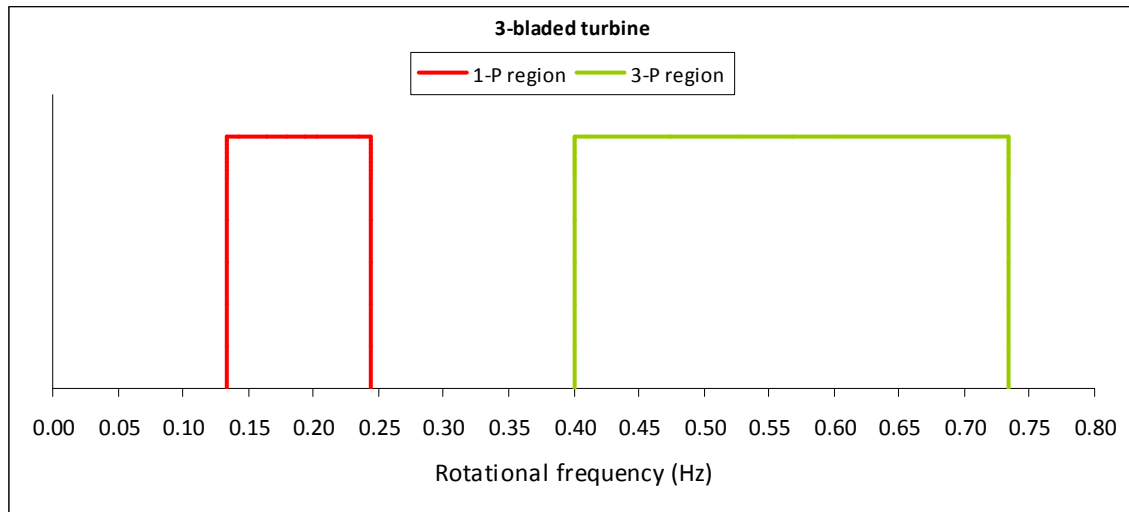


Figure 8-16: 1-P and 3-P regions for the three-bladed turbine with $\lambda_{\text{design}}=8.3$

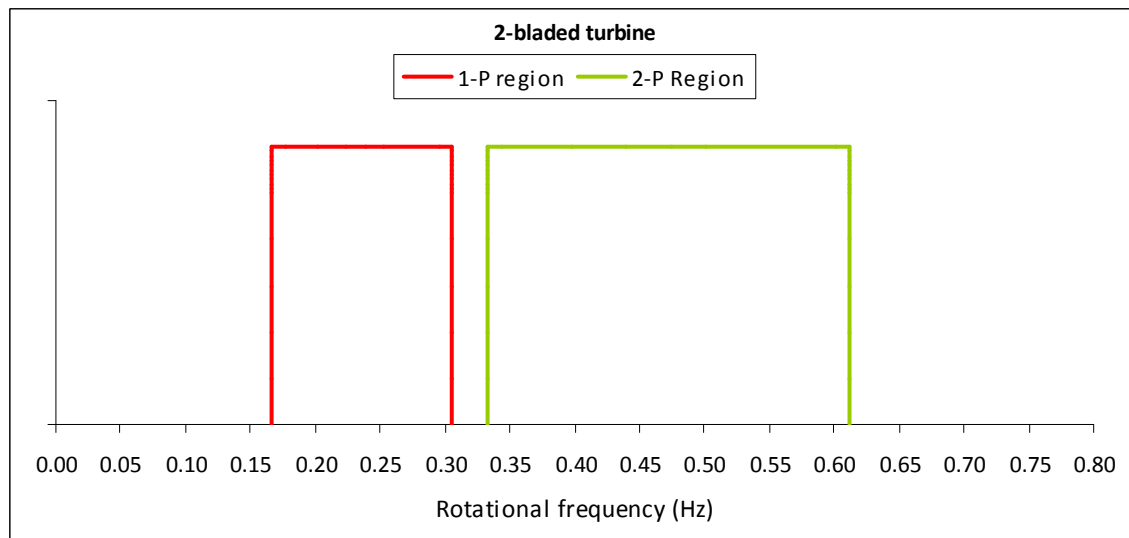


Figure 8-17: 1-P and 2-P regions for the two-bladed turbine with $\lambda_{\text{design}}=9.8$

Finally an optimum outer diameter and wall thickness for the two concepts were obtained. Optimum in this case means most economical. These dimensions were utilized for all two-bladed and three-bladed turbines designed as it resulted in the most economic usage of steel. Figure 8-18 shows the difference in support structure costs which resulted from a mass difference of around 150 tons of steel. This extra steel for the two-bladed turbine was used near the seabed because the fatigue analysis showed that the two-bladed turbine's support structure at the seabed was more prone to failure than the three-bladed turbine's.

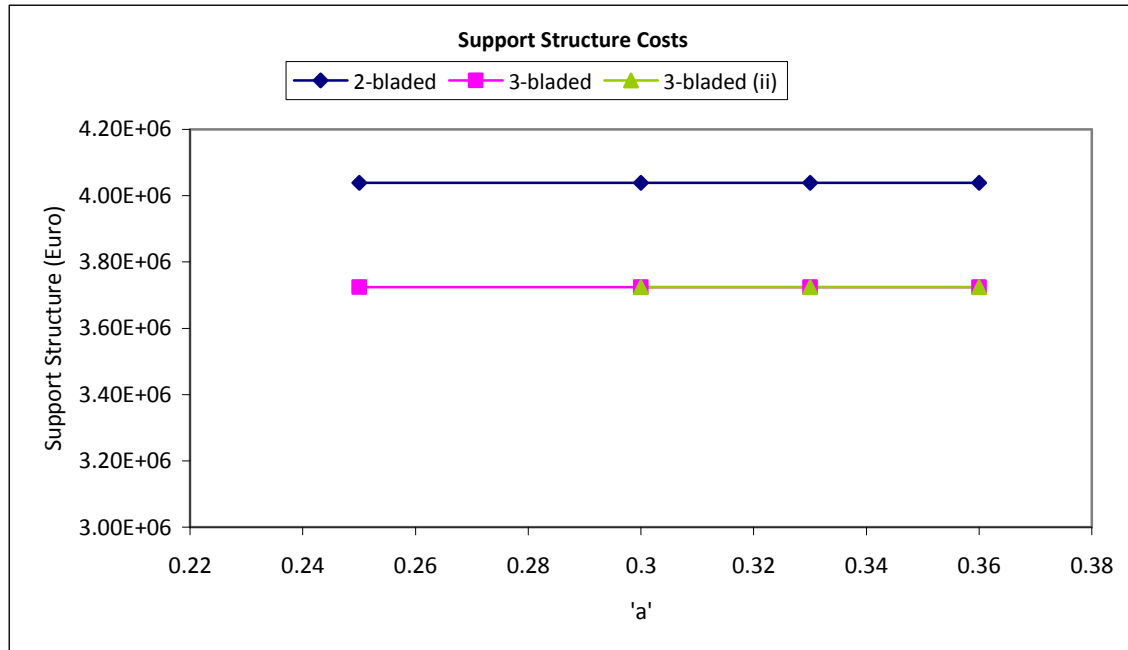


Figure 8-18: Support Structure Costs

8.5.4 Results for all iterations

Table 8-4 shows the tabulated results for the component masses, rotor thrust, rotor torque, root flapwise bending moment and tower top mass for all iterations undertaken. Table 8-5 shows the tabulated results for the AEY, component costs, installation and O&M costs for all iterations undertaken along with the LPC obtained.

Table 8-4: Tabulated results for component masses, rotor thrust, rotor torque, root flapwise bending moment and tower top mass for all iterations

Sl. No.	Axial Induction Factor	Mass (kg)								Rotor Thrust (N)	Rotor Torque (Nm)	Root Flapwise moment (Nm)	Tower top mass (kg)
		Blade (single)	Support Structure	Hub	Pitch mechanism (total)	Gearbox	Generator	Yaw drive	Nacelle				
3-bladed $\lambda_{design}=8.3$													
1	0.25	2.81E+04	1.96E+06	3.25E+04	6.04E+03	3.22E+04	1.67E+04	8.73E+03	1.66E+05	6.20E+05	3.40E+06	8.20E+06	3.46E+05
2	0.3	2.63E+04	1.96E+06	3.08E+04	5.73E+03	3.22E+04	1.67E+04	9.71E+03	1.66E+05	6.70E+05	3.40E+06	8.80E+06	3.40E+05
3	0.33	2.64E+04	1.96E+06	3.08E+04	5.74E+03	3.22E+04	1.67E+04	1.04E+04	1.66E+05	7.00E+05	3.40E+06	9.20E+06	3.41E+05
4	0.36	2.98E+04	1.96E+06	3.41E+04	6.34E+03	3.22E+04	1.67E+04	1.07E+04	1.66E+05	7.30E+05	3.40E+06	9.40E+06	3.55E+05
2-bladed $\lambda_{design}=9.8$													
1	0.25	2.55E+04	2.13E+06	3.00E+04	5.59E+03	2.77E+04	1.67E+04	1.55E+04	1.66E+05	6.10E+05	2.80E+06	1.20E+07	3.12E+05
2	0.3	2.65E+04	2.13E+06	3.10E+04	5.76E+03	2.77E+04	1.67E+04	1.75E+04	1.66E+05	6.50E+05	2.80E+06	1.30E+07	3.18E+05
3	0.33	2.82E+04	2.13E+06	3.26E+04	6.06E+03	2.85E+04	1.67E+04	1.85E+04	1.66E+05	6.90E+05	2.90E+06	1.35E+07	3.25E+05
4	0.36	2.93E+04	2.13E+06	3.36E+04	6.24E+03	2.85E+04	1.67E+04	1.92E+04	1.66E+05	7.00E+05	2.90E+06	1.38E+07	3.29E+05
3-bladed $\lambda_{design}=9.8$													
1	0.3	2.47E+04	1.96E+06	2.92E+04	5.45E+03	2.85E+04	1.67E+04	9.38E+03	1.66E+05	6.60E+05	2.90E+06	8.60E+06	3.29E+05
2	0.33	1.75E+04	1.96E+06	2.24E+04	4.22E+03	2.85E+04	1.67E+04	1.02E+04	1.66E+05	6.90E+05	2.90E+06	9.10E+06	3.00E+05
3	0.36	1.76E+04	1.96E+06	2.24E+04	4.23E+03	2.85E+04	1.67E+04	1.09E+04	1.66E+05	7.20E+05	2.90E+06	9.50E+06	3.01E+05

Table 8-5: Tabulated results for AEY, component costs, installation costs, O&M costs and LPC for all iterations

Sl. No.	Axial Induction Factor	AEY (GWhr)	Investment cost (Euro)									Total investment cost (Euro)	Annual O&M cost (Euro)	LPC (€/kWh)
			Rotor	Support Structure	Hub	Pitch mechanism (total)	Gearbox	Generator	Yaw drive	Nacelle	Installation			
			3-bladed $\lambda_{design}=8.3$											
1	0.25	26.1816	1.11E+06	3.72E+06	3.05E+05	1.06E+05	7.49E+05	4.26E+05	9.86E+04	1.63E+06	6.47E+05	1.05E+07	1.80E+05	0.04011
2	0.3	26.4224	1.04E+06	3.72E+06	2.89E+05	1.01E+05	7.49E+05	4.26E+05	1.10E+05	1.63E+06	6.47E+05	1.04E+07	1.80E+05	0.039474
3	0.33	26.5035	1.04E+06	3.72E+06	2.90E+05	1.01E+05	7.49E+05	4.26E+05	1.17E+05	1.63E+06	6.47E+05	1.05E+07	1.80E+05	0.039397
4	0.36	26.5293	1.18E+06	3.72E+06	3.21E+05	1.12E+05	7.49E+05	4.26E+05	1.21E+05	1.63E+06	6.47E+05	1.06E+07	1.80E+05	0.039934
2-bladed $\lambda_{design}=9.8$														
1	0.25	25.9572	6.72E+05	4.04E+06	2.82E+05	9.83E+04	6.47E+05	4.26E+05	1.75E+05	1.63E+06	5.18E+05	1.02E+07	1.80E+05	0.039464
2	0.3	26.256	6.99E+05	4.04E+06	2.91E+05	1.01E+05	6.47E+05	4.26E+05	1.98E+05	1.63E+06	5.18E+05	1.03E+07	1.80E+05	0.039208
3	0.33	26.3652	7.45E+05	4.04E+06	3.06E+05	1.07E+05	6.64E+05	4.27E+05	2.09E+05	1.63E+06	5.18E+05	1.03E+07	1.80E+05	0.03935
4	0.36	26.3464	7.72E+05	4.04E+06	3.16E+05	1.10E+05	6.64E+05	4.26E+05	2.16E+05	1.63E+06	5.18E+05	1.04E+07	1.80E+05	0.039516
3-bladed $\lambda_{design}=9.8$														
1	0.3	26.4614	9.78E+05	3.72E+06	1.52E+05	9.60E+04	6.64E+05	4.26E+05	1.06E+05	1.63E+06	6.47E+05	1.02E+07	1.80E+05	0.038505
2	0.33	26.5578	6.94E+05	3.72E+06	1.16E+05	7.43E+04	6.64E+05	4.26E+05	1.15E+05	1.63E+06	6.47E+05	9.82E+06	1.80E+05	0.037335
3	0.36	26.3683	6.96E+05	3.72E+06	1.17E+05	7.44E+04	6.64E+05	4.26E+05	1.23E+05	1.63E+06	6.47E+05	9.83E+06	1.80E+05	0.037444

8.5.5 LPC

The final LPC's obtained are shown below in graphical form. The lowest LPC of the three-bladed turbine with $\lambda_{\text{design}}=8.3$ is 3.94 €/kWhr and was obtained at a design axial induction factor of 0.33. See Figure 8-19.

The lowest LPC of the two-bladed turbine with $\lambda_{\text{design}}=9.8$ is 3.92 €/kWhr and was obtained at a design axial induction of 0.3. See Figure 8-20.

The lowest LPC of the three-bladed turbine with $\lambda_{\text{design}}=9.8$ is 3.73 €/kWhr and was obtained at a design axial induction factor of 0.33. See Figure 8-21. This was the lowest LPC of all design iterations.

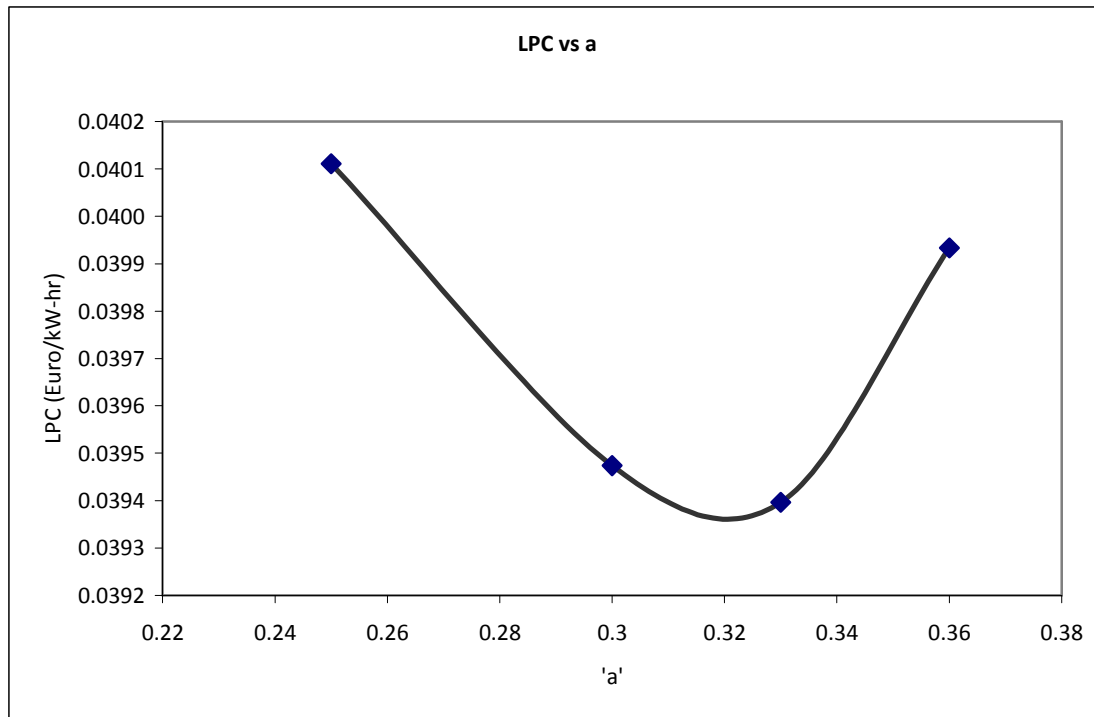


Figure 8-19: LPC variations for the three-bladed turbine with $\lambda_{\text{design}}=8.3$

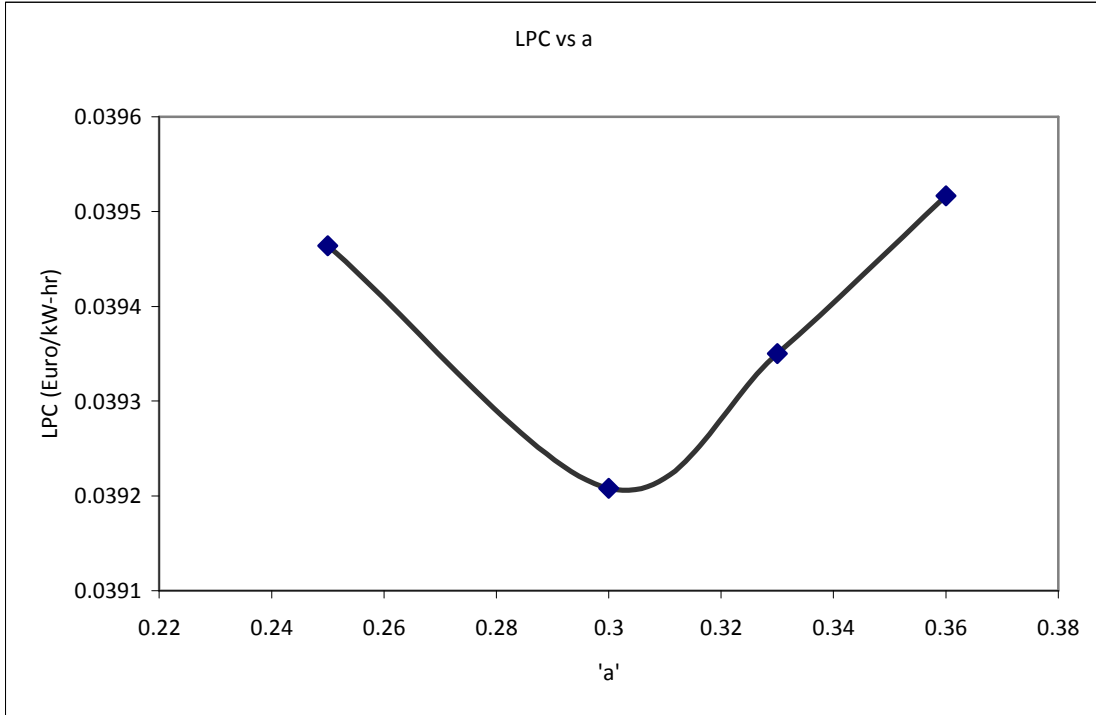


Figure 8-20: LPC variations for the two-bladed turbine with $\lambda_{\text{design}}=9.8$

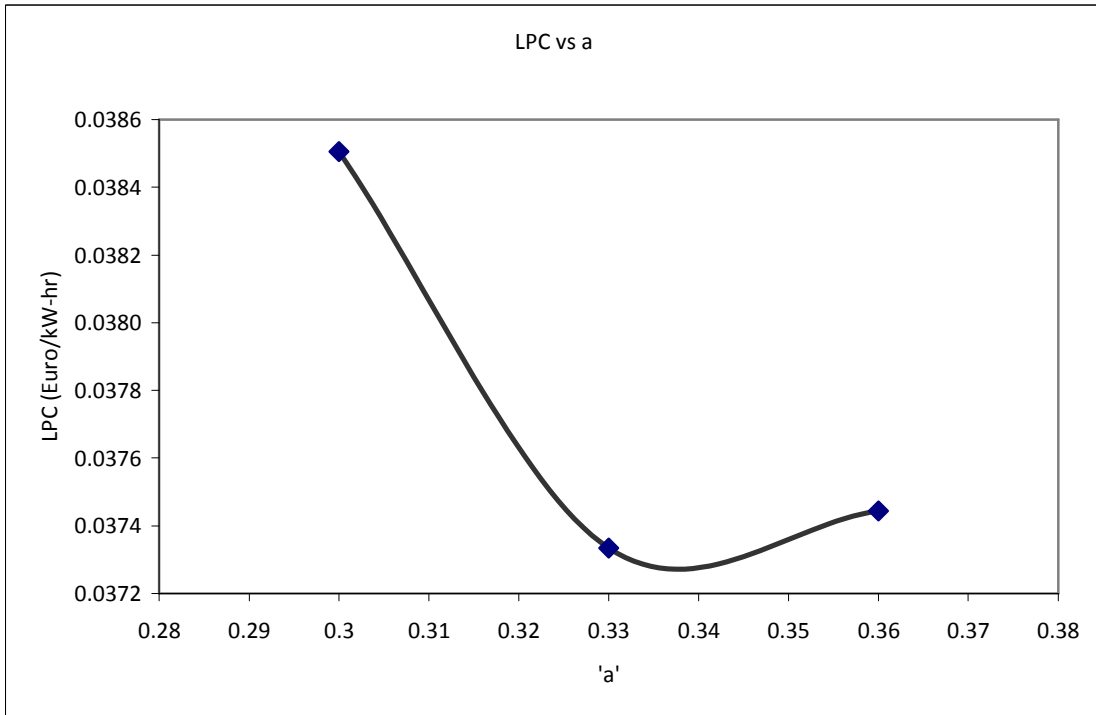


Figure 8-21: LPC variations for the three-bladed turbine with $\lambda_{\text{design}}=9.8$

8.6 Final note

Finally, it may be conceivable that as turbines become larger, the rotor could play a more significant role in contributing to the investment cost thus implying that the two-bladed turbine would yield a lower LPC. With this in mind, a fictional 10 MW turbine with a rotor diameter of 170m was modeled using the NREL scaling relations. The contributions are shown below in Figure 8-22, along with turbines used in the industry today.

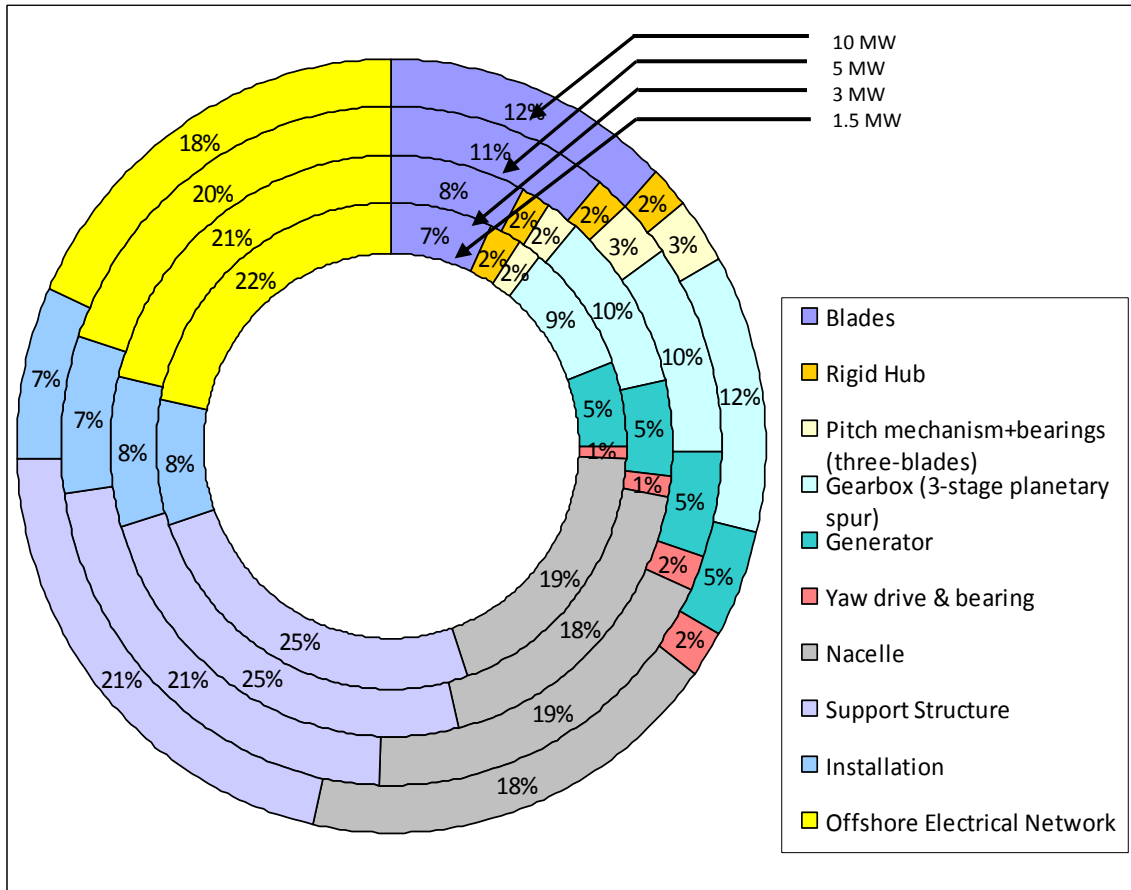


Figure 8-22: Cost breakup for turbines with ratings of 1.5MW, 3MW, 5MW and 10 MW

From the figure it can be seen that the contributions of the blades have increased slightly and the support structure costs have hardly changed as the turbine rating increases from 5MW to 10MW. Of course, all this is based on the premise that the NREL scaling relations is applicable for a turbine with a 170m rotor diameter.

As turbines become bigger and are installed further offshore, it is most probable that the monopile type support structure becomes less favorable economically and there would be a preference for other types of support structures. This would more or less put the two-bladed and three-bladed concepts on an equal footing with regard to support structures.

9 Conclusions and Recommendations

After the design implementation of the previous chapter the conclusions reached are presented below. After this some recommendations are given.

9.1 Conclusions

All discussions in this section pertain to the turbines with the lowest LPC's.

The results of this thesis show that the differences in LPC between the three-bladed turbine with $\lambda_{\text{design}}=8.3$ and the two-bladed turbine with $\lambda_{\text{design}}=9.8$ is minimal. However the difference in LPC between the two-bladed turbine with $\lambda_{\text{design}}=9.8$ and the three-bladed turbine with $\lambda_{\text{design}}=9.8$ is significantly larger. A discussion with regard to this difference follows:

9.1.1 Rotor Cost

The rotor of the three-bladed turbine with $\lambda_{\text{design}}=8.3$ costs about 1.04 million Euro. This is about 0.3 million Euro larger than the rotor cost of the two-bladed turbine. However the rotor cost of the three-bladed turbine with $\lambda_{\text{design}}=9.8$ is approximately equal to that of the two-bladed turbine.

The lightest blade belonged to the three-bladed turbine with $\lambda_{\text{design}}=9.8$. Each blade had a mass of about 17.5 tons leading to a total blade mass of about 53 tons (three blades). The mass of the blade of the two-bladed rotor was 26.5 tons which also lead to a total blade mass of about 53 tons (two blades).

9.1.2 AEY

The AEY of the two-bladed concept is lower than that of the three-bladed concept. The difference between the concepts is approximately 0.25 GWhr per year. This contributed significantly to the difference in LPC's.

9.1.3 Nacelle

The difference in gearbox mass between the turbine with $\lambda_{\text{design}}=8.3$ and turbines with $\lambda_{\text{design}}=9.8$ was found to be a little over 4 tons. However, the yaw drive of the two-bladed turbine was about 7 tons higher because its mass was modeled on the basis of the root flapwise bending moment. The hub masses of all turbines were modeled on the basis of individual blade mass. This lead to the three-bladed turbine with $\lambda_{\text{design}}=9.8$, having the lowest hub mass.

The tower top mass of the three-bladed turbine with $\lambda_{\text{design}}=9.8$ was about 300 tons which was the lowest. The two-bladed turbine had a tower top mass of 316 tons and the three-bladed turbine with $\lambda_{\text{design}}=8.3$ had a tower top mass of 341 tons.

9.1.4 Support Structure

As explained earlier, fatigue was the design driver and so the outer diameter and wall thickness of the monopile were chosen such that it resulted in the most economic usage of steel. This led to the steel mass of the two-bladed concept being higher than that of

the three-bladed turbine(s) which translated to cost difference of 0.32 million Euro. This difference more or less closed the gap between the three-bladed turbine with $\lambda_{\text{design}}=8.3$ and the two-bladed turbine with regard to investment cost. However it gave a further advantage to the three-bladed turbine with $\lambda_{\text{design}}=9.8$.

Even though the tower top mass of the three-bladed with $\lambda_{\text{design}}=9.8$ and two-bladed turbine was lower than the three-bladed turbine with $\lambda_{\text{design}}=8.3$, it did not yield any advantage with respect to support structure design. This is because at this site, fatigue considerations determined the design of the support structure.

9.1.5 Installation

The installation cost of the two-bladed concept was lower than that of the three-bladed concept(s). The difference was approximately 0.13 million Euro which gave the two-bladed turbine a slight advantage over the three-bladed turbine with $\lambda_{\text{design}}=8.3$ when the total investment cost was calculated. However, this was not enough to go lower than the investment cost of the three-bladed turbine with $\lambda_{\text{design}}=9.8$.

9.2 Recommendations

9.2.1 Better blade design

The blade designs used in this report were very basic in nature and the ideal chord and twist distribution were linearised for ease of manufacturing. This serves well for a first iteration. For the next iteration, it might be possible to use blade designs which more closely follow the ideal chord and twist distribution.

The blade designs in this report were obtained using an axial induction factor which was constant over the length of the blade. This need not necessarily give the lowest LPC. Varying the axial induction factor along the blade length (to deal with manufacturing requirements near the blade root or to design for tip loss effects at the blade tip) may result in lower LPC's.

Thus aero-structural design of the rotor with a view to reducing the LPC, both by increasing AEY and by decreasing amount of material used for the rotor seems to be the way forward.

In this report blade erosion was not considered. From offshore turbine designs prevalent today, it is clear that many operate at a λ_{design} of 7. It is though that blade erosion is a major factor for this. For the next iteration, it is therefore recommended to investigate the effect of choice of λ_{design} on blade erosion.

9.2.2 New airfoils

With current airfoils available it can be seen that the AEY of a two-bladed turbine will not be higher than that of a three-bladed turbine. This is an important factor as it seems to be the primary reason that the LPC of the two-bladed turbine is not much lower than that of the three-bladed turbine. Therefore one of the main recommendations would be to investigate new airfoils for the two-bladed turbine or design specific airfoils for the two-bladed turbine.

It is not certain if this will give the two-bladed concept an advantage as the same can be done for the three-bladed turbine. However, it can be said that from the fatigue analysis of the three-bladed turbine with $\lambda_{\text{design}}=9.8$ a slender blade requires more material to satisfy structural requirements. This might give the two-bladed turbine an advantage in terms of lesser material usage because of its (expected) larger chord.

9.2.3 New Support Structure

With the monopile design it was seen that large diameters were used and due to the nature of the loading, monopile design was governed by fatigue. This led to large thicknesses, especially at the seabed level. The pile thickness at the seabed was 13cm for the three-bladed turbine and 15 cm for the two-bladed turbine. This led to a larger amount of steel usage and therefore a higher cost for the two-bladed turbine.

Alternate support structures that can be used are the jacket support structure or the tripod support structure. These structures use a lower amount of steel but the labor costs involved in fabricating them thus far have ensured that they are more expensive than monopiles. However, for these site conditions and turbine size a tripod or jacket type support structure may turn out to be cheaper than the monopile.

9.2.4 Teetering Hub Effects

A teetering hub provides significant cost reduction on the nacelle, the yaw drive and the low speed shaft, but the complexity of the system offsets these savings (Burton, et al., 2001). In this report, the load reducing effects of the teetering hub were not taken into account, although the higher cost of the teetering hub was factored into the LPC calculation. Modeling the cost reduction on the above mentioned components due to the teetering hub will give a more accurate picture of the LPC of the two-bladed turbine.

References

- Areva Multibrid, 2010.** Viewed 10th May 2010. <<http://www.multibrid.com/>>
- Auszac EcoBalsa, 2007.** Balsa Wood Properties guide. <www.auszac.com>. Australia.
- BARD Offshore, 2010.** Viewed 3rd May 2010. <<http://www.bard-offshore.de/>>
- Benschop, H. 1996.** *Windsnelheidsmetingen op zeestations en kuststations: herleiding warden windsnelheid naar 10-meter niveau.* KNMI, the Netherlands.
- Burton, T., Sharpe, D., Jenkins, N., Bossanyi, E., 2001.** *Wind energy Handbook.* West Sussex. John Wiley & Sons, Ltd.
- van Bussel, G.J.W Henderson, A.R. , Morgan, C.A., Smith, B., Barthelmie,R.,Argyriadis,K., Arena, A., Niklasson, G., Peltola, E., N.D.** *State of the Art and Technology Trends for Offshore Wind Energy: Operation and Maintenance Issues.*CA-OWEE.
- van Bussel, G.J.W., Zaaier, M.B., 2001.** *Reliability, Availability and Maintenance aspects of large-scale offshore wind farms, a concepts study.* Section Wind Energy, Technical University of Delft, the Netherlands.
- Cockerill, T.T., Harrison, R., Kühn, M., van Bussel, G.J.W., 1997.** *Opti-OWECS Final Report Vol. 3:Comparison of Cost of Offshore Wind Energy at European Sites.* Delft University of Technology, the Netherlands.
- Danish Energy Authority, 2006.** <<http://193.88.185.141/>>
- Fingersh, L., Hand, M. and Laxson, A., 2006.** *Wind Turbine Design Cost and Scaling Model.* Technical Report NREL/TP-500-40566, National Renewable Energy Laboratory, USA.
- GE Drivetrain Technologies, N.D.** *Wind Turbine gearbox brochure.*
- Gerdes, G., Tiedemann, A., Zeelenberg, S., N.D.** *Case Study: European Offshore Wind Farms – A survey to analyze lessons learnt by developers of offshore wind farms.* POWER.
- Germanischer Lloyd IV-2, 2004.** *Guidelines for Certification of Offshore Wind Turbines.* Germanischer Lloyd, WindEnergie.
- GL, beaufort 6, 2008.** *Wind energy newsletter for customers and business partners. Edition 1/2008.* Germanischer Lloyd.
- Green, J., Bowen, A., Fingersh. L.J., Wan, Y., March, 2007.** *Electrical Collection and Transmission Systems for Offshore Wind Power.* Conference Paper NREL/CP-500-41135. National Renewable Energy Laboratory, USA.
- Hau, E., 2006.** *Wind Turbines: Fundamentals, Technologies, Application, Economics.* Berlin. Springer-Verlag Berlin Heidelberg.
- Horns Rev Offshore Wind Farm, N.D.** <<http://www.hornsrev.dk>>
- IEC 61400-3, 2006.** *Part 3: Design requirements for offshore wind turbines.* International Electrotechnical Commission.
- Jamieson, P., 2009.** *Light Weight, High Speed Rotors for Offshore.* Paper presented at European Offshore Wind, 2009.
- Jonkman, J., Butterfield, S., Musial, W. and Scott, G., 2009.** *Definition of a 5MW Reference Wind Turbine for Offshore System Development.* Technical Report NREL/TP-500-38060, National Renewable Energy Laboratory, USA.

- LM Glasfiber, 2010.** LM Glasfiber, Denmark, viewed 22nd March, 2010 < www.lmglasfiber.com>
- Lund, E., Johansen, L.S., N.D.** *On buckling optimization of a wind turbine blade.* Department of Mechanical Engineering, Aalborg University, Denmark.
- Malcolm, D.J. and Hansen, A.C., 2006.** *WindPACT Turbine Rotor Design Study.* Subcontract Report NREL/SR-500-32495. National Renewable Energy Laboratory, USA.
- Manwell J.F., McGowan J.G., Rogers A.L., 2006.** *Wind Energy Explained.* West Sussex John Wiley & Sons, Ltd.
- Menck Offshore Pile Driving, 2010.** Menck GmbH, Kaltenkirchen, Germany.
- Nedergaard, L., 2008.** *Transport, Installation and Service Support of Offshore Wind Turbines.* A2Sea, Denmark.
- Offshore Standard DNV-OS-J101, 2004.** *Design of Offshore Wind Turbine Structures.* Det Norske Veritas.
- Offshore Wind Energy Europe, 2008.** *Technology of Offshore Wind Energy.* Viewed 6th April 2010 < www.offshorewindenergy.org>
- Optimat Blades, 2006.** *Reliable optimal use of materials for Wind Turbine Rotor Blades.* Project funded by the European community under the EESD Program (1998-2002).
- Opti-Owecs, 1996.** *E-mail correspondence within the Opti-Owecs team dated 18th October 1996.*
- Oud, J.C., 2002.** *Foundation design monopile: Comparison, extra steel consumption versus scour protection.* DOWEC, the Netherlands.
- Paul, A.J., 2010.** *A qualitative analysis of the two-bladed wind turbine for offshore wind farms.* System Integration Project – II, Technical University of Delft, the Netherlands
- Polinder, H., Morren, J., 2005.** *Developments in wind turbine generator systems.* Paper presented at Electrimacs, 2005.
- RE Power Systems, 2009.** Viewed 3rd May 2010. < <http://www.repower.de>>
- van Rooij, R.P.J.O.M., 2003.** *Description of the aerodynamic design process for a wind turbine rotor.* Section Wind Energy, Technical University of Delft, the Netherlands.
- Snel, H., N.D.** *Appendix A of Task 11 of the DOWEC Project: Selection of feasible concepts.* Energy Research Centre of the Netherlands, the Netherlands.
- Sørensen, T., Nielsen, P., Thøgersen, M.L., 2006.** *Recalibrating Wind Turbine Wake Model parameters – Validating the wake model performance for large offshore wind farms.* Paper presented at EWEC 2006.
- van der Tempel, J., 2006.** *Design of Support Structures for Offshore Wind Turbines.* PhD Dissertation, Technical University of Delft, the Netherlands.
- The British Wind Energy Association, N.D.** *Prospects for Offshore Wind Energy.* A report written for the EU (Altener contract XVII/4.1030/Z/98-395)
- Viterna, L.A., Corrigan, R.D., 1981.** *Fixed pitch rotor performance of large horizontal axis wind turbines.* NASA Lewis Research Centre, USA.
- de Vries, E., 2007.** *Heading Offshore-fast: Bard Engineering.* Renewable Energy World International Magazine. <www.renewableenergyworld.com> Viewed 14th June, 2010.
- de Vries, E., 2009.** *REPower Systems: Less is more offshore.* Renewable Energy World International Magazine. <www.renewableenergyworld.com>. Viewed 14th June, 2010.
- de Vries, W.E., 2009.** *Email correspondence from W.E., de Vries.*

de Vries, W.E., Krolis, V.D. 2007. *Effects of deep water on monopile support structures for offshore wind turbines.* Paper presented at EWEC 2007.

de Vries, W., and van der Tempel, J., 2007. *Quick Monopile Design.* Paper presented at EWEC 2007.

Zaaijer, M.B., 2000. *Starting-point and Methodology of Cost Optimisation for the Conceptual Design of DOWEC.* Section Wind Energy, Technical University of Delft, the Netherlands.

Zaaijer, M.B., 2003. *O&M aspects of the wind farm.* DUWIND, Technical University of Delft, the Netherlands.

Appendix I: Example Design and Operating curves for one iteration

Design Curves

Figure 1 through Figure 6 show the axial tangential factor, power coefficient, thrust coefficient, rotor thrust, rotor power and rotor torque along the length of the blade.

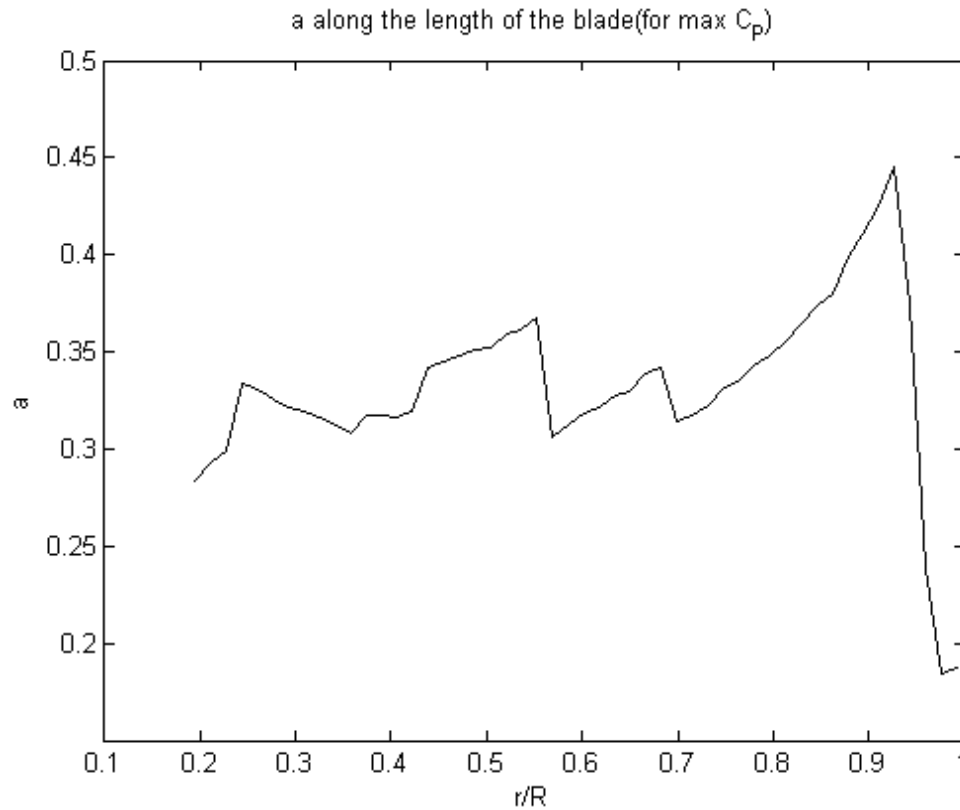


Figure 1: Axial induction factor along the length of the blade

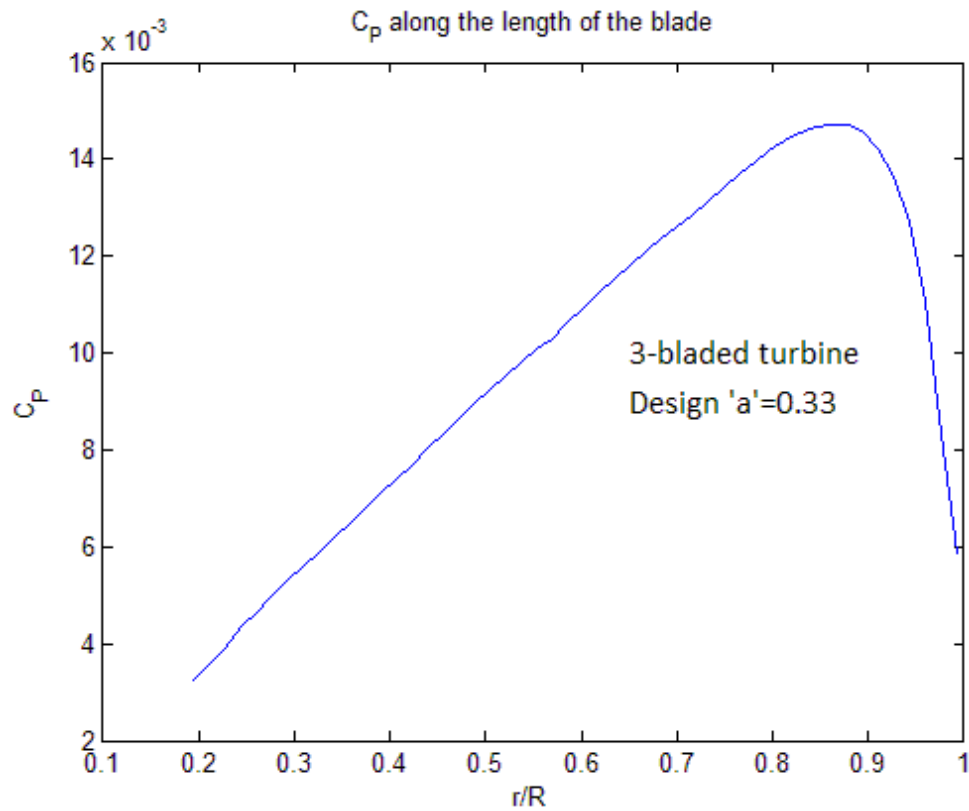


Figure 2: Power coefficient along the length of the blade

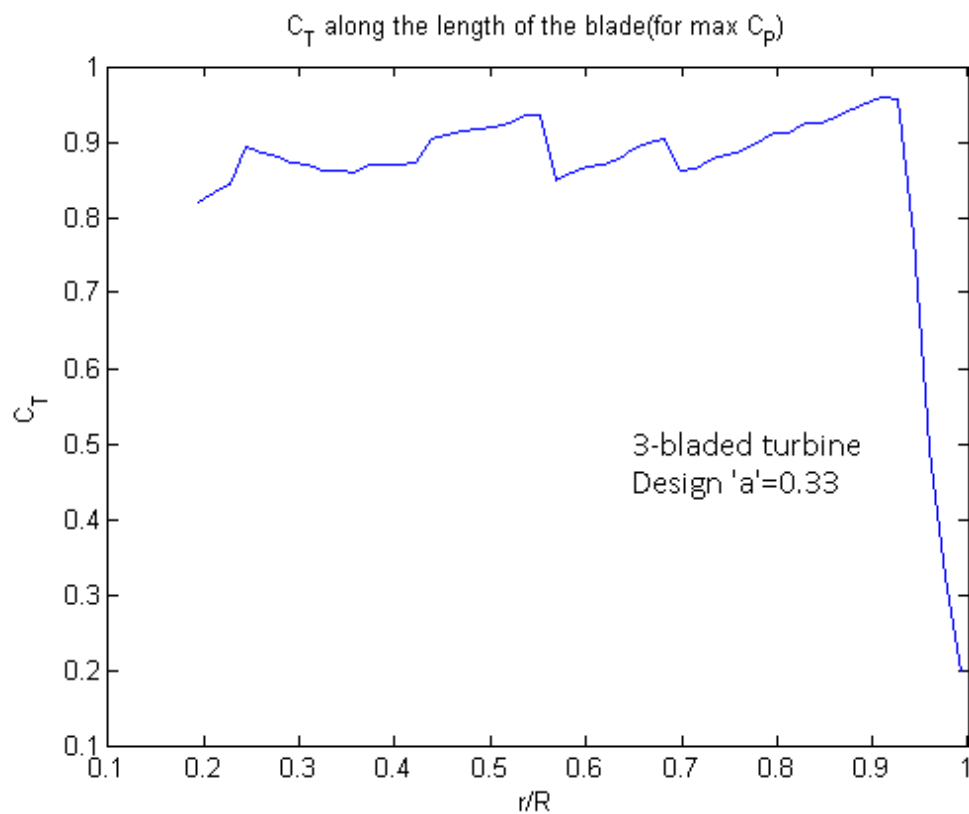


Figure 3: Thrust coefficient along the length of the blade

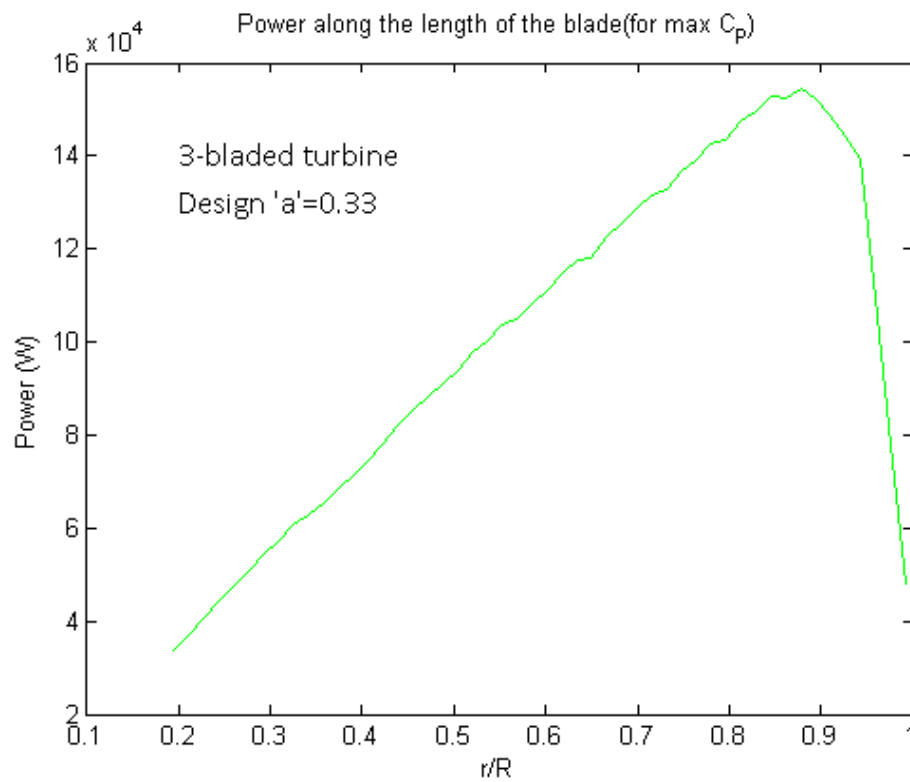


Figure 4: Power along the length of the blade

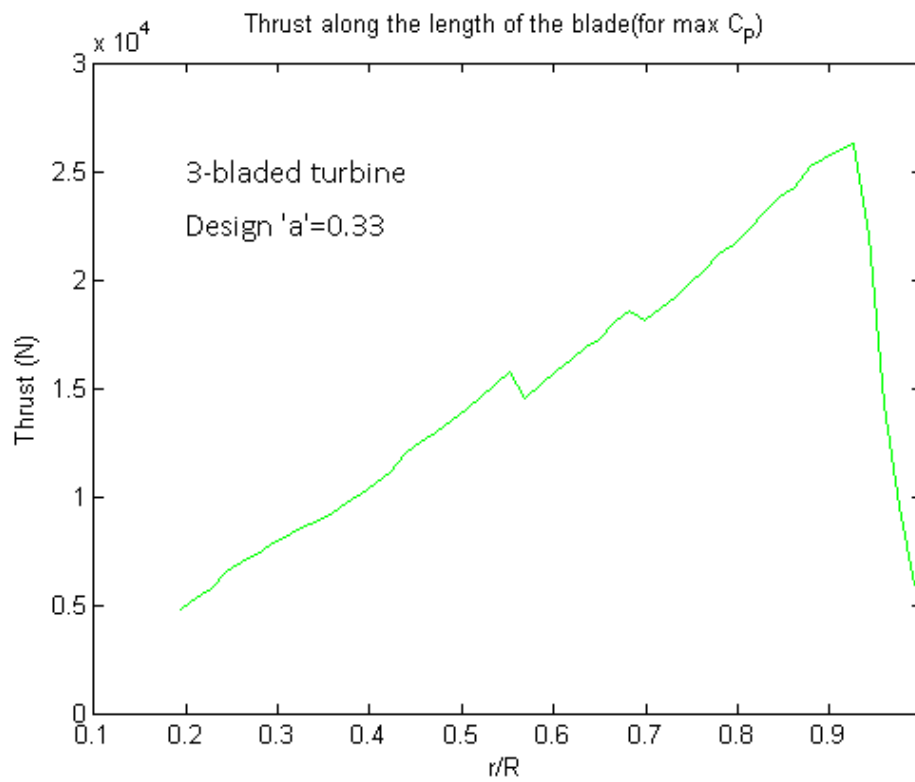


Figure 5: Thrust along the length of the blade

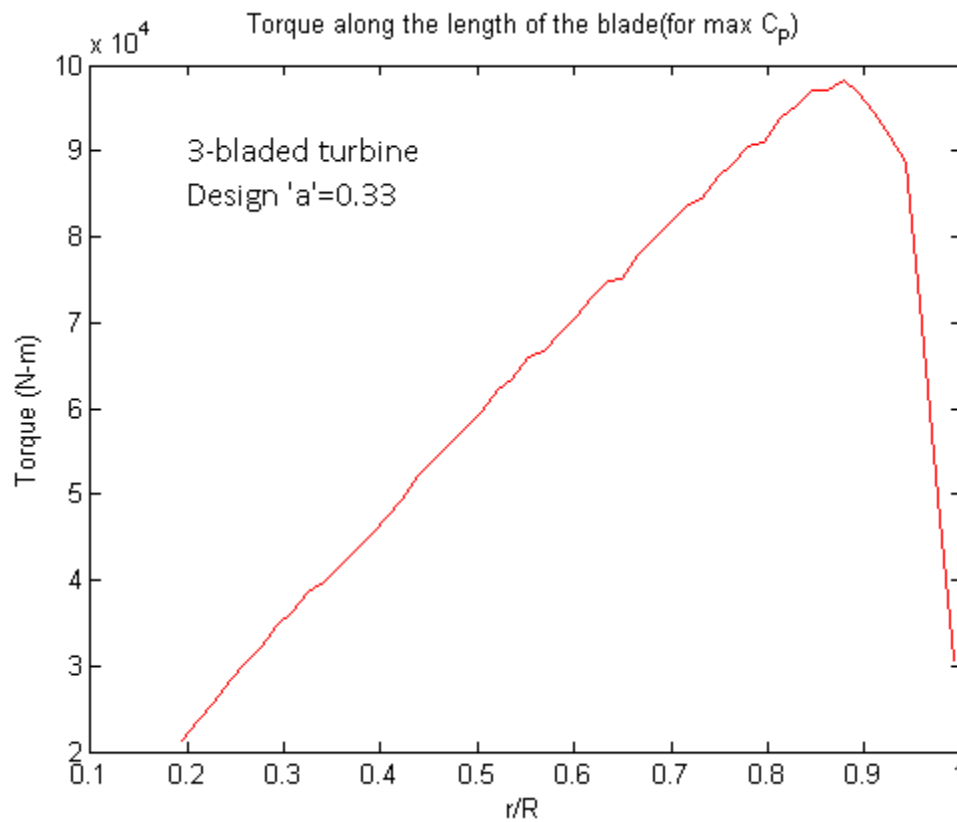
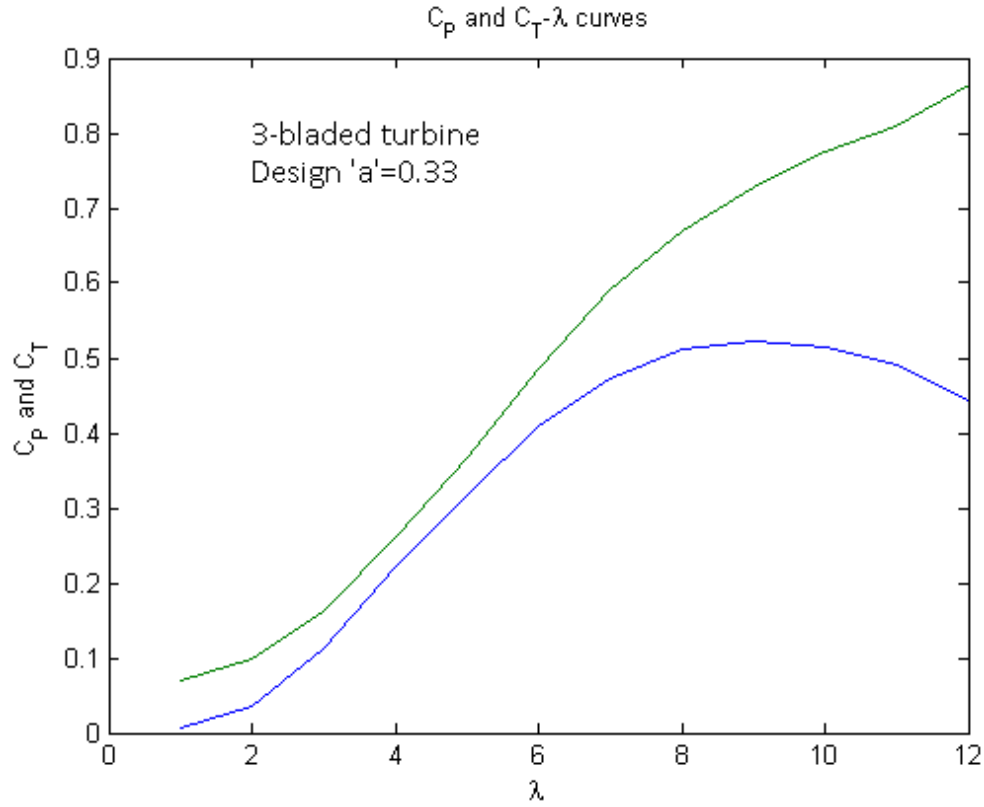
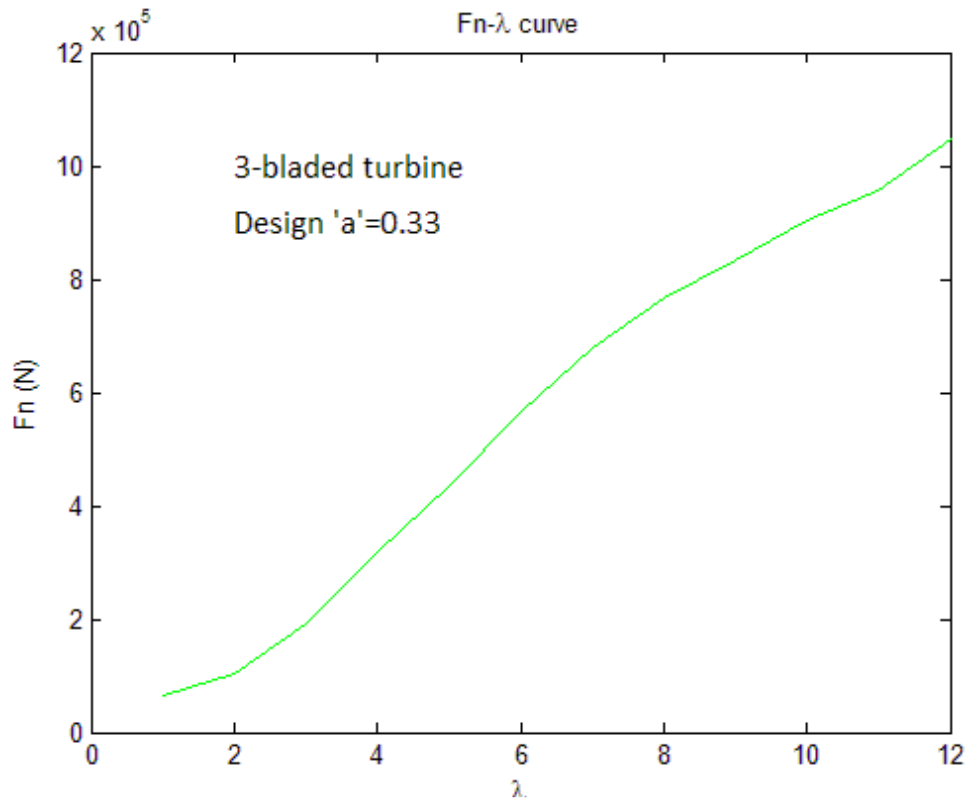
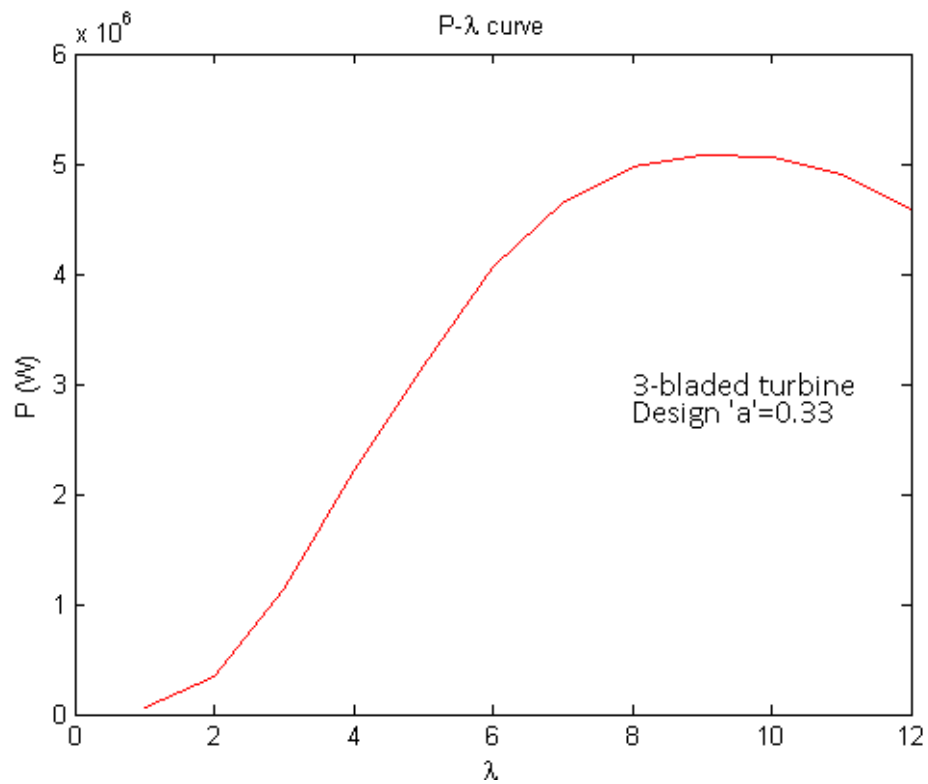
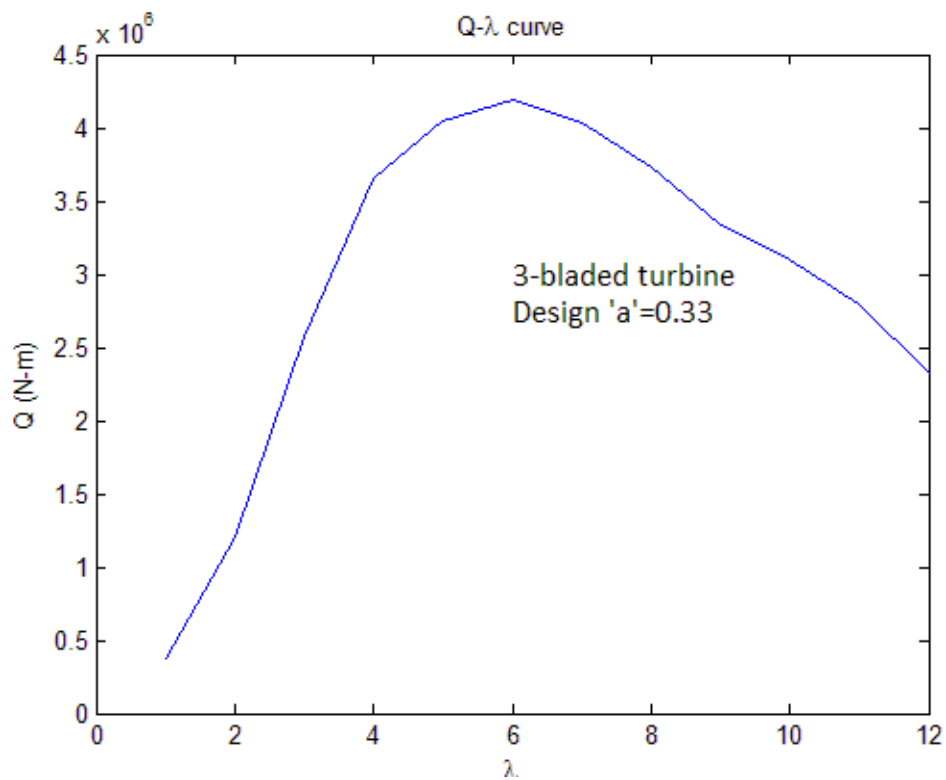


Figure 6: Torque along the length of the blade

Figure 7 through Figure 10 show the power coefficient, thrust coefficient, rotor thrust, power and torque versus λ .

Figure 7: Power coefficient and thrust coefficient Vs. λ Figure 8: Thrust Vs. λ

Figure 9: Power Vs. λ Figure 10: Torque Vs. λ

Operating Curves

Figure 11 through Figure 14 shows the annual energy yield, the operational C_p and C_T curves, the power curve, the thrust curve and the pitch curve.

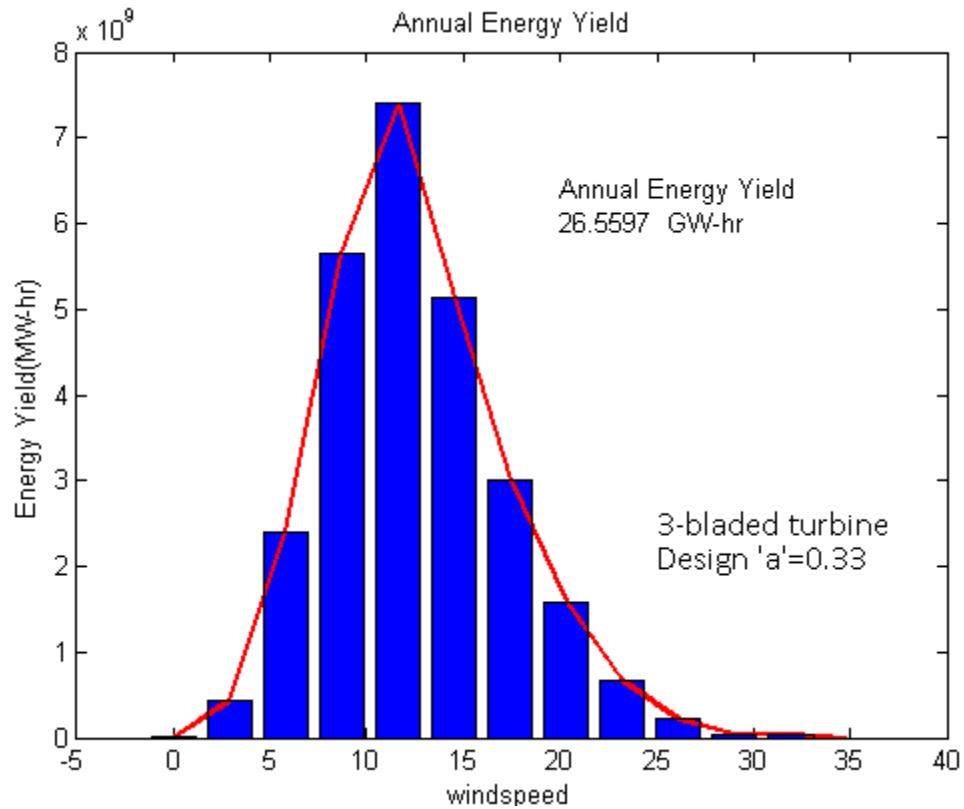


Figure 11 : Annual Energy Yield

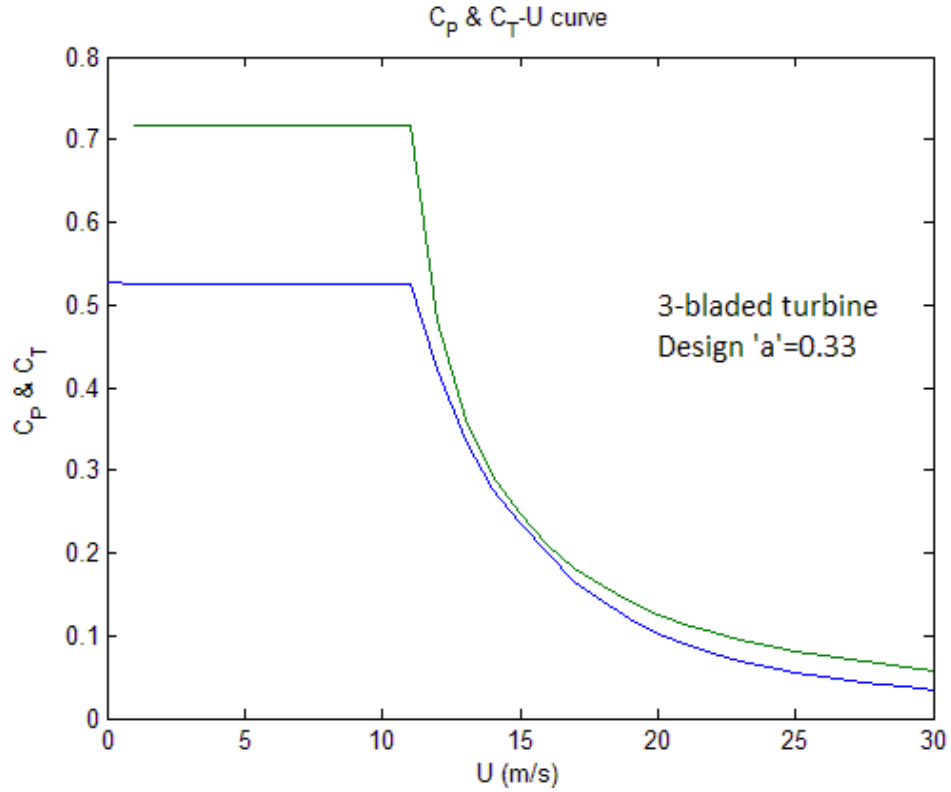
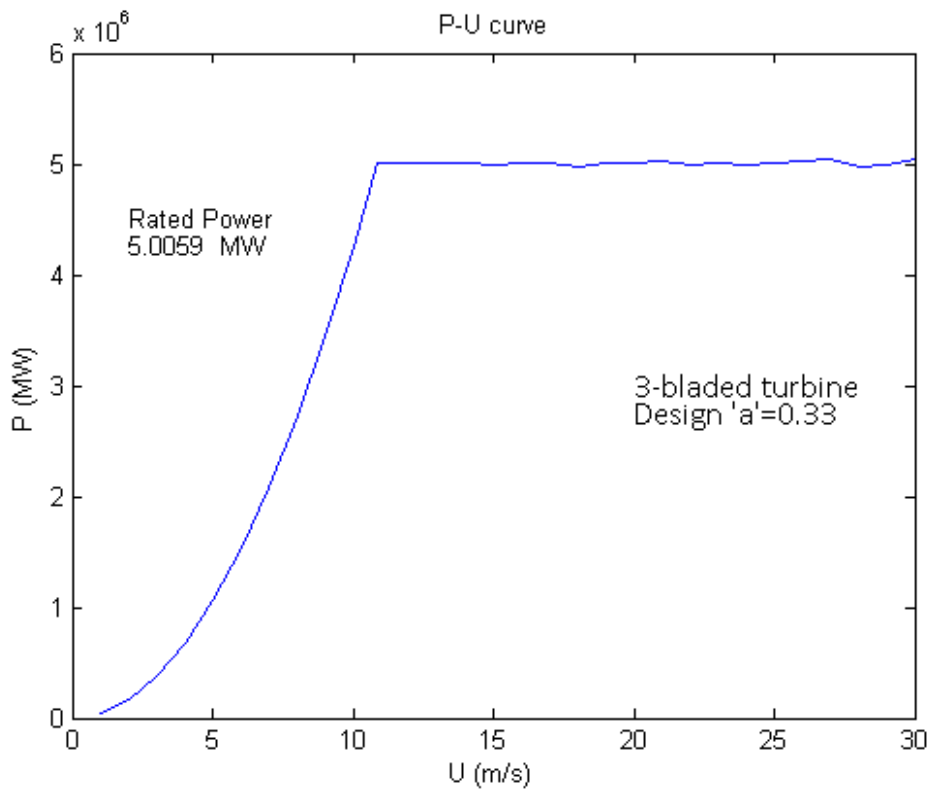
Figure 12: C_p and C_T Vs. Wind speed

Figure 13: Power Vs. Wind speed

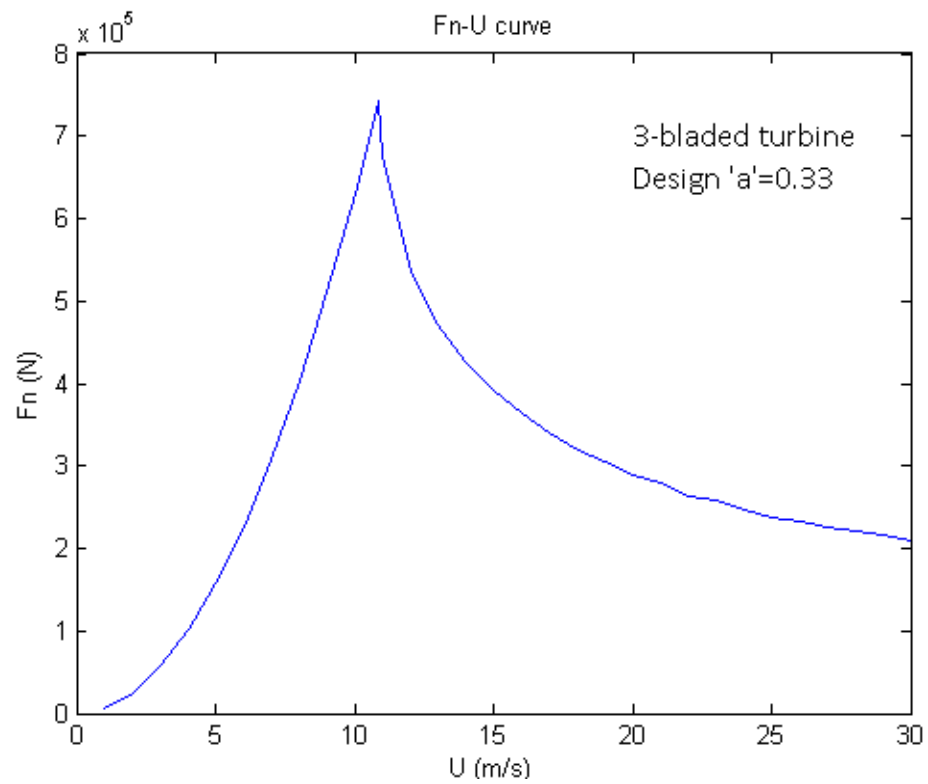


Figure 14: Thrust Vs. Wind speed

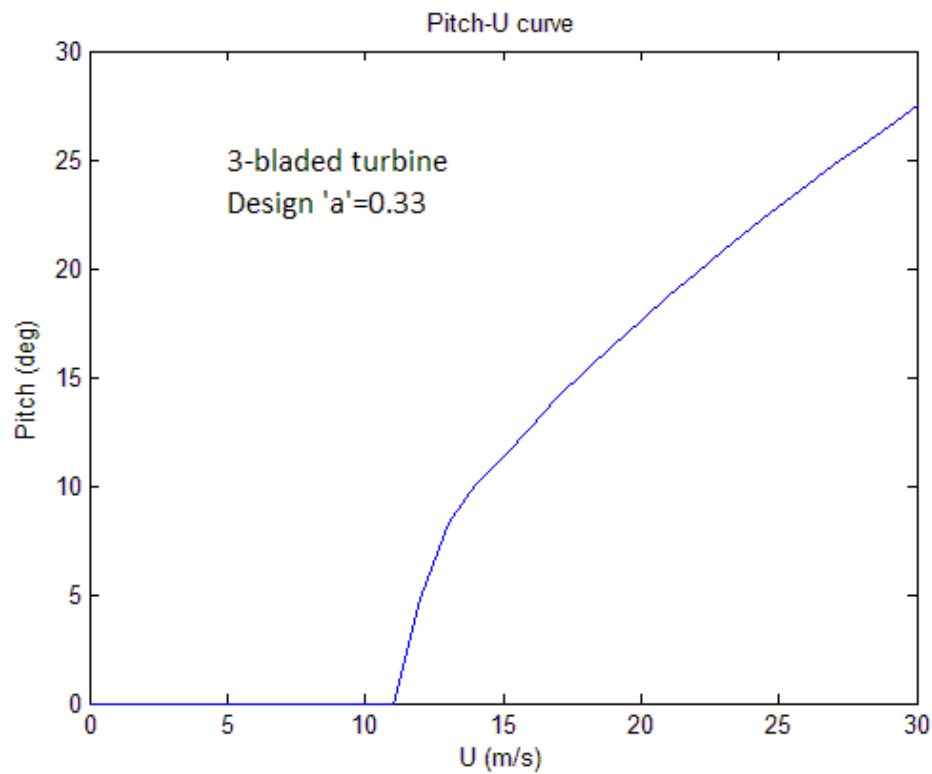


Figure 15: Pitch angle Vs. Wind speed